NUMERICAL MODELING OF KIZILDERE GEOTHERMAL FIELD

A MASTER THESIS SUBMITTED TO
THE GRADUATE SCHOOL OF NATURAL AND APPLIED SCIENCES
OF
MIDDLE EAST TECHNICAL UNIVERSITY

BY

MELİKE ÖZKAYA

IN PARTIAL FULFILLMENT OF THE REQUIREMENTS
FOR
THE DEGREE OF MASTER OF SCIENCE
IN
GEOLOGICAL ENGINEERING

DECEMBER 2007

Approval of the thesis:

NUMERICAL MODELING OF KIZILDERE GEOTHERMAL FIELD

submitted by **MELİKE ÖZKAYA** in partial fulfillment of the requirements for the degree of **Master of Science in Geological Engineering Department, Middle East Technical University** by,

Prof. Dr. Canan ÖZGEN
Dean, Graduate School of **Natural and Applied Sciences** _____

Prof. Dr. Vedat DOYURAN
Head of Department, **Geological Engineering** _____

Prof. Dr. Nurkan KARAHANOĞLU
Supervisor, **Geological Engineering Dept., METU** _____

Prof. Dr. Vedat TOPRAK
Co-Supervisor, **Geological Engineering Dept., METU** _____

Examining Committee Members:

Prof. Dr. Mahmut PARLAKTUNA
Petroleum and Natural Gas Engineering Dept., METU _____

Prof. Dr. Nurkan KARAHANOĞLU
Geological Engineering Dept., METU _____

Prof. Dr. Vedat TOPRAK
Geological Engineering Dept., METU _____

Prof. Dr. Nilgün GÜLEÇ
Geological Engineering Dept., METU _____

Assoc. Prof. Dr. Serhat AKIN
Petroleum and Natural Gas Engineering Dept., METU _____

Date: 17.12.2007

I hereby declare that all information in this document has been obtained and presented in accordance with academic rules and ethical conduct. I also declare that, as required by these rules and conduct, I have fully cited and referenced all material and results that are not original to this work.

Name, Last name : Melike Özkaya

Signature :

ABSTRACT

NUMERICAL MODELING OF KIZILDERE GEOTHERMAL FIELD

ÖZKAYA, Melike

Ms., Department of Geological Engineering
Supervisor: Prof. Dr. Nurkan KARAHANOĞLU
Co-Supervisor: Prof. Dr. Vedat TOPRAK

December 2007, 95 pages

This research is dedicated to make a foreseeing of the future state of the Kızıldere Geothermal Field in order to suggest acceptable solutions to the current problems. The non-isothermal mechanism of the geothermal field is simulated for the pressure and temperature variables. For this purpose, a finite element model (696 four-nodal elements with 750 nodes) of the field is formulated by considering the geological conditions and the present wells already drilled in the area. Then the model is calibrated to the field for the natural state by using appropriate physical properties, boundary and initial conditions. Comparison of the simulated and the observed pressures and temperatures has emphasized a very successful calibration study. After the calibration, response of the field to the production and injection for the period of 1984-2006 has been simulated by applying a history matching study. History matching runs have yielded very good correlations between the observed and the computed values of the pressure and temperature variables.

The calibrated and history matched model has been applied to the field to simulate the future performance of the field for different production and injection scenarios. In the first scenario the field is simulated for the next 10-year production period keeping the on-going production conditions. Then, the influence of the production of two new wells has been investigated in two different scenarios. In the forth scenario, the effect of injection from one of the production wells has been simulated.

Keywords: Kızıldere Geothermal Field, Numerical Modeling, Geothermal Models

ÖZ

KIZILDERE JEOTERMAL SAHASI'NIN SAYISAL MODELLENMESİ

ÖZKAYA, Melike
Yüksek Lisans, Jeoloji Mühendisliği Bölümü
Tez Yöneticisi: Prof. Dr. Nurkan KARAHANOĞLU
Ortak Tez Yöneticisi: Prof. Dr. Vedat TOPRAK

Aralık 2007, 95 sayfa

Bu araştırmada, Kızıldere Jeotermal Sahası'nın güncel problemlerine kabul edilebilir çözümler getirmek maksadıyla sahanın gelecek durumunu öngörmek amaçlanmıştır. Jeotermal sahanın eşısıl olmayan mekanizması, basınç ve sıcaklık değişkenleri için simüle edilmiştir. Bu amaçla, jeolojik durum ve alanda daha önceden açılmış bulunan kuyular dikkate alınarak, sahanın bir sonlu elemanlar modeli (750 nod ve 696 dört-nodlu eleman) formüle edilmiştir. Daha sonra, uygun fiziksel özellikler, sınır ve başlangıç koşulları kullanılarak model, doğal hal için sahaya kalibre edilmiştir. Simüle edilen ve gözlenen basınç ve sıcaklıklar çok başarılı bir kalibrasyon çalışmasını vurgulamaktadır. Kalibrasyondan sonra, 1984–2006 zaman aralığında sahanın üretim ve enjeksiyona tepkisi tarihsel eşleştirme çalışması uygulanarak simüle edilmiştir. Tarihsel eşleştirme çalışması, basınç ve sıcaklık değişkenlerinin gözlenen ve hesaplanan değerleri arasında çok iyi korelasyon sağlamıştır. Kalibre edilen ve tarihsel eşleştirmesi yapılan model, sahanın değişik üretim ve enjeksiyon senaryolarındaki gelecek performansını simüle etmek için sahaya uygulanmıştır. Birinci senaryoda saha, halen devam eden üretim koşulu sonraki on yıllık üretim sürecinde de sürdürülerek simüle edilmiştir. Daha sonra, yeni iki kuyunun üretimlerinin etkisi iki değişik senaryoda araştırılmıştır. Dördüncü senaryoda, üretim kuyularından birinden uygulanan enjeksiyonun etkisi simüle edilmiştir.

Anahtar Kelimeler: Kızıldere Jeotermal Sahası, Sayısal Modelleme, Jeotermal Modeller

To My Family

ACKNOWLEDGMENTS

It is an honor for me to express my deepest gratitude to my supervisor Prof. Dr. Nurkan Karahanoğlu for his major contributions, valuable guidance and unlimited patience throughout the study.

Again, I would like to express my gratitude to my co-supervisor Prof. Dr. Vedat Toprak for his constant support, guidance, trust and friendly attitude.

I would also like to thank Prof. Dr. Mahmut Parlaktuna for his valuable suggestions and comments.

I am deeply indebted to Mr. Kadri Yeltekin from General Directorate of Mineral Research and Exploration (MTA in Turkish Initials) whose technical support and stimulating suggestions helped me in all the time of research for and writing of this thesis.

I would like to give my special thanks to my friends Deniz Türkmen, Nesrin Tüfekçi Başak Şener and Özgür Aktürk because of their great motivational help to go ahead in difficult times and of their precious comments during the study.

Finally, I am really grateful to my family whose patient support enabled me to complete this work.

TABLE OF CONTENTS

LIST OF TABLES

TABLE

LIST OF FIGURES

FIGURE

CHAPTER 1

INTRODUCTION

Energy demand is increasing all over the world as a result of gradually fastening technological developments. Countries tend to meet their energy demand by the utilization of primary energy sources such as coal and petroleum. Nevertheless, these sources are limited. Therefore, it is obvious that, new and renewable energy sources have to be found or developed.

One of the renewable energy resources that holds the most promise is the geothermal energy. Especially in countries that are in an earthquake zone, geothermal energy has an important potential (Murathan et al., 1999).

Turkey is a country with significant potential in geothermal energy. This is basically because of the fact that it is located on the Alpine-Himalayan Orogenic Belt and the Miocene or younger grabens are developed as the result of this orogeny. Widespread volcanism, fumarole hydrothermal alterations, and the existence of more than 1,000 hot and mineral water springs—up to 373 and 413 K—in geothermal fields with a temperature range of 313 to 505 K have been discovered in Turkey (Günerhan et al., 2001). Studies on the exploitation and exploration were started in the 1960s by the Mineral Research and Exploration Institute of Turkey (MTA in Turkish initials), and approximately 140 geothermal fields, with a wellhead temperature above 313 K were explored (Mertoğlu and Başarır, 1995; Şimşek, 1997).

Turkey has a place among the world's first 7 countries with respect to the abundance of its geothermal resources (Mertoğlu et al., 1993). The domestic coal, geothermal, and hydropower reserves of Turkey are approximately 1% of the world's total (WECTNC, 1994). The most significant developments in production are observed in hydropower and geothermal energy production. However, this usage is not larger than 2% of its potential (Eltez, 1997).

The overall geothermal potential in Turkey is about 38,000 MW. According to the data accumulated since 1962, around 88% of this potential (approximately 31,000 MW) is appropriate for thermal use (temperature < 473 K) and the remainder (approximately 4.500 MW) for electric power production (temperature > 473 K) (Ediger and Kentel, 1999; Kaygusuz, 1996).

Taking the current development of geothermal energy in Turkey into consideration, it is estimated that by the year 2010 about 6,500 MW shall be installed in district heating and also a capacity of 258 MW (Hepbaşlı et al., 2001).

The Büyük Menderes fault zone at Western Anatolia contains an important part of the abovementioned potential. Especially the Denizli-Kızıldere Geothermal field at the eastern part of Büyük Menderes graben has one of the operating geothermal power plants in Turkey.

The Kızıldere Geothermal Power Plant was installed as the first geothermal pilot plant of Turkey, in February 1984, with a capacity of 20.4 MW. This 20MW plant produces about 85 GW/h of electricity using high- temperature geothermal fluid (200–212 ◦C), with a 10% steam ratio, from wells tapping the second reservoir (Şimşek et al., 2005). Because of the high noncondensable gas (NCG) content of the field (average 13% by weight of the steam) and also NCGs consist mainly of CO_2 (97–99%) and NH^3, a liquid CO_2 and dry-ice production was built adjacent to the field in 1986. Since then, a factory with a capacity of 40,000 tons/yr has been continuing to extract CO_2 gas from the steam to meet the demand of the indigenous industry. Besides electricity and dry ice production, the resources of the field are also used for green-house heating and space heating of offices and residences of the plant. Greenhouses of approximately 10,700 m^2 have been heated by using the waste water of the plant (Günerhan et al., 2001; MTA, 1993).

1.1. Geographical Setting of the Study Area

The Kızıldere geothermal field is located at 12 km northwest of the Sarayköy village of Denizli city. The field is found between the latitudes of North 37° and 38° and longitudes of East 29° and 30° in the eastern part of the Büyük Menderes Graben (Figure 1). It is situated between the city borders of Denizli and Aydın.

The Büyük Menderes River, in the vicinity of the study area, flows through the Büyük Menderes Graben with a meandering flow pattern and braided distributaries. The region has a dry maritime climate with an annual average temperature of 22.5 °C.

1.2. Overview of Tectonic Evolution of the Study Area

Kızıldere Geothermal Field is situated at Western Turkey which is a structurally complex region exhibiting all the superimposed imprints of extensional, compressional and strike-slip tectonics. Generally, the active deformation of this region is governed by interaction of three major plates (Eurasia, Arabia and Africa), as well as other small plates (blocks). The bulk deformation in the region appears to have originated from subduction and collision-related processes, i.e. the forces applied at the plate boundaries (Şengör et al., 1985).

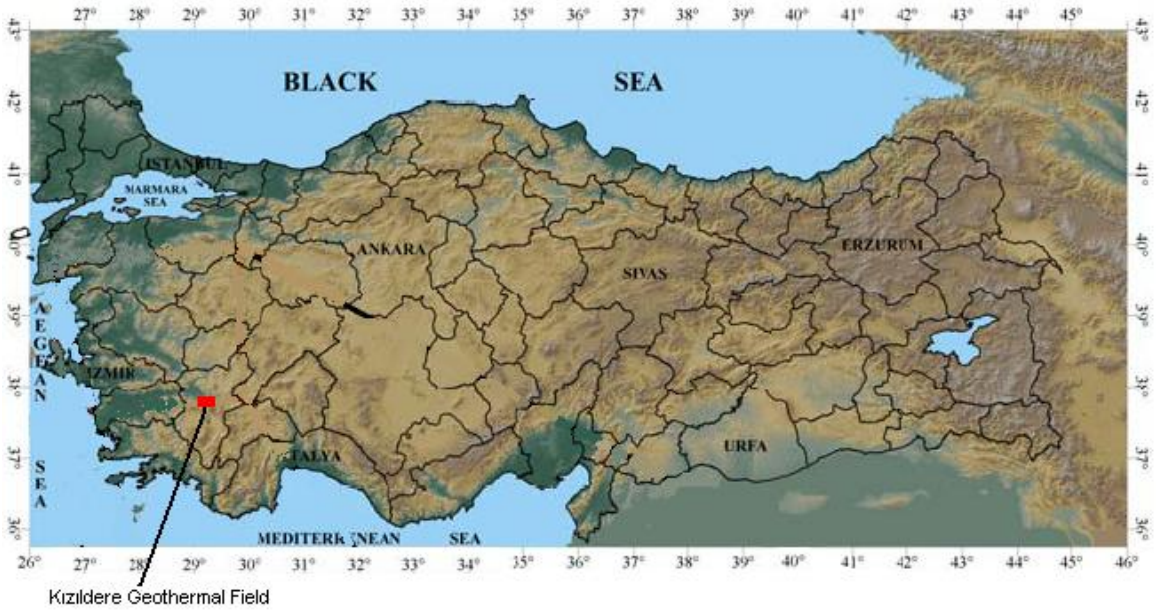

Figure 1.1 Geographical setting of the study area

Extension in this region has been attributed to:

1. Westward escape of the Anatolian block along the North Anatolian Transform Fault
2. Neogene to recent subduction in the Hellenic Trench
3. Gravitational collapse of thickened crust following Paleogene Alpine–Himalayan compression (Bozkurt, 2001 and the references there in).

East–West grabens like Büyük Menderes Graben where the study area is found and their basin-bounding active normal faults are the most prominent neotectonic features of western Turkey (Dumont et al., 1979; Duvarcı, 2001, Bozkurt, 2001). The Menderes Massif is one of the largest metamorphic massifs in Turkey, with a length of about 200 km N–S between the Simav and Gökova grabens, and about 150 km E–W between Denizli and Turgutlu in western Anatolia (Ketin, 1983) (Figure 1.2).

Extension continues today and major earthquakes have occurred in the Gediz and Büyük Menderes grabens. In western Turkey, the north–south extension inferred from major earthquakes is about 13.5 mm/year (Eyidoğan, 1988).

Regional uplift across western Turkey has been no more than 700–800 m in the past 7–8 My, as estimated from the elevation of Miocene marine sediments to the east of the Büyük Menderes graben (Westaway, 1993). GPS data show that the westernmost part of the Anatolian plate is rapidly escaping to the SW at a rate of 30.1 mm/year motion (Oral, 1994; Şalk et al., 1999; McClusky et al., 2000).

Kaya (1982) reported that the older Miocene structure in Western Turkey consists of a N to NE-trending graben-horst system and the ENE-trending Büyük Menderes fullgraben. The superimposed late Miocene structure is represented by WNW and ENE-trending half grabens (the Gediz, Simav and Kütahya grabens). In this context, the Büyük Menderes graben would have been influenced by the late Miocene-Pliocene half-graben tectonics, and half-grabens characterized by the older N to NE-trending normal faults.

In terms of total displacements and extent of strike, the Gediz and Büyük Menderes fault zones could be considered as the most important ones. Each has a Neogene basin in its hanging-wall, visible as low-lying sediment up to 2 km thick in its uplifted footwall. According to borehole data obtained for geothermic purposes (Erisen, 1996), the thickness of the sediments is 1241 m in Kızıldere - Denizli (KD-9). Both the Büyük Menderes and Gediz basins are asymmetric, with their dominant active extensional fault traces on their southern and northern margins, respectively (Roberts, 1988; Paton, 1992). These faults separate the recent basin from belts of exhumed Neogene sediments in faulted and depositional contact with the basement. In addition, Neogene sediments are uplifted along the northern margin of the Gediz graben, and within isolated sub-basins on the southern margin of the Büyük Menderes graben.

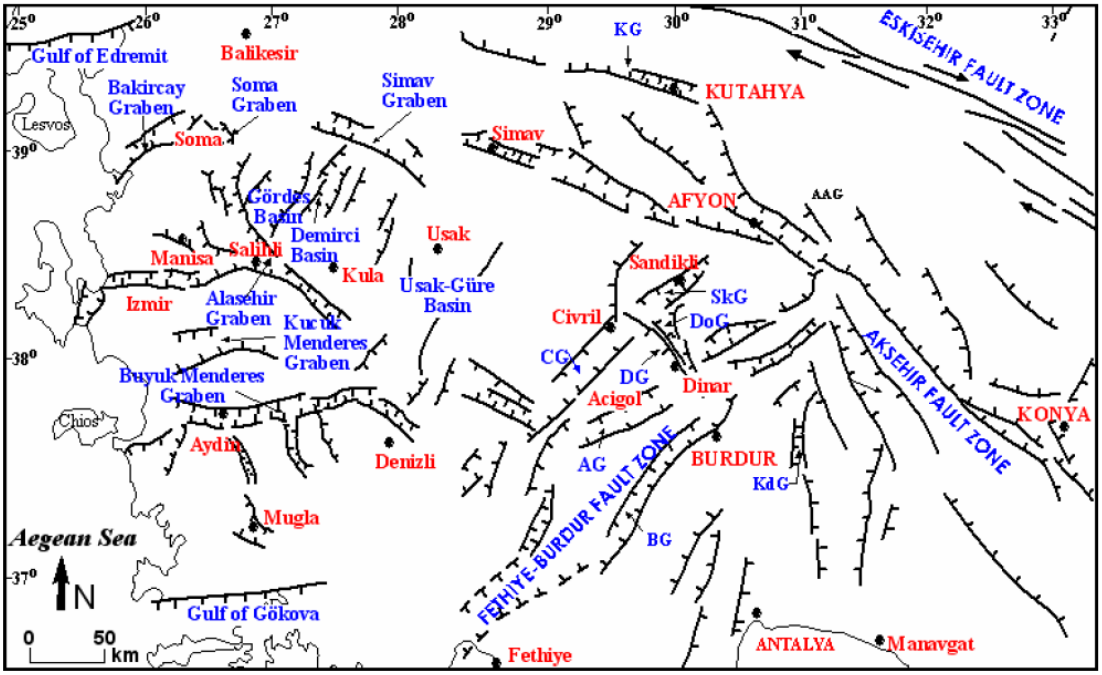

Figure 1.2 Simplified map showing major structural elements of Western Anatolia. Heavy lines with hachures show normal fault: hachures indicate down-thrown side, other heavy lines show strike-slip faults and the arrows along them show the relative direction of movement (from Bozkurt, 2001).

In each graben, one margin is characterized by steeper topography and more extensive and thicker exposures of Neogene sediments; and has been associated with surface breaks during earthquakes in historic times. The depositional systems in the Gediz, Büyük Menderes grabens are syn-tectonic. Locally, major structures have been modified by antithetic faulting. These basins, while being mainly half-grabens, exhibit synthetic and antithetic faulting on their hanging wall margins which created topographic relief and generated locally derived coarse detrius (Cohen et al., 1995).

The proposed ages of the Menderes Massif metamorphic rocks and the granodiorite are Precambrian to Paleocene (Dora et al, 1997) and Early Miocene in age (Erdoğan and Güngör, 1992), respectively.

In Kızıldere, the general trends of the most recent faults are E – W and SE – NW. Some older fault systems trending N – S have also been observed. Overturned cover folding and local reverse faulting consistent with graben tectonics have also been observed in the area.

The denudation surfaces, valley forms and alluvial fans indicate that the E –W fault systems are the youngest and that the largest displacements of these faults occurred during the Pli – Quaternary and Quaternary. The seismic data obtained during the earthquakes indicate that Kızıldere Geothermal Field is in the first degree earthquake zone. Average vertical displacement is annually about 2.4 cm.

1.3. Geology of the Study Area

Kızıldere geothermal field is in the Sarayköy–Buldan area, and is associated with the major fault along the northern boundary of the Büyük Menderes Graben (Figure 1.3).

The basement rocks in the vast areas of West Anatolia are Menderes metamorphics of the Paleozoic or older period. Same as other fields in the graben, the basement in the Kızıldere field is made up of metamorphic rocks of the Menderes Massif. At the base of the metamorphics are augen gneisses. These are typically exposed within the massif in the deeply eroded horsts of Buldan and Yenice. These gneisses are classified as augen, biotite-bearing and lustre gneiss, according to their texture and mineral composition, but are classified as ortho and para according to their origin.

The upper parts of the gneiss appear to alternate with quartzites and schists in some places, reaching thicknesses of 150 m in parts. Generally this unit is overlain by a rather thick unit of schists, known as micaschist unit, and bearing considerable amounts of garnet, muscovite and biotite.

İğdecik Formation forms the uppermost unit of the metamorphics in the study area. It is composed of marble, calcschist, quartzite and schist alteration and the rocks of this unit are commonly fractured and faulted.

These rocks are overlain by fluvial and lacustrine Pliocene sediments, which have been divided into four lithologic units (Şimşek, 1985) (Figure 1.3). Lower Pliocene units are the earliest continental – lacustrine deposits that cover the massif. A large stratigraphic gap exists between these rocks and the basement units.

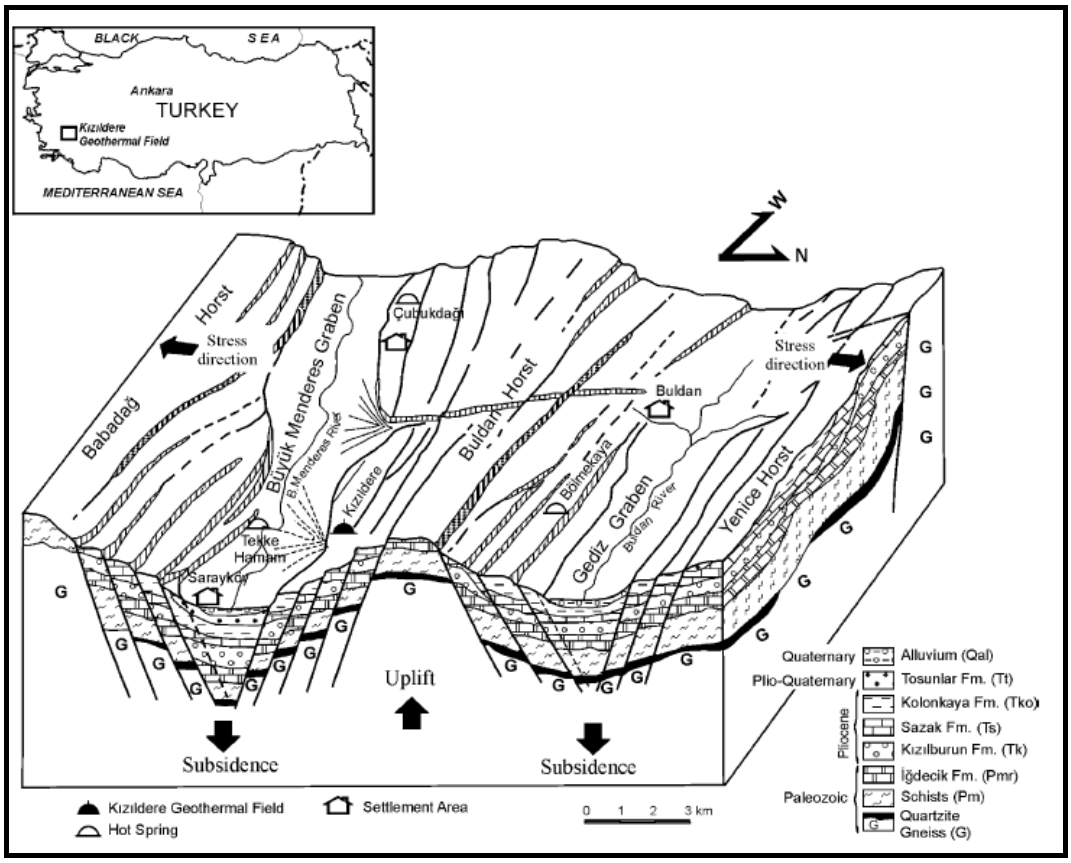

Figure 1.3 Geological block diagram of the Sarayköy–Buldan area (from Şimşek, 1985).

From bottom to top these are listed below.

Sazak Formation (Ts) comprises intercalated gray limestones, marls and siltstones and has a 100–250 m thickness

Kolonkaya Formation (Tko), made up of yellowish green marls, siltstones and sandstones, 350–500 m in thickness,

Kolonkaya Formation appears to contain alternations of yellowish and light brown sandstone, claystone and clayey limestone. Within this succession there are district marker beds composed of limestones. Their thickness is 350–500 m in thickness.

Finally, Pli – Quaternary Tosunlar Formation (Tt), overlies the Lower Pliocene and Paleozoic units with an angular unconformity. It consists of alternations of a grey, poorly consolidated, partly bouldery conglomerate, sandstone and mudstone with fossiliferous clayey limestone. Thickness of this formation is about 500 m.

Quaternary alluvium (Qal) which is characterized by terrace deposits, alluvium, slope debris, alluvial fans and travertine unconformably overlies these sedimentary units.

The regional geological structure is controlled by E–W trending faults associated with the Büyük Menderes Graben, but some NW–SE trending, active faults have caused the uplift and dissection of the northern and southern flanks of the metamorphic basement.

1.4. Hydrogeology of the Study Area

The permeability within the Menderes Massif rocks is highly variable. The carbonates (marbles and dolomitic marbles) of the Menderes Massif rocks are highly fractured and karstified and act as an aquifer for both cold ground waters and thermomineral waters depending on the location. Fractured parts of granodiorite, gneiss and quartz-schist units of the Menderes Massif act as aquifers for low-salinity cold ground waters, hot waters and for thermomineral waters. These rocks form the reservoir for waters to be heated at depth and fractures and faults provide a means for circulation and rise of the heated waters to the surface (Gemici and Tarcan, 2002). Schists and phyllites have relatively low permeability. The Neogene terrestrial sediments, which are made up of alluvial fan deposits including poorly cemented clayey levels, have very low permeability as a whole and may locally act as cap rocks for the geothermal systems. Clayey levels of the Neogene sediments occur as impermeable barrier rocks. Sandy to gravely and limestone levels of this Neogene unit contain minor aquifers (Tarcan et al, 2005).

There are three main reservoirs in the Kızıldere field: (1) the First (upper) Reservoir, within the limestones of the Sazak Formation; (2) the Second Reservoir, within the marble–quartzite–schist intercalations of the İğdecik Formation, and (3) the Third (deep) Reservoir, hosted within the gneisses and quartzites that are intercalated with, and underlie the schists (Figure 1.4).

1.4.1. The First Reservoir

Within the units of the Pliocene, Sazak Formation represents the first reservoir. Its continuity is, however, broken by lateral facies variations in the formation. These changes in the formation restrict the distribution of the first reservoir. The thickness of the limestones in this unit varies and they grade into marls and sandstones laterally and vertically.

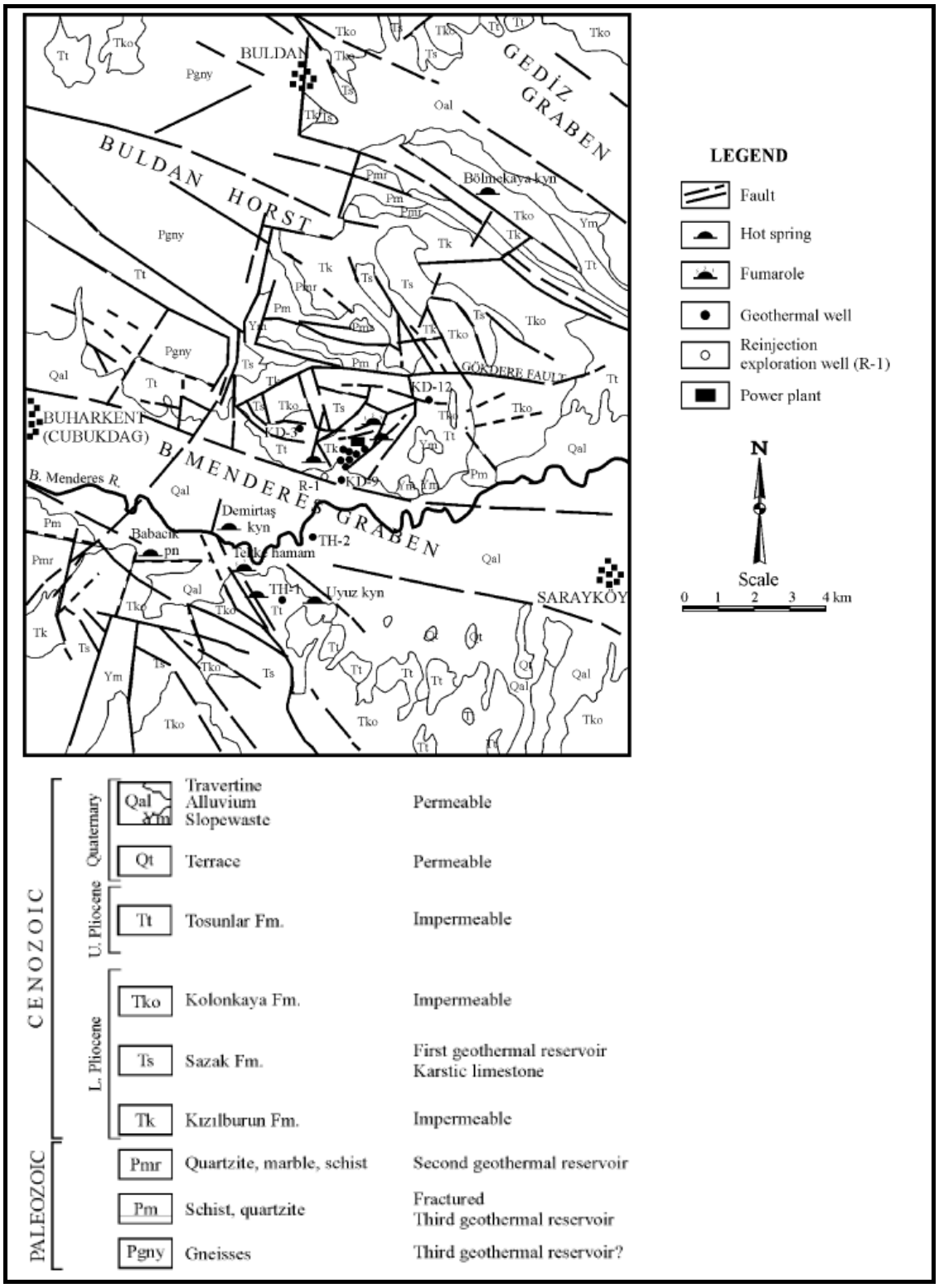

Figure 1.4 Hydrogeological map of the Kızıldere geothermal area (Modified from Şimşek, 1985)

According to the drilling data in the Kızıldere geothermal field, production in wells KD-1, KD-1A, KD-2, KD-3, KD-4, KD-12 and KD-8 are from the first reservoir of Pliocene limestones, whereas the other wells (KD-6, KD-7, KD-9, KD-13, KD-14, KD-15 and KD-16) crossed marls and sandstones instead of limestones. The maximum temperature recorded in the first reservoir was 198 °C in KD-1 well. The average temperature is about 170 °C for this reservoir. The thickness of the reservoir rock varies between 100 – 250 m.

1.4.2. The Second Reservoir

The alternations of marble – quartzite – schists of the İğdecik Formation in the Menderes metamorphic massif represent the second reservoir. It exhibits a lateral continuity over a large area and has relatively high secondary porosity and permeability compared to the first reservoir. As this reservoir lies at greater depths, it has higher temperatures. A temperature of 212 C was recorded at well bottom in KD-16. The wells; KD-6, KD-7, KD-9, KD-13, KD-14, KD-15, KD-16 and KD-111 have reached the second reservoir. Its thickness varies between 100 – 300 m. The first and second reservoirs are related by faulting.

1.4.3. The Third Reservoir

According to geological data, thick and impermeable micaschists underlie the alternation of marble – quartzite – schist that forms the second reservoir. Gneiss and quartzites lie beneath the micaschists according to the general sequence, indicating that the transition zone could form a suitable reservoir formation. Furthermore, the dam site investigations of the DSI (State Hydraulics Works) in the same area revealed that some parts of the basement gneiss (particularly the quartzitic gneiss), which are in fact composed of various gneiss, are permeable and could act as a reservoir, judging by the results of water permeability tests. The wells R-1 and R-2 tap the deep reservoir (Şimşek et al., 2000a). The Na – K – Ca and SiO_2 geothermometers indicate a temperature of 250 – 260 ° C for this third hypothetical reservoir in the Kızıldere field. This reservoir is associated with the main graben boundary fault line at depth (Şimşek et al., 2005).

1.4.4. Cap Rocks

The alternations of Pliocene claystone, marl and sandstone act as an impermeable cap rock in the study area, impeding any loss of heat and entrapping the geothermal fluid within the reservoir rock. Folding, instead of faulting, has developed in these rocks as a result of intense tectonic activity. Two cap rocks have been identified from drilling data.

1.4.4.1. First Cap Rock

Kolonkaya Formation, which overlies the Sazak Formation containing the first reservoir, together with the alternations of claystone, marl and sandstone of the Tosunlar Formation forms a suitable cover for the first reservoir. In the Kolonkaya Formation, joints and other discontinuity planes have very little effect on the permeability of the unit.
The very fine-grained dendritic drainage that characterizes the existence of impermeable beds could be taken as a distinguishing feature of this unit. The thickness of the cap rock varies between 350 and 600 m.

1.4.4.2. Second Cap Rock

The alternations of well-consolidated conglomerate, sandstone and claystone of Kızılburun Formation, which lies under the first reservoir, act as a very efficient cap rock. The characteristics of this unit at various points in the measured stratigraphical sections suggest that this unit represents an ideal cap rock. Its thickness varies between 100 and 250 m.

1.5. Geochemistry

Kızıldere geothermal reservoir is liquid-dominated. Two percent of the total fluid in the reservoir is CO_2, but at 70 psia separation pressure at the surface about 10 % of the fluid is steam and about 10-20 % of this steam is composed of noncondensable gases, especially CO_2 (Tan, 1985). There is also a large amount of scaling in the well bore and in the surface equipment due to pressure drop. The calculated saturation pressure of gas for the Kızıldere reservoir is 52,4 kg/cm^2 (Ölçenoğlu, 1986). In static conditions, it is possible to keep the gas in the reservoir in the fluid phase, but during flow, as the pressure decreases in the well, gas starts to separate and because of this gas phase, steam starts to evaporate with its partial pressure corresponding to its temperature. These two phenomena occur spontaneously resulting in an increased gas pressure due to the partial pressure of steam. Thus, flashing occurs at a deeper level.

1.5.1. Chemical Characteristics

Chemical analyses of hot and cold waters in and around Kızıldere and Tekkehamam (Table 1.1) show that three types of water exist in the region:

a) Alkaline bicarbonate (NaHCO3); 4500 ppm < TDS < 6000 ppm; Kızıldere geothermal water, that interacts for a long time with high-grade metamorphic rocks.

b) Alkaline earth bicarbonate (CaHCO3); TDS < 500 ppm; cold springs related to shallow groundwater circulations, feeding the aquifer of Kızıldere. Like the type (a) waters, these waters have interacted with the same high-grade metamorphic rocks, but at lower temperatures and only for a short time.
c) Alkaline sulfate (NaSO4); TDS < 3000 ppm; Tekkehamam hot spring waters that occur in the marginal parts of Kızıldere.

The chemical composition of the fluid in the second reservoir changes according to the direction of mixing with the cold water.
Analyses of the geothermal water and separated steam reveal high B, NH_4 and CO_2 concentrations, which may be derived from the ascent of magmatic emanations from depth. The high concentrations of dissolved solids (especially boron and fluoride), together with the high alkalinity, make Kızıldere geothermal fluids unsuitable for domestic and irrigation uses. The waters from this liquid-dominated geothermal field contain moderate sulfate and low chloride concentrations. The chemical composition of the geothermal water samples is Na+K>Ca>Mg and HCO_3 +CO_3 > SO_4 > Cl; on a Na–K–Mg diagram they are partially equilibrated fluids.

1.5.2. Isotope Analyses

Analyses were made of the chemical and isotopic compositions of 12 water samples taken from well R-1, which cuts the Third (deep) Reservoir, and from several wells (KD-6, KD-13, KD-15, and KD-21) which cut the Second Reservoir. These analyses show that the water type for well R-1 is $NaHCO_3$, which is the same as for the other wells in the field (Şimşek et al., 2000). The stable isotope analyses of the water samples indicate that the geothermal waters are of meteoric origin. There is a clear shift from the Mediterranean Meteoric Water Line and cold-water values. This suggests that water–rock interaction is an important process in the Kızıldere geothermal system, and implies deep circulation and high temperatures. Both the hot spring waters and the deep geothermal well fluids have almost no tritium so the thermal fluids in the field are older than 50 years (Şimşek et al., 2000).

1.6. Production History and Operational Problems of the Field

The first deep well in Kızıldere Geothermal field, KD-1, drilled in 1968 at a depth of 540 m, produced a mixture of water and steam with a temperature of 198 °C in the reservoir, indicating the existence of water-dominated geothermal system. Then 16 more wells have been drilled in the field between 1968 and 1975. The depths of those wells are between 370

m – 1241 m. After well completion tests it was found that KD-6, KD-7, KD-13, KD-14, KD-15, KD-16 wells were suitable to generate electricity.

After completion of feasibility studies, the geothermal power plant with an installed capacity of 20.4 MW_e was put in operation in 1984 with 6 production wells (KD-6, KD-7, KD-13, KD-14, KD-15, KD-16). Three additional production wells (KD-20, KD-21, KD-22) were drilled in between 1985-1986, due to the shortage of steam. KD-7 well has been used as observation well since 1991 because of small diameter of production casing.

There are four observation wells in Kızıdere Geothermal Field, namely KD-1A, KD-7, KD-8 and KD-9. Water level is measured daily at KD-1/A and KD-8. Reservoir pressure was measured daily by interference tools at KD-7 and KD-9 wells up to 1998. Since then these wells are not used because of break down of interference tools (Yeltekin and Parlaktuna, 2006). General properties of each well in Kızıdere Geothermal Field are tabulated in Table 1.2.

After Kızıldere geothermal field started electricity production in 1984, the field has faced with some operational problems. These problems are mainly; calcite scaling in production wells, depletion of reservoir pressure and waste water disposal (Yeltekin et.al. 2002).

Table 1.1: Chemical compositions of geothermal waters from Kızıldere, Tekkehamam and surrounding cold waters (Yıldırım and Ölmez, 1999)

	KD-6	KD-13	KD-14	KD-15	KD-16	KD-20	KD-21	KD-22	Wastewater	R-1	TH-2	Tekkehamam	Cold waters	
	W.B.	W.B.	W.B.	W.B.	W.B.	W.B.	W.B.	W.B.		W.B.	W.B.		Kızıldere	Tekkehamam
Sampling date (month/year)	4/96	4/96	4/96	4/96	4/96	4/96	4/96	4/96	4/96	9/98	12/98	10/87	10/87	
Reservoir temperature (°C)	196	195	207	205	211	201	202	202	92	242	171	190	–	–
Sampling temperature (°C)	92.5	92.1	93.6	94.2	96	89.6	92.3	96	63.6	96	96	97.2	16.6	15.3
Conductivity (µS@25 °C)	5830	5940	6160	5890	5835	6180	5940	5830	5500	5820	4800	4000	550	850
pH (@25 °C)	8.97	8.89	8.96	8.82	8.94	8.92	9.02	9.3	9.25	8.8	9.4	7.71	8.25	7.53
TDS (ppm)	4550	4880	6010	4910	5100	4720	4740	4910	4870	6380	4370	2950	390	740
Na	1220	1300	1410	1340	1400	1375	1325	1275	1400	1556	1240	750	11.9	44.8
K	116	138	152	138	148	140	131	140	138	245	120	75	1.5	0.9
Ca	1.2	2.0	1.2	1.2	3.2	1.6	1.8	1.2	1.2	2.67	2.0	12.	65	72
Mg	0.36	0.25	0.2	0.15	0.24	0.15	0.24	0.24	0.6	0.23	1.2	12	1.0	5.2
B	20.4	26.5	24.4	24.6	24	24.1	24.5	25	26	30	3.1	12.1	0.3	0.5
SiO_2	364	364	392	393	398	367	387	392	345	416	77	210	27	52
HCO_3	1586	1525	2403	1464	1525	1159	1220	1586	1342	3074	1335	446	250	450
CO_3	540	600	720	660	730	780	780	600	720	100	738	-	<10	<10
SO_4	560	773	737	730	714	710	710	729	735	792	727	1350	23	108
Cl	124	128	144	140	136	140	140	136	136	134	112	76	7.5	7
F	17.8	20.0	24.8	22.3	23.5	22.5	21	22.5	21.7	26.4	18.5	8.3	1.7	1.8

Water samples from the geothermal wells were taken from the weir boxes installed at the wellhead separators. Concentrations of chemical species in mg/kg (ppm).

1.6.1. Calcite scaling in production wells

Geothermal fluid of Kizildere Geothermal field contains high $CaCO_3$ and 1-1.5 % dissolved CO_2 by weight. The CO_2 partial pressure drop that takes place during the up flow of geothermal fluid causes calcite scaling. The flashing point, where the scaling starts is around 450-500 m. Calcite scale causes a reduction in well bore radius thus a decrease in productivity of the well bore.

Table 1.2 General properties of wells in Kızıldere Geothermal field (MTA, 1996)

Well	Year	Max. Depth (m)	Depth to İğdecik Formation (m)	Bottom-hole Temperature (C°)
KD-1	1968	540	436	203
KD-1A	1968	452	431	198
KD-2	1968	707	651	175
KD-3	1969	370	248	158
KD-4	1969	368	310	166
KD-111	1969	505	299	164
KD-6	1970	851	670	196
KD-7	1970	645	530	204
KD-8	1970	577	-	193
KD-9	1970	1241	1105	170
KD-12	1970	405	393	160
KD-13	1971	760	585	196
KD-14	1970	597	450	208
KD-15	1971	510	440	208
KD-16	1973	667	490	207
KD-17	1975	350	-	157
KD-20	1986	810	490	204
KD-21	1985	898	525	205
KD-22	1985	888	565	204
R-1	1997	2261	1048	242
R-2	1998	1372	750	204

1.6.2. Waste water disposal

Since 1984, that separated water having a boron concentration of 25-30 ppm was discharged to Büyük Menderes River with an average rate of 700 ton/h – 1000 ton/h.

Büyük Menderes River is used to irrigate the fertile lands of Büyük Menderes valley. During the arid months of spring and summer, the discharge of separated water of Kızıldere Geothermal Power Plant to river, causes an increase in boron content of Büyük Menderes River over allowable limits. It has been the practice to shutdown the Kizildere Geothermal power plant during the arid months of spring and summer to cope with the adverse effect of boron in irrigation water.

1.6.3. Depletion of reservoir pressure

Reservoir pressure is continuously monitored using observation wells KD-1A and KD-8. The changes in water levels in those wells for the period 1989-2001 are presented in Figure 1.5. There was a continuous decline in water level as a response of the reservoir to fluid production. The decline is 3.3 m/year in average.

The best solution for fluid disposal and decline in reservoir pressure problems has seemed to be the re-injection of produced fluid. Thus, since these problems were recognized, various re-injection trials were implemented in the field.

A re-injection project was initiated in 1995. The first well (TH-2) for this purpose was drilled in 1996 at Tekkehamam region which is situated approximately 3 km away at south of Kızıldere field. Well TH-2 did not show suitable permeability for reinjection purposes. Then, a second well (R-1) closer to the production region was drilled in 1997.

It was found from well completion and production tests that well R-1 is not suitable for reinjection but a very powerful producer with the highest temperature (242.7 °C) encountered in Kızıldere field. As the third trial to find a suitable injector well R-2 was drilled in 1999 to a depth of 1371.89 m. The completion tests proved that R-2 is a good candidate of being an injector (Yeltekin and Erkan 2002a).

Reinjection trials on well R-2 showed that, well R-2 is suitable for reinjection, holding 20 – 25 % of waste fluid of Kizildere Geothermal Field (Yeltekin and Parlaktuna, 2006). But there is still a need of increasing reinjection rate without avoiding not to experience the adverse affects of reinjection (early breakthrough, cooling, etc.).

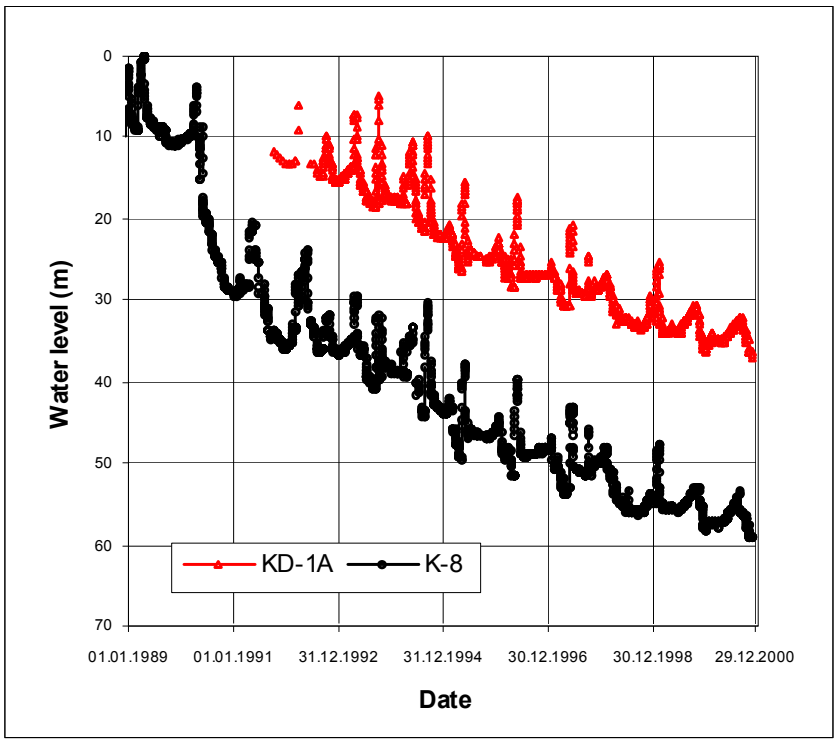

Figure 1.5 Pressure decline in observation wells (1989-2000) (from Yeltekin and Parlaktuna, 2006)

CHAPTER 2

GEOTHERMAL RESERVOIR SIMULATION

2.1. Initiative Works

With the advent of digital computers, the numerical solution of complex non-linear partial differential equations became possible in the late 1960s. However, the application of these techniques to modeling the behavior of geothermal reservoirs lagged behind their application in groundwater, and oil and gas reservoir modeling. This is not surprising, as the coupling between mass and energy transport in a geothermal reservoir adds considerable complexity (O'Sullivan et al., 2001).

The earliest work on the subject began to appear in the early 1970s (e.g. Cheng and Lau, 1973; Mercer and Pinder, 1973). Some further modeling studies were published during that decade, but the effective starting point for the acceptance by the geothermal industry of the usefulness of computer simulation was the 1980 Code Comparison Study (Stanford Geothermal Program, 1980).

Coupled heat and mass transfer in the highly heterogeneous environment of a geothermal reservoir is a very complex physical process. Often phase changes are involved and the flow is complicated by the presence of additional chemical species such as gases or dissolved salts. Fundamental studies have resulted in a steady advance of the range of physical phenomena that it is possible to include in a geothermal reservoir model, and in improvements in the numerical techniques used in the reservoir simulators (O'Sullivan et al., 2001).

The enhanced techniques for modeling geothermal reservoirs have found extensive application in investigations of other complex multiphase, multi-component fluid flows underground, such as nuclear waste storage (e.g. Tsang and Birkholzer, 1999; Wu et al., 1999), mining engineering (e.g. Menzies and Forth, 1995; Lefebvre et al., 1998) and environmental restoration (e.g. Battistelli et al., 1998; Hodges et al., 1998).

The use of computer modeling in the planning and management of the development of geothermal fields has become standard practice during the last 10–15 years (O'Sullivan et al., 2001).

During that time models have been set up for more than 100 geothermal fields worldwide. The reports on many of these modeling studies remain confidential but from the published work, it is possible to obtain a general picture of the nature of recent models (Antunez et al., 1994; Bodvarsson et al., 1991; Sanyal, 2000).

The software and/or the modeling techniques used in most of these studies were developed during the 1980s by a number of pioneering groups, both in the public sector (Lawrence Berkeley National Laboratory, Los Alamos National Laboratory, US Geological Survey, University of Auckland) and in private industry (GeothermEx, S-Cubed (now Maxwell Technologies), Unocal). The computer power available in the 1980s limited the size of the computational meshes used and many of them were based on geometrically simple models. For example often two-dimensional models were used, either vertical slices (Tulinius and Sigurdsson, 1989) or single layer models (Tulinius et al., 1987). In some cases radial symmetry was assumed (Bodvarsson, 1988).

These simple models were limited in the detail of the systems they could represent but often gave good results for the gross behavior of the system and were used to develop the natural state and history matching model calibration techniques that are discussed below. Most of the early three-dimensional models were simplified in some way, usually by omitting low permeability zones entirely (Halfman et al., 1986) or by using a relatively small number of blocks. However, during the 1980s, and particularly towards the end of the decade, a few quite complex three-dimensional models were developed (Pruess et al., 1983; Bodvarsson et al., 1988; Aunzo et al., 1989).

2.2. New Developments and Emerging Trends

2.2.1. Improved Process Description

In early geothermal reservoir simulations the reservoir fluids were idealized as pure water (Stanford Geothermal Program, 1980). Subsequent more realistic representations of geothermal fluids included carbon dioxide, which is usually the most prominent non-condensable gas (O'Sullivan et al., 1985), and dissolved solids typically represented as NaCl (Burnell, 1992; Battistelli et al., 1997). Later developments include interactions between several different dissolved and gaseous chemical species in geothermal flows (Kissling et al., 1996; Battistelli et al., 1997), and porosity and permeability changes from dissolution and precipitation of minerals (Weir and White, 1996; White and Mroczek, 1998).

More sophisticated multi-species chemical models that describe reactions between aqueous, gaseous, and solid species have usually been limited to zero dimensional systems in which no flow and transport effects are taken into account (Moller et al., 1998). A fully-coupled treatment of three-dimensional fluid flow and mass transport with detailed chemical interactions between aqueous fluids, gases, and primary mineral assemblages is very difficult. Such treatment can potentially provide a more realistic description of geothermal reservoir processes during natural evolution as well as during exploitation, and can provide added constraints that can help reduce the inherent uncertainty of geothermal reservoir models.

Ongoing research is exploring different approximations for coupled processes with vastly different intrinsic time scales, and is addressing uncertainties in thermodynamic parameters, reactive surface areas and kinetic rate constants (Cheng and Yeh, 1998; Xu and Pruess, 1998, 2000).

High-resolution and stochastic techniques borrowed from the extensive literature on stochastic hydrology (Gelhar, 1993; Dagan and Neuman, 1997) are being adopted for improved description of reservoir heterogeneity (Glover et al., 1998; Pruess, 1997).

2.2.2. Model Calibration

Major advances have been made in the development of automatic history matching (model calibration) capabilities, using inverse modeling techniques (Finsterle and Pruess, 1995).

These techniques replace the tedium of manual model adjustment by trial-and-error with an automated process that obtains optimal model parameters by computer. In addition to reorganization of the model calibration process, inverse techniques provide quantitative model acceptance criteria, potentially leading to more reliable models with less subjective bias. The increased computational demands of inverse modeling have prompted the development of parallel processing techniques, not only for high-end massively parallel platforms, but also for economical clusters of workstations or PCs (Finsterle and Pruess, 1999).

Geothermal reservoir models have usually been constrained by natural state modeling and well test analyses, and have been calibrated against reservoir engineering type data (flow rates and enthalpies of wells, reservoir pressures and temperatures, tracer concentrations). A relatively new trend is the utilization of geophysical and geochemical observations for model calibration, such as resistivity and microgravity changes, self-potential, micro-seismics, and tracer data (Rose et al., 1999; Simiyu, 1999).

2.2.3. Numerics and Graphics

In addition to the areas highlighted above, improvements continue to be made in numerical algorithms, to be able to solve larger reservoir problems more efficiently (Moridis and Pruess, 1998). Enhanced user features include coupling between reservoir and well bore flow with capabilities for flexible, dynamic scheduling of production and injection wells (Murray and Gunn, 1993; Hadgu et al., 1995). This idea has been extended recently to include the characteristics of surface plants such as separators and turbines (Pritchett, 1995). These developments allow the inclusion in a realistic manner of the performances of wells and surface plants in a field-wide reservoir simulation.

Graphical user interfaces (GUIs) are being developed that integrate simulation and grid generation capabilities, and preparation and visualization of input and output data (Bullivant et al., 1995; Osato et al., 1998). A number of databases have been developed specifically for geothermal applications (Stevens et al., 1995). Soon databases, grid generation facilities, pre- and post-processing facilities may all be linked and managed through a GUI.

2.3. Current State-of-Practice

In this section, the steps of the procedure which is currently applied in geothermal reservoir modeling are explained and the prominent references to the applications of this procedure are given.

2.3.1. Conceptual Models and Data Collection

Before a computer model of a geothermal field can be set up, a conceptual model must be developed. A good understanding of the important aspects of the structure of the system and the most significant (physical and chemical) aspects in it is referred to as its ‘‘conceptual model’’ (O’Sullivan et al., 2001).

Setting up a conceptual model requires the synthesis of a set of multidisciplinary information from geology, geophysics and geochemistry to reservoir engineering and project management. Some of the raw data require expert interpretation before they can be used. For example, the down-hole temperature logs that are used to construct the isotherm plots are often affected by internal well bore flows, or the previous production and injection history of the well (see Grant et al., 1982).

In addition, the data sets tend to be incomplete and often the conceptual models proposed by the various contributing scientists and engineers are inconsistent or incorrect (O'Sullivan et al., 2001). Thus, the ''art'' of computer modeling involves the synthesis of conflicting opinions, interpretation and extrapolation of data to set up a coherent and sensible conceptual model that can be developed into a computer model.

2.3.2. Model Design

2.3.2.1. Structure

Recent models have a complex 3D structure and often consist of as many as 3000–6000 blocks or elements (e.g. Menzies and Pham, 1995; Okita et al., 1995; Butler et al., 2000). Even with these large site-specific models, the smallest block size is still quite large. A typical minimum horizontal dimension is 200 m and a minimum vertical dimension is 100 m. The problem of how best to represent the fractured rock in a geothermal reservoir with large blocks has received a considerable amount of attention. Most modelers have simply used a porous medium approach while a few have used double porosity or MINC (Pruess and Narasimhan, 1985) models (Butler et al., 2000; Nakanishi and Iwai, 2000). Others have included explicit representation of a few dominant fractures and faults (Antics, 1998; Yamaguchi et al., 2000).

The use of large blocks in a geothermal model also makes the task of matching well-by-well performance difficult. Some modelers have overcome this difficulty by introducing embedded sub-grids around each well (Suarez Arriaga et al., 1996).

The most widely used simulators that have been used to implement these complex 3D models are STAR (Pritchett, 1995), TETRAD (Vinsome and Shook, 1993) and TOUGH2 (Pruess et al., 1998). A few other codes have been developed but not widely used. Examples of these are AQUA (Hu, 1995), GEMMA (Parini et al., 1995), SIM.FIGS (Hanano and Seth, 1995) and GEOTHER/HYDROTHERM (Ingebritsen and Sorey, 1985).

A regular rectangular mesh structure is required by TETRAD and STAR, whereas TOUGH2 can handle general unstructured meshes. However, most geothermal models set up using TOUGH2 have some structure, such as layering. The major codes all have the capability of handling multiphase, multi-component flows, and several models have included a reservoir fluid that is a mixture of water and carbon dioxide (Bertani and Cappetti, 1995; Calore et al., 1990) or a mixture of water and NaCl (Burnell, 1992; McGuinness et al., 1995) or both (Kissling et al., 1996; Battistelli et al., 1997).

2.3.2.2. Boundary Conditions

Two important matters to be decided in setting up a model of a geothermal system are its size and the boundary conditions to be applied on the sides of the model. Geothermal systems, apart from low-temperature systems, involve the large-scale convection of heat and mass, driven by the deep input of heat (O'Sullivan et al., 2001). Usually the whole of this convective system is not included in a model, so that aspects of the convective system must be represented by the boundary conditions. In particular, at the base of the model the deep upflow is represented by a suitable source of heat and mass. The only exception to this procedure is the special case of vapor-dominated systems, where it is not possible to set up a stable natural state using flow boundary conditions. Instead, constant pressure and vapor saturation boundary conditions must be applied (O'Sullivan et al., 1990; McGuinness et al., 1993).

Constant pressure and temperature boundary conditions instead of flow boundary conditions have been used for modeling hot water or liquid-dominated, two-phase systems. This procedure works satisfactorily but should be used with care as it may lead to a spurious quasi-steady state in future scenario simulations where the unlimited recharge from a constant pressure boundary matches the specified production rate. At the side or lateral boundaries of the model, a number of strategies have been adopted. In general it is advisable to have the side boundaries of the model sufficiently remote from the production and injection zones so that the choice of boundary conditions does not significantly affect the performance of the model over the simulated lifetime of the project (say 25 years).

Some modelers have implemented no-flow boundary conditions (heat or mass), while others have applied background linear temperatures and hydrostatic pressures or other constant temperature and pressure ‘‘open’’ boundary conditions. The latter boundary condition allows the free flow of cool water into (or out of) the model. An intermediate approach adopted by some is to apply ‘‘recharge’’ boundary conditions that allow mass flow into (or out of) the boundary blocks at a rate proportional to the pressure drop (or increase).

In the opinion of the authors, the model should be self-contained as much as possible, with the model structure determining its behavior and not the lateral boundary conditions. If these conditions have a large influence on the behavior of the model it means that the modeled domain is not large enough and the lateral boundaries of the model should be pushed farther out.

For the top boundary there are examples where the model was truncated well below the ground surface and either a closed top (no flow of heat and/or mass) corresponding to a low-permeability layer/cap-rock, or an open top with a constant pressure and temperature, was implemented. In some cases a condition of no mass flow is implemented but conductive heat loss is allowed. Probably the most common approach is to assume a constant atmospheric pressure and temperature at the top of the model.

In most cases these atmospheric conditions are implemented not at the ground surface but at the estimated position of the water table. Some modelers have used an approximate flat water table at a constant elevation while others have adjusted the thickness of the top blocks of the model to match the variable elevation of the water table (O'Sullivan et al., 1998).

The difficulty with using a top boundary condition of constant atmospheric conditions is that it may allow the unlimited inflow of cold water or the unlimited outflow of warm fluids, depending on whether the pressure in the top block decreases or increases, respectively. In fact the inflow of cold water cannot exceed the natural infiltration rate. In a real geothermal system, if the shallow pressures fall far enough, the water table will be lowered as well as water being drawn in. There is no easy way of representing this lowering of the water table in a standard geothermal model. The shallow temperature regime, moreover, may not be well represented by a single atmospheric temperature at the water table level. Some have added complexity by estimating the variable temperature at the water table and implementing constant pressure and temperature conditions with a different temperature at each block at the top of the model.

The relatively large size of blocks in present computational meshes prevents modeling of the direct flow from depth to small surface features such as hot springs and steaming ground. Several models (e.g. Parini et al., 1995; O'Sullivan et al., 1998) have used artificial wells, located in near surface layers and operating on deliverability to represent surface features.

Recently, some modelers have tried to improve the representation of the shallow zone in a geothermal field by including the unsaturated zone (e.g. O'Sullivan et al., 2001). This was carried out by making the reservoir fluid a mixture of air and water, and then applying atmospheric conditions at the ground surface. The unsaturated zone, between the ground surface and the water table, then appears as blocks with a high mass fraction of air, whereas in the saturated zone the mass fraction of air is very low. This approach is an improvement on the standard method of including only the saturated zone but it is still approximate as the resolution of the movement of the water table is limited by the thickness of the top blocks. To obtain high accuracy either a number of very thin layers would have to be used at the top of the model, or, alternatively, a new technique for tracking the movement of the water table, similar to that used for modeling unconfined flow in a groundwater aquifer, could be developed.

2.3.3. Calibration

A general procedure for model calibration has been developed by (O'Sullivan, 1985; Bodvarsson et al., 1986). It consists of natural state modeling followed, if possible, by history matching. Most modelers have carried out at least the first step of natural state modeling, which consists of running the model for a long time in a simulation of the development of the geothermal field over geological time. The temperature distribution and surface outflows of heat and fluid (water and steam) in the model are compared with measured field data and the permeability structure of the model is adjusted to achieve a satisfactory match. The magnitude and location of the deep hot upflow may also need to be adjusted. The calibration of the natural state may require many iterations before a good match to the field data is achieved.

A second history matching stage of calibration has been carried out for most systems that have some production history. It is aimed at matching the measured behavior of the geothermal field, in response to production, with the simulated behavior. In this process the past production for the wells is assigned to the relevant blocks in the model (based on information about the locations of the feed-zones) and a simulation of the total production period is carried out. The pressures and temperatures in the model at the start of production are taken from the natural state model. The model results for pressure declines are then compared to field data and adjustments made to permeabilities and porosities if necessary.

In some cases production enthalpies from the model can be compared with field data. This process is particularly useful for calibrating the porosity in reservoirs whose wells discharge at two-phase enthalpies (e.g. O'Sullivan et al., 1998; Nakanishi and Iwai, 2000; Sanyal et al., 2000b) and for calibrating permeabilities in reservoirs where production temperatures are affected by re-injection returns (e.g. Tokita et al., 1995; Parini et al., 1996).

For hot water systems where the injection zone is well separated from the production zone the production enthalpies change slowly; therefore, for reservoirs with only a few years of production history, enthalpies may not be useful for calibration. Similarly, in vapor-dominated systems production enthalpies remain almost constant and pressures change slowly, so calibration by history matching is not possible if only a short production history is available (e.g. O'Sullivan et al., 1990).

In a few cases the history matching process can be carried out by using wells on deliverability in the model and matching the simulated production rate decline to the measured data (e.g. Bodvarsson et al., 1993). This technique is only applicable if the wells in the field have been operated in a stable manner because it assumes that the deliverability state of the wells does not change.

Recently, some modelers have used tracer test results (e.g. Parini et al., 1996) or chemical changes to assist calibration (e.g. Burnell, 1992; Kissling et al., 1996). The tracer test calibrations are particularly useful for calibrating models of highly fractured reservoirs such as Dixie Valley (Rose et al., 1997) where the rapid return of re-injected water is an important phenomenon. A few modelers have used geophysical data such as gravity measurements (Ishido et al., 1995; Osato et al., 1998) or electro-potentials (Ishido and Tosha, 1998) to assist with model calibration.

The process of model calibration both for natural state matching and past history matching is difficult and time consuming. It is sometimes difficult to decide which part of the model structure should be adjusted to improve the match to a particular field measurement. Some use of computerized model calibration (for example: TOUGH2, Finsterle and Pruess, 1995) has been made in improving a few geothermal models (O'Sullivan et al., 1998; White et al., 1998). In this case the computer is used to systematically adjust a few parameters until the differences between model results and field data are at a minimum. It is demanding in terms of computer time and requires some manual intervention to select the particular parameters to be adjusted.

CHAPTER 3

NUMERICAL SIMULATION OF THE STUDY AREA

In this study, it is aimed to simulate the past and present behavior of Kızıldere Geothermal Field by using the data of existing production wells in order to forecast the possible responses of the geothermal field under different scenarios.

A numerical simulator, SUTRA-VERSION 1284-2D has been utilized throughout the study. SUTRA (Saturated-Unsaturated TRAnsport) is a finite element program written in the FORTRAN environment and used for saturated and/or unsaturated groundwater flow and thermal energy or solute transport (single species reactive) simulation models. The SUTRA code and documentation were prepared under a joint research project of the U.S. Geological Survey, Department of the Interior, Reston, Virginia, and the Engineering and Services Laboratory, U.S. Air Force Engineering and Services Center, Tyndall A.F.B., Florida.

The program uses a hybrid galerkin-finite-element method and integrated-finite-difference method with two-dimensional quadrilateral finite elements and finite-difference time discretization to solve for two-dimensional areal or cross-sectional simulation either in cartesian or radial/cylindrical coordinates. The basic function of the simulation code is to calculate the areal distribution of pressure, concentration or temperature and fluid velocity at the determined points which correspond to the nodes in the grid model. It has the non-linear iterative, sequential or steady-state solution modes. Complete explanation of function and use of this code is given in (Voss, 1984).

3.1. Construction of the Conceptual Model and Data Evaluation

There are two hydrogeological model in the literature describing the Kızıldere Geothermal Field [(Dominco, 1974) (Figure 3.1), Serpen and Satman, 2000) (Figure 3.2)]. Both models consider infiltration of meteoric water into deeper sections of the Earth (about 3000 m depth) and upflow of it after heating. The other feature of the field extracted from the model by Dominco (1974) (Figure 3.1) is the two faults (Main Feeding Fault Zone and Southern Fault Zone) dividing the Kızıldere Region into three blocks, Upper Block, Middle Block and Lower Block (Yeltekin, 2001). These two features of the field described below have been utilized while developing the conceptual model.

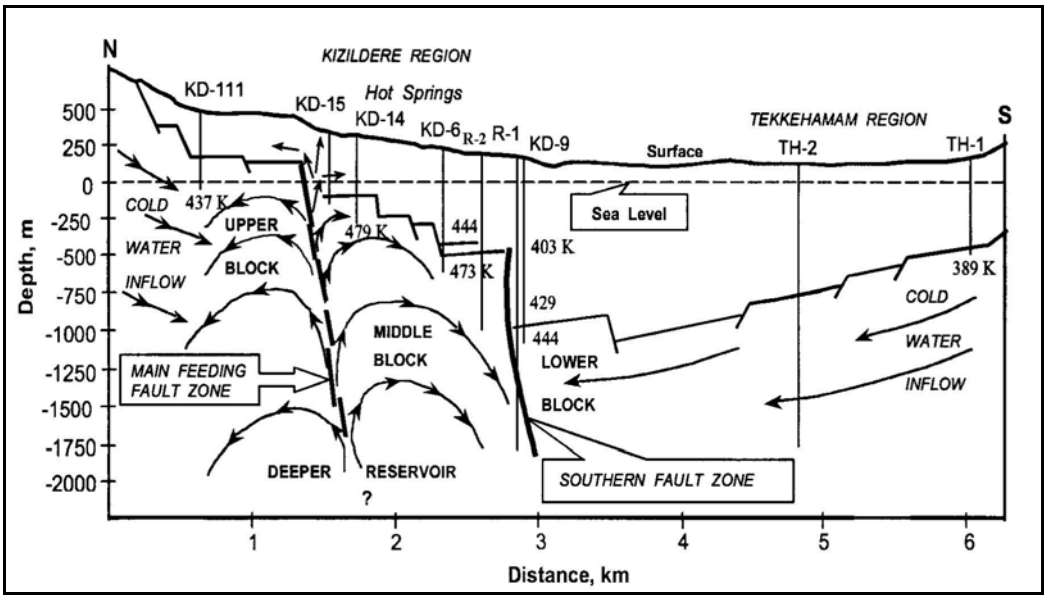

Figure 3.1 Kızıldere Geothermal Field: Sketch of Probable Hydrothermal Conditions (Revised after Dominco, 1974).

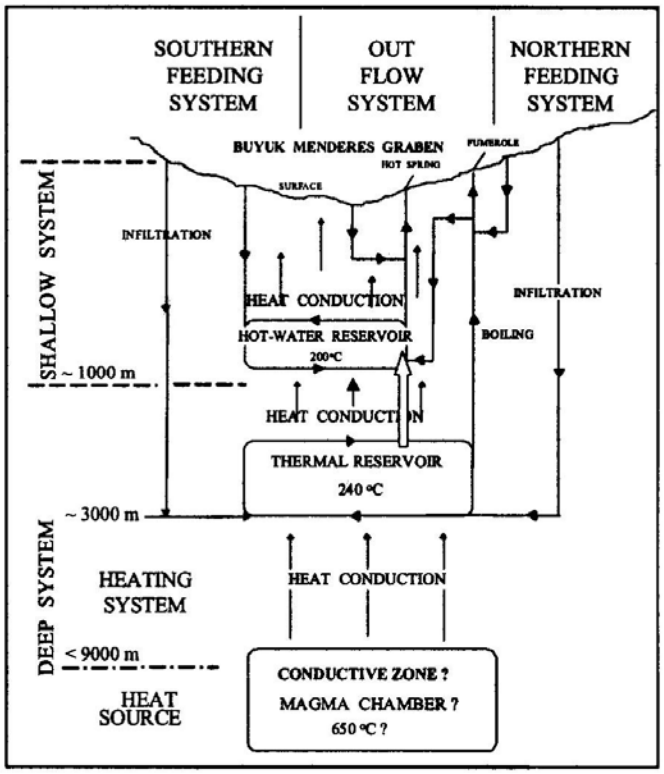

Figure 3.2 A model for Kızıldere Geothermal system (Serpen and Satman, 2000)

Basically, the assumptions made before forming the grid model have been;

1. Modeling area is considered as a porous medium with varying permeability within the boundaries.
2. Only saturated flow and steady-state transport are assumed to be effective within the domain.
3. Because that the model is two dimensional the thickness of producing zone is fixed to a level at the vertical extent of reservoir which is equal to the depth of İğdecik Formation.
4. As two deep wells R-1 and R-2 have very high pressure values, their pressures are normalized by subtracting the hydrostatic pressures below the depth of İğdecik Formation. Thus, they have been considered as shallow wells with high production capacities.
5. The fault zones found in the region possess lower permeabilities compared to the rest of the area.
6. The areal extent of the model shown in Figure 3.3 is assumed to be chosen adequately remote from the production and injection zones.

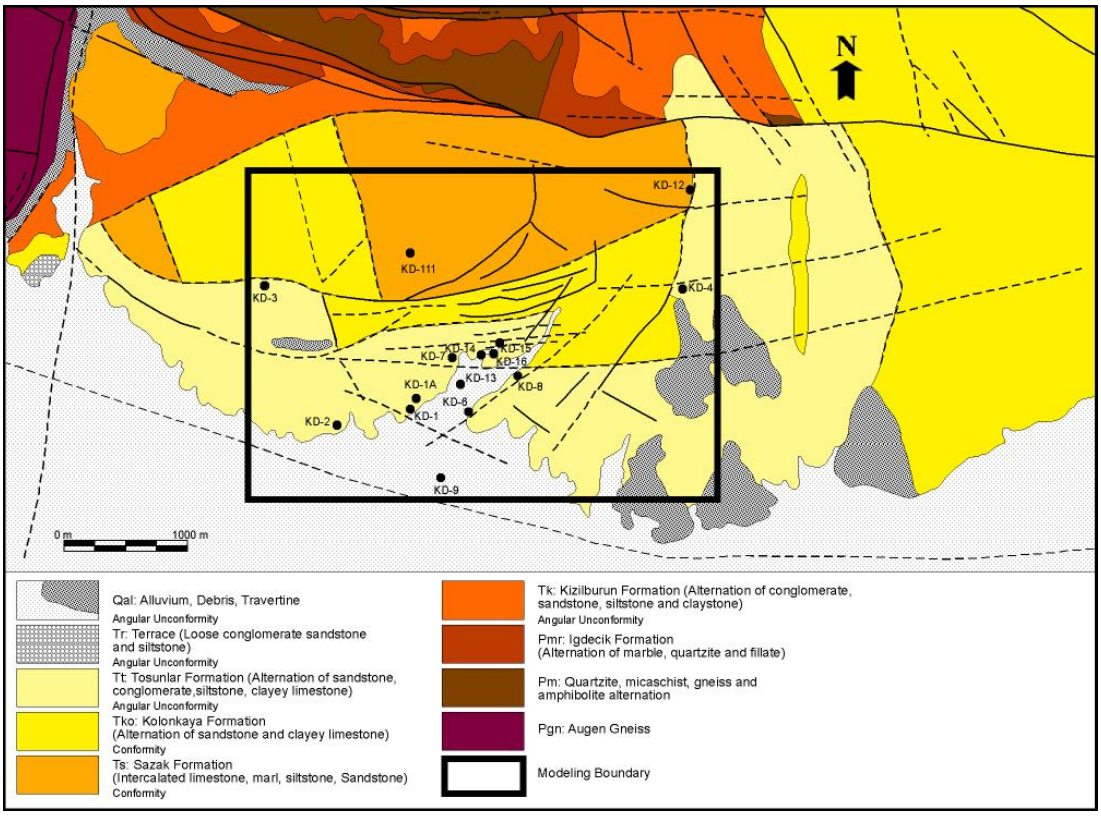

Figure 3.3 Geological Map of Kızıldere Geothermal Field showing the modeling area (Revised after Şimşek, 1985)

3.2. Finite Element Discretization

3.2.1. Generation of the Mesh

The areal extent of the model covers all of the production wells: KD-6, KD-13, KD-14, KD-15, KD-16, KD-20, KD-21, KD-22, R-1; the monitoring wells: KD-1, KD-1A, KD-2, KD-3, KD-4, KD-111, KD-7, KD-8, KD-9, KD-12; and the re-injection well: R-2. Knowing that the two wells, KD-1 and KD-1A are very similar in their geological aspects and found in the same location, they are considered and shown as one well: KD-1. Also the wells are shifted from their original positions in order to prevent the formation of very thin elements and to bring the well locations to the nodes of the elements.

With these considerations, reservoir grid model given in Figure 3.4 was created. It is a rectangular mesh with quadrilateral (rectangular) elements having numbers as 29×24 in x and y directions, respectively. The grid lengths in x and y direction are approximately 30 m. The vertical thickness of the model is assumed to be the drilled thickness of İğdecik formation of the production wells.

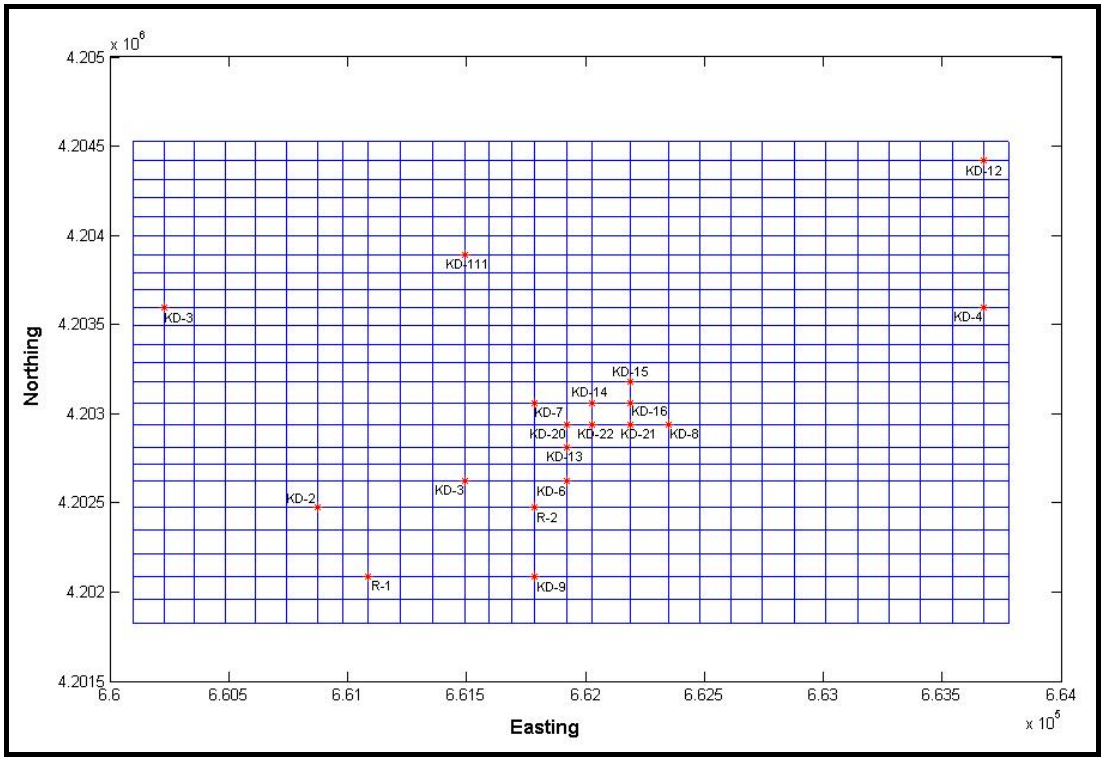

Figure 3.4 Areal view of reservoir model grid diagram.

3.2.2. Boundary Conditions

As it is stated in Chapter 2, it is suitable to have the side boundaries of the model sufficiently remote from the production and injection zones so that the choice of boundary conditions does not significantly affect the performance of the model over the simulated lifetime of the project (O'Sullivan et al., 2001). The lateral boundaries of the model is selected quite far away from the production wells in accordance with this statement, and also covering all the wells belonging to the geothermal area.

Applying the simplest assumption, constant temperature and constant pressure values were specified at the boundaries.

These hypothetic initial values have been selected according to the some calculated values at the wells nearest to the boundaries. These values have been changed, during the calibration process, to catch the measured values at the production wells which are found at the known nodes in the grid model. This procedure has been used until the average error has been decreased to an optimum value.

3.3. Calibration

The general procedure for model calibration consists of natural state modeling followed by history matching.

Before beginning these processes, the appropriate reservoir parameters taken from literature are supposed to be entered in the program. Values tabulated in Table 3.1 are given for the initiation of the program.

Table 3.1 Initial reservoir parameters used in the simulation program

Parameter	Value	Unit
Fluid Compressibility	4.47×10^{-10}	$(kg/(m.s^2))^{-1}$
Fluid Specific Heat	4182	(Joule/(kg.°C))
Fluid Thermal Conductivity	0.001	(Joule/(m.°C.s))
Fluid Base Density	1000	(kg/m^3)
Fluid Viscosity	1	(kg/(m.s))
Solid Matrix Compressibility	1.00×10^{-10}	$(kg/(m.s^2))^{-1}$
Solid Grain Specific Heat	840	(Joule/(kg.°C)
Solid Grain Diffusivity	3.5	(Joule/(m.°C.s))
Density of a Solid Grain	2650	(kg/m^3)

3.3.1. Natural State Modeling

At this stage, it is aimed to approach the measured pressure and temperature values belonging to the beginning of the modeling period taken from literature (Yeltekin, 2001).
After the boundary conditions and reservoir parameters are optimized permeability values which are specified at each element have been modified.
This option is basically used to determine the fault zones passing through the geothermal field and affecting the groundwater flow between the production wells (Figure 3.5). That is mostly based on the idea that the faults act as discontinuous flow boundaries showing very low permeability values compared to the neighboring zones. This assumption has been applied to the model with giving low permeability values to the elements in which the faults pass.

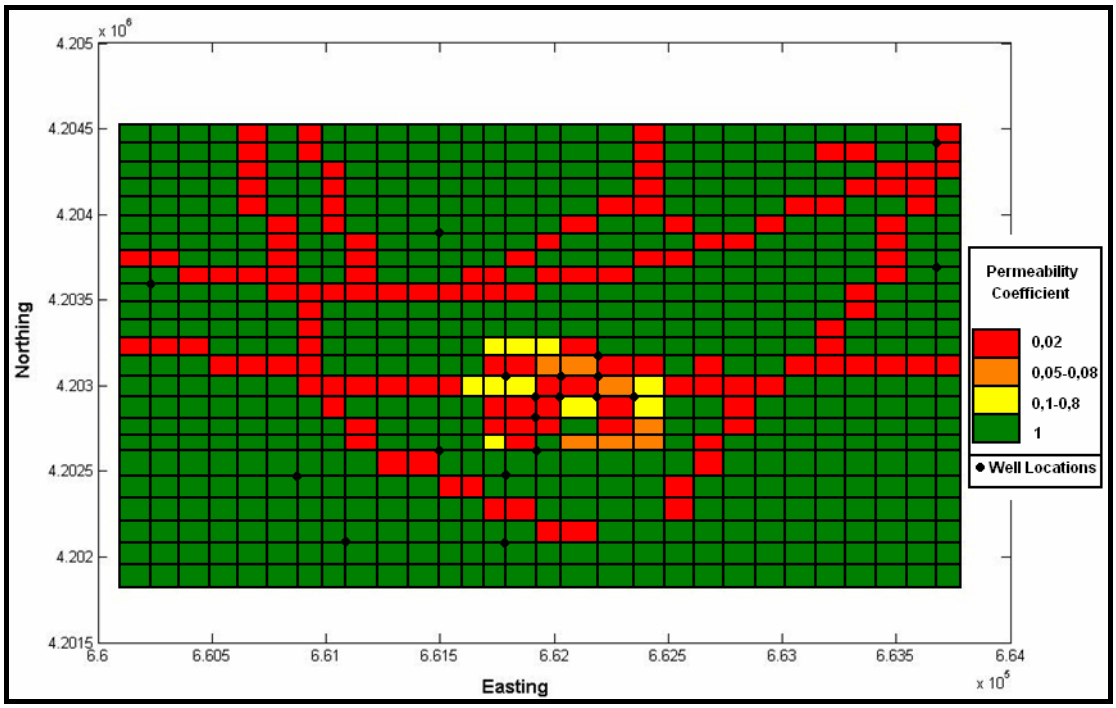

Figure 3.5 Distribution of the permeability coefficient over the modeling area

The area between the control points (the production wells) has been identified in a more detailed manner on the grid model. Basic considerations having made here are not only the existence of three blocks between the production wells (Dominco, 1974) in terms of groundwater flow but also maintaining the best fit for the pressure responses.

After the calibration process by using trial & error method, the error between observed and calculated values in pressure and temperature are optimized.

For this purpose, an average error is calculated by using the pressure and temperature data of all production wells at the beginning of modeling period. This error is found by taking the squares of errors in pressure or temperature and taking the square root of the summation of these values.

Reduction behavior of the average error in pressure could be seen in Figure 3.6 and in temperature in Figure 3.8. From this graph it is suggested that the error for the calculated pressure values within the domain is acceptable and the natural state modeling has been completed. The calibration results for pressure and temperature at the production wells are tabulated in Table 3.2 and Table 3.3, respectively.

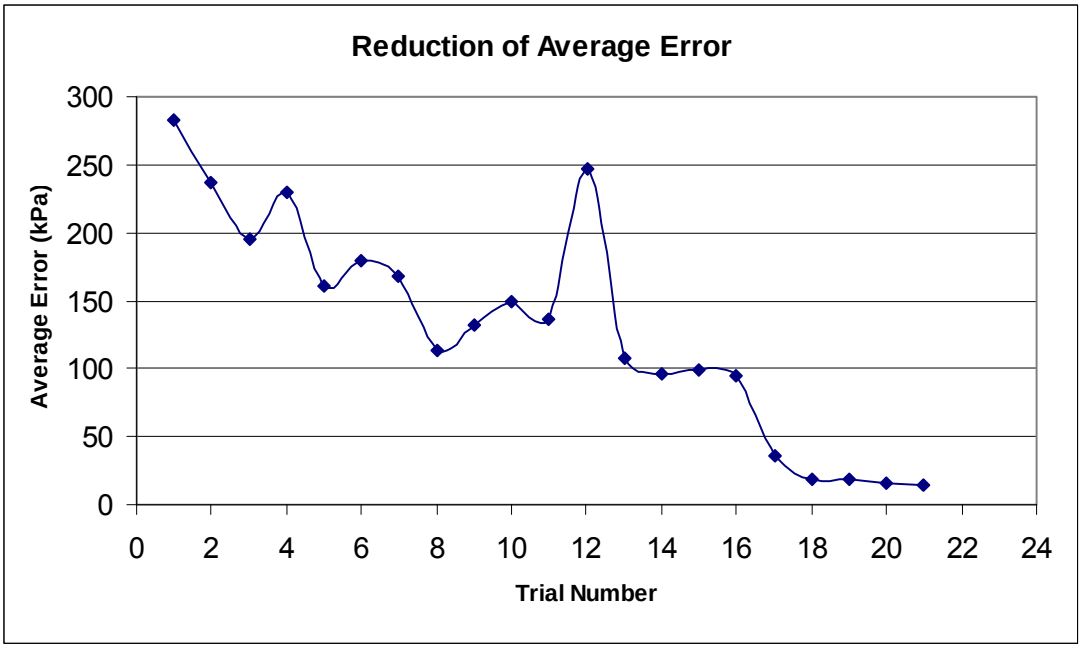

Figure 3.6 Reduction of average error in pressure values calculated in the production wells

In Figures 3.7 and 3.9, respectively, the pressure and temperature distributions in the modeling domain are tabulated. These contour maps show the natural state of pressure and temperature parameters within the modeling area calculated in the simulation code. These maps are constructed by using the calibrated values of the nodes in the model grid diagram at the end of natural state modeling process.

Table 3.2 Calibrated pressure values at the production wells

Well	Node No.	Observed Pressure (kPa)	Computed Pressure (kPa)	Error (kPa)	Error %	Dev^2_2 (kPa)
KD-6	382	8500	8473.7	26	0.3	692.2
KD-13	384	7500	7492.1	8	0.1	62.4
KD-14	411	5500	5443.9	56	1.0	3148.5
KD-15	437	5000	5049.1	-49	-1.0	2413.3
KD-16	436	6200	6245.9	-46	-0.7	2104.7
KD-20	385	7200	7188.9	11	0.2	123.0
KD-21	435	7400	7458.6	-59	-0.8	3434.5
KD-22	410	8100	8064.4	36	0.4	1268.1
					Total Error (kPa)	**115.1**
					Average (kPa)	**14.4**

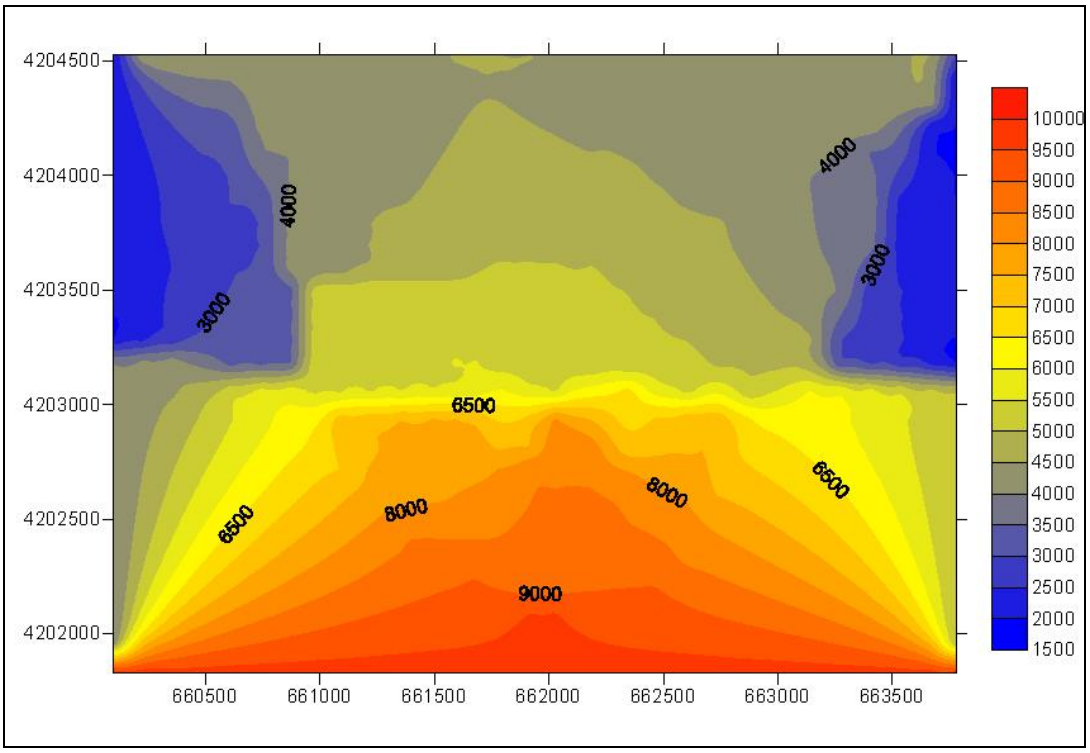

Figure 3.7 Natural state pressure distribution of the modeling area

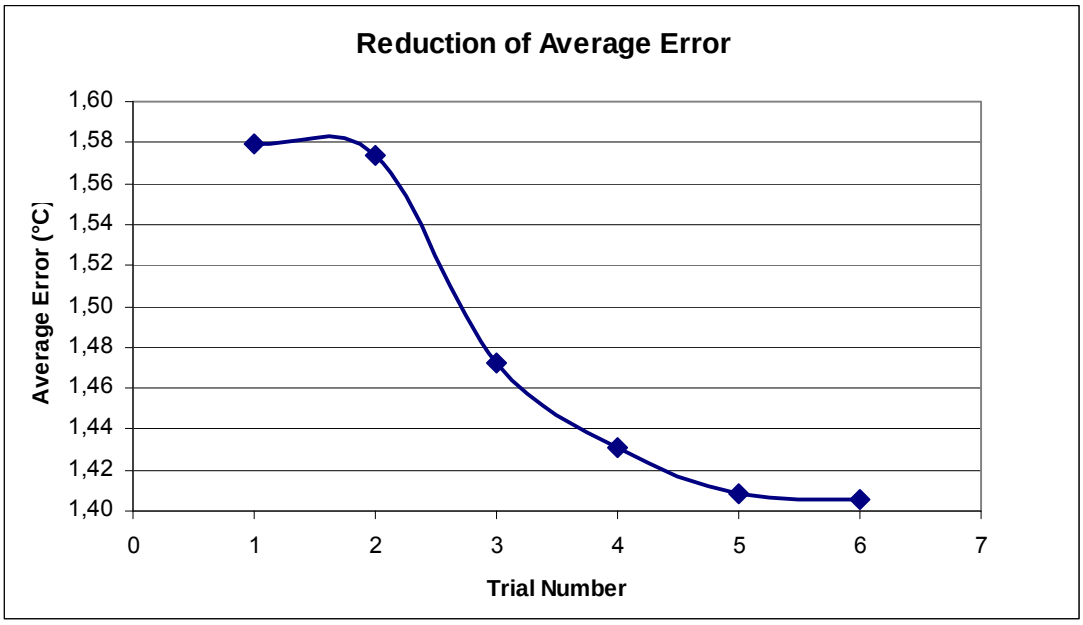

Figure 3.8 Reduction of average error in temperature values calculated in the production wells

Table 3.3 Calibrated temperature values at the production wells

Well	Node No.	Observed Temperature (°C)	Computed Temperature (°C)	Error (°C)	Error %	Dev^2 $(°C)^2$
KD-6	382	197,5	201,09	-3,59	-1,82	12,91
KD-13	384	196,5	202,37	-5,87	-2,99	34,49
KD-14	411	207,9	203,93	3,97	1,91	15,75
KD-15	437	205,7	204,71	0,99	0,48	0,98
KD-16	436	209,1	203,99	5,11	2,44	26,12
KD-20	385	204,4	203,20	1,20	0,59	1,45
KD-21	435	208,9	203,26	5,64	2,70	31,83
KD-22	410	201,4	203,20	-1,85	-0,92	3,42
					Total Error (°C)	**11,27**
					Average (°C)	**1,41**

3.3.2. History Matching

The basic purpose of a history match or transient calibration is to calculate reservoir performance using the best data available. The results are compared with the field recorded histories of the wells. If agreement is satisfactory, the simulator is then used to predict performance for alternate plans (scenarios) of operating the reservoir.
As it is mentioned in Chapter 1, there has been a decrease since 1984 in reservoir pressure of the field due to the production from KD wells. This reduction has ended up with cutting of the production efficiency of these wells within a short period of time. The disposal of the operational waste water to the Büyük Menderes River is also another serious deficiency of the field.
For solving these problems, a re-injection project has been put into practice and two deep wells R-1 (producer) and R-2 (injector) started operation after year 2000. Since these wells started operation, there appear steady and even increasing trends in pressures of KD wells (Yeltekin and Parlaktuna, 2006). Effects of these wells to the system are discussed at the end of the chapter in section 3.5.

In the model, pressure response of the Kızıldere Geothermal Field to fluid production from 1984 to the end of 2005 has been used for history matching. The pressure data used in the study have been taken from literature (Yeltekin, 2001) and from the test reports of the field made by MTA. Production data is taken from measurements of MTA test group at Kızıldere field. The change in the well-bore pressures (measured and calculated) in the history-matching period are given in between Figure 3.10- Figure 3.18. Also the calibrated pressure values in the production wells at the end of this process are given in Table 3.4.

From these illustrations it could be suggested that an appropriate profile is achieved.

As similar to the natural state modeling, the contour map showing the pressure distribution within the modeling area is demonstrated in Figure 3.19. In this figure, it could be identified that, there is a decrease in the region where the production well R-1 is situated and an increase in the region where the reinjection well R-2 is found.

3.4. Limited Convenience of the Model for Temperature Simulation

At this study, it has been considered that, both pressure responses and temperature declines of the reservoir would be modeled separately throughout all the modeling period in order to have a better approach to the reality.

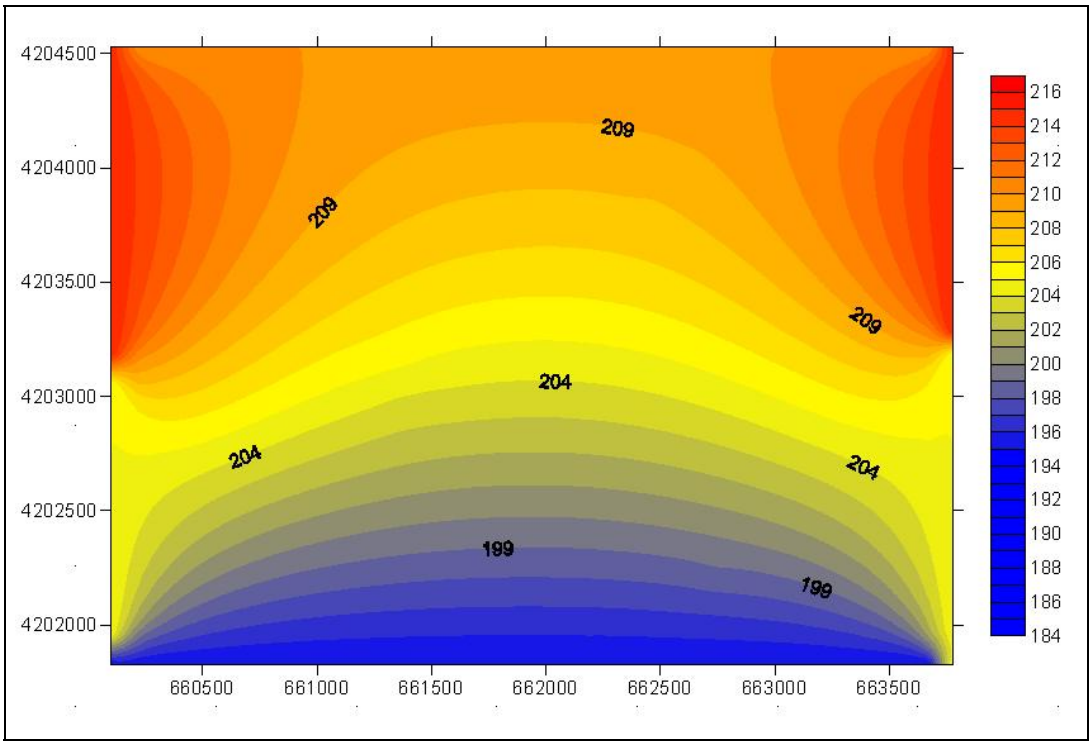

Figure 3.9 Natural state temperature distribution of the modeling area

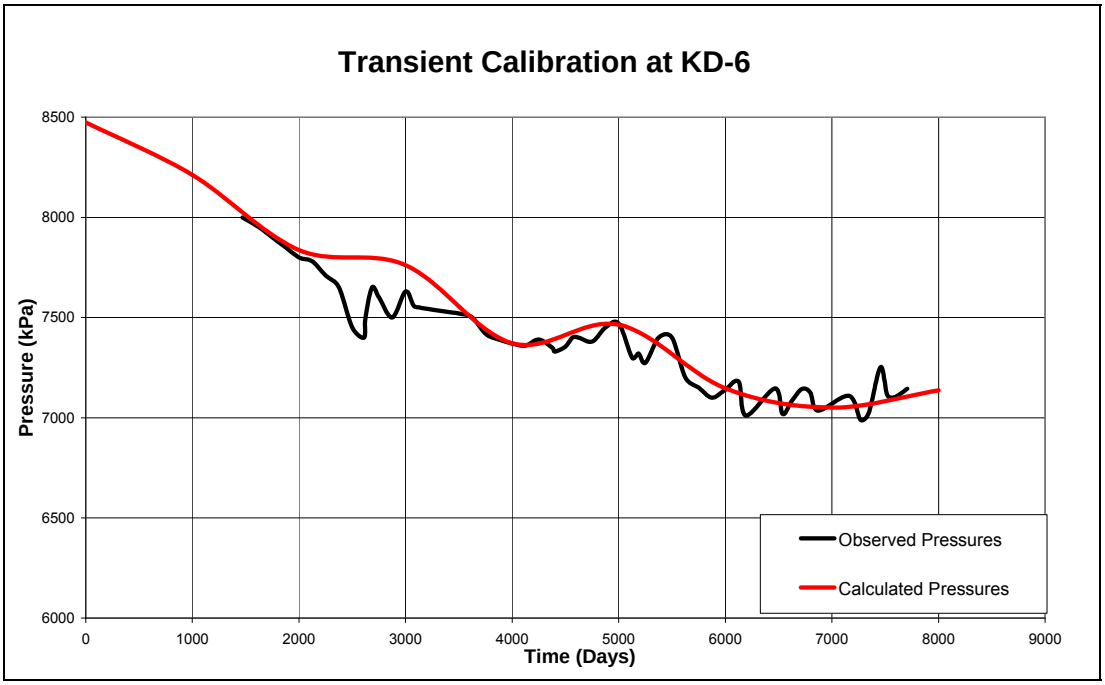

Figure 3.10 Observed and calculated pressure profiles of KD-6

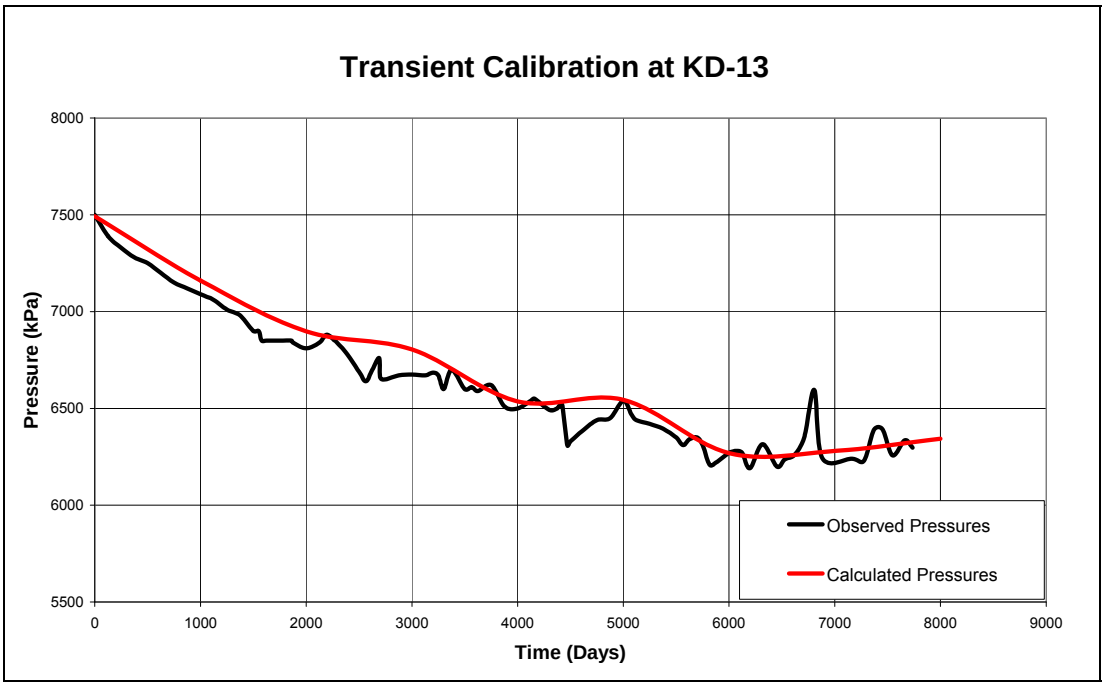

Figure 3.11 Observed and calculated pressure profiles of KD-13

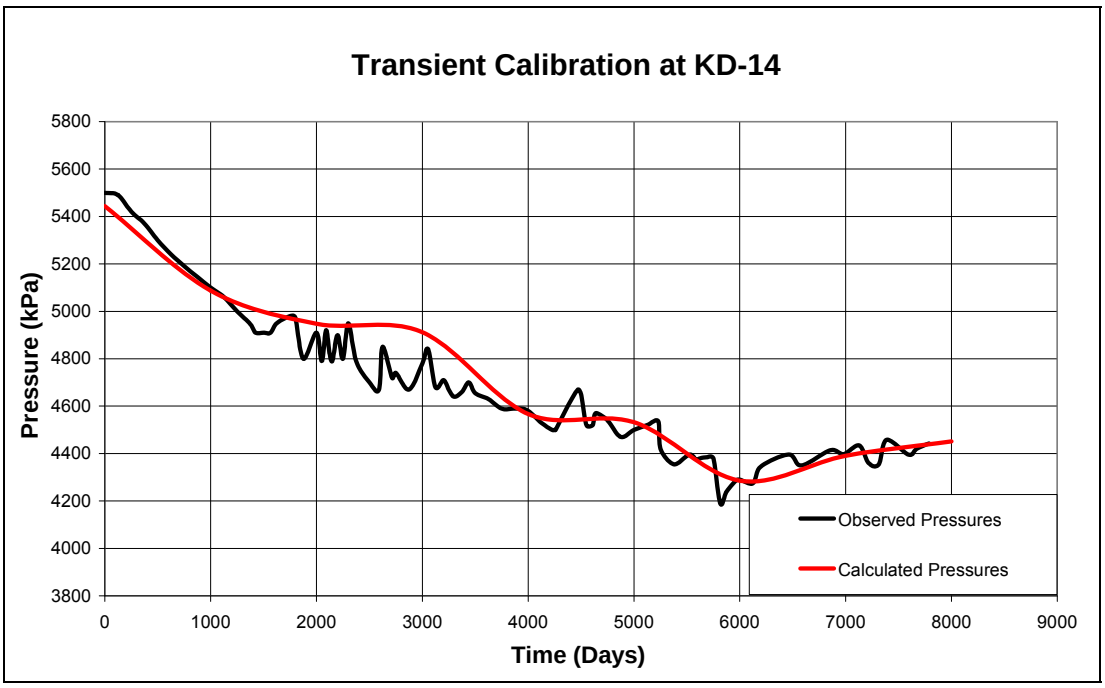

Figure 3.12 Observed and calculated pressure profiles of KD-14

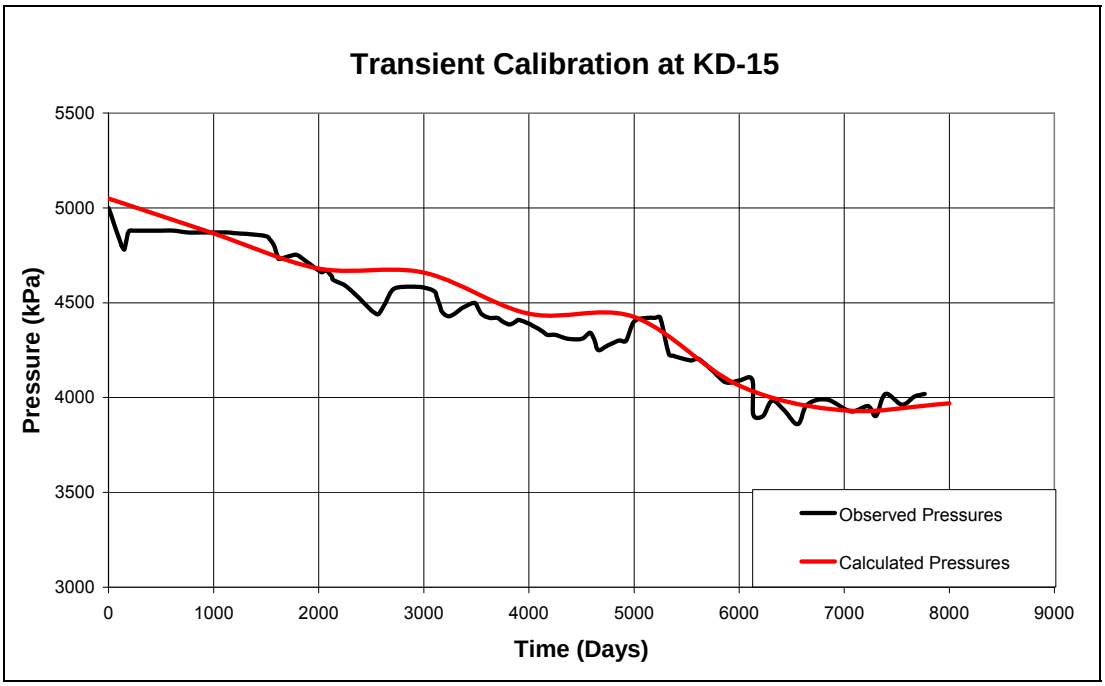

Figure 3.13 Observed and calculated pressure profiles of KD-15

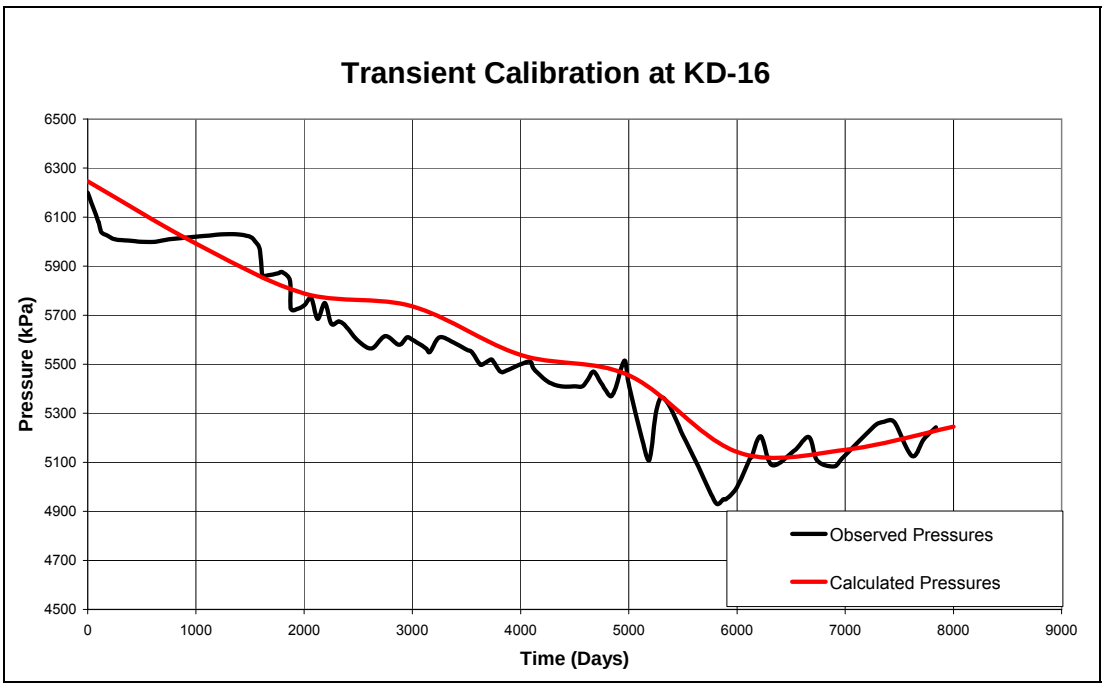

Figure 3.14 Observed and calculated pressure profiles of KD-16

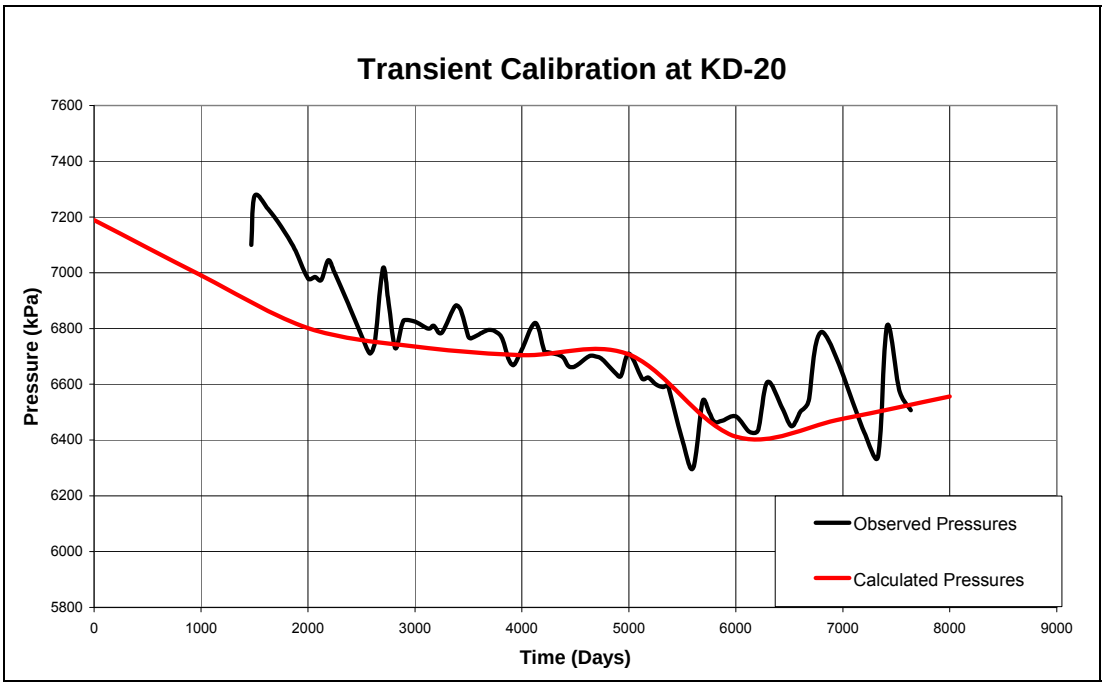

Figure 3.15 Observed and calculated pressure profiles of KD-20

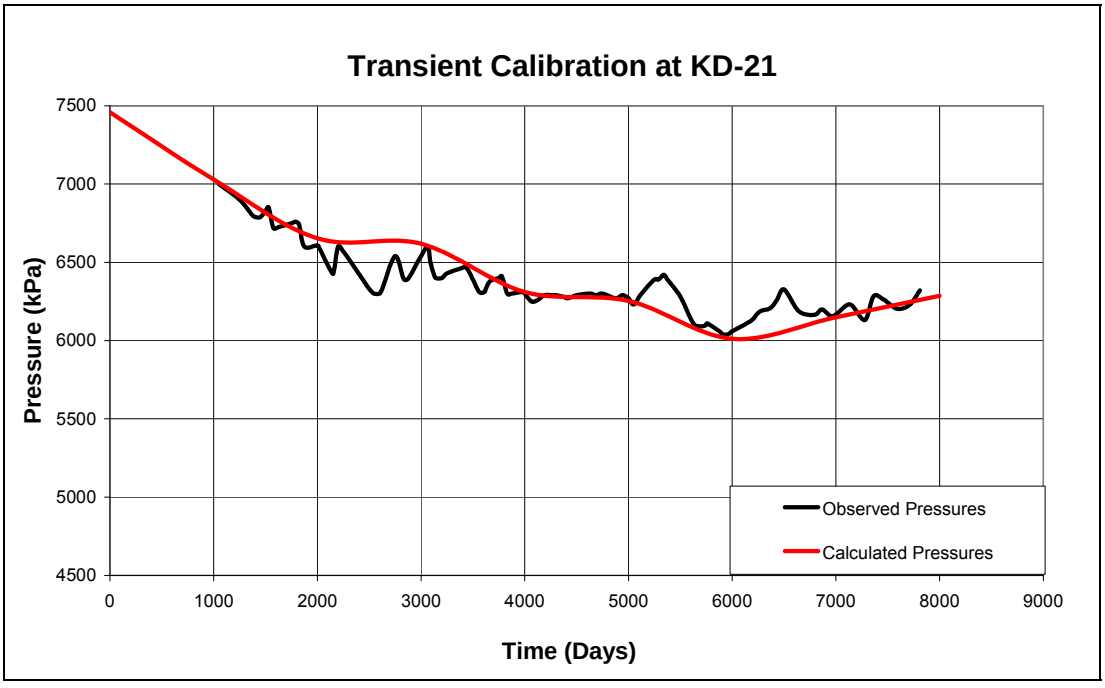

Figure 3.16 Observed and calculated pressure profiles of KD-21

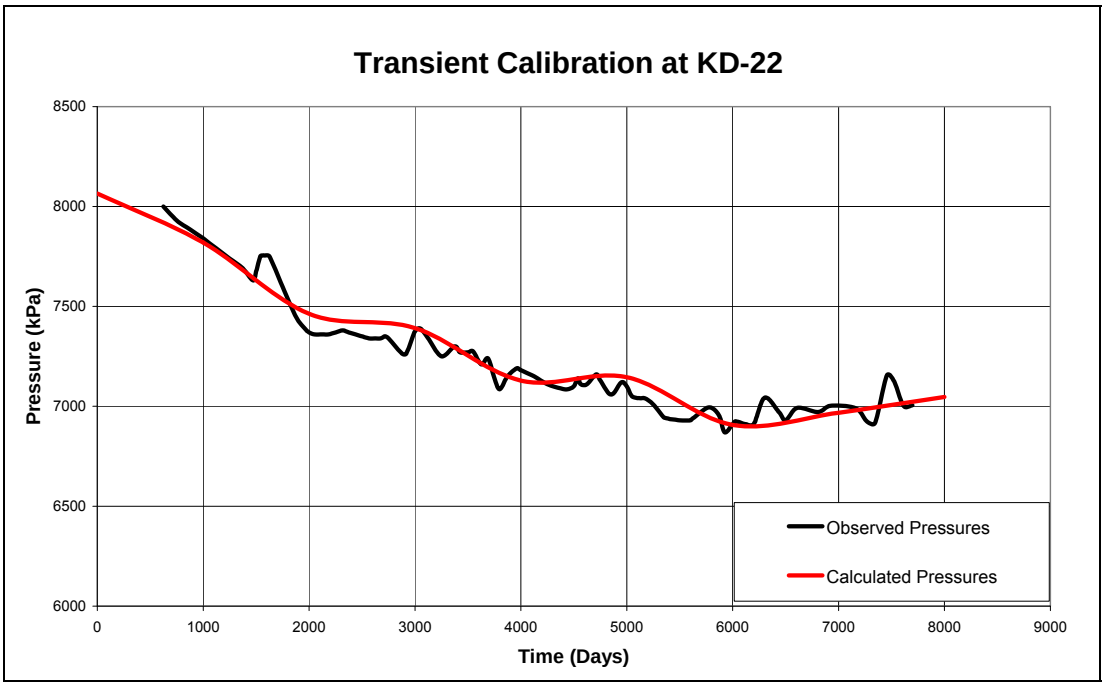

Figure 3.17 Observed and calculated pressure profiles of KD-22

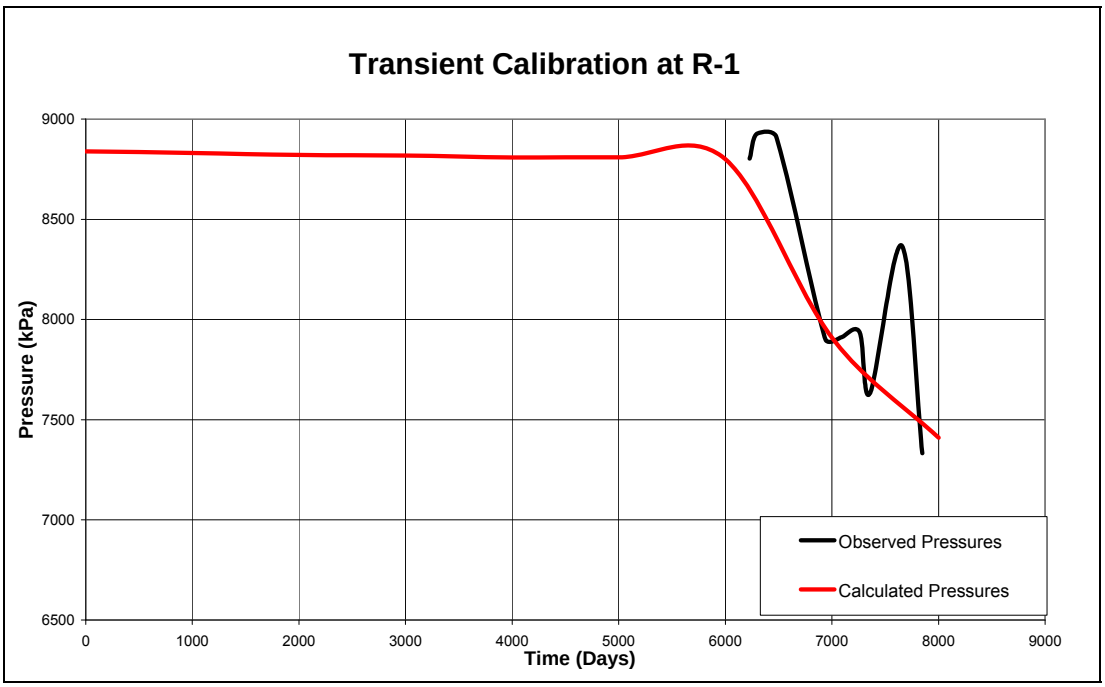

Figure 3.18 Observed and calculated pressure profiles of R-1

Well	Node No.	Observed Pressure (kPa)	Computed Pressure (kPa)	Error (kPa)	Error %	Dev^2 (kPa)
R-1	203	7400	7410,2	-10	-0,1	**104**
KD-6	382	7120	7137,0	-17	-0,2	**288**
KD-13	384	6345	6343,6	1	0,0	**2**
KD-20	385	6565	6556,8	8	0,1	**66**
KD-22	410	7060	7046,7	13	0,2	**177**
KD-14	411	4450	4451,4	-1	0,0	**2**
KD-21	435	6270	6286,3	-16	-0,3	**265**
KD-16	436	5235	5245,3	-10	-0,2	**107**
KD-15	437	3980	3969,1	11	0,3	**120**
					Total Error	**32**
					Average	**4**

Table 3.4 Transient Calibration Results (between 1.1.1984 and 31.11.2005)

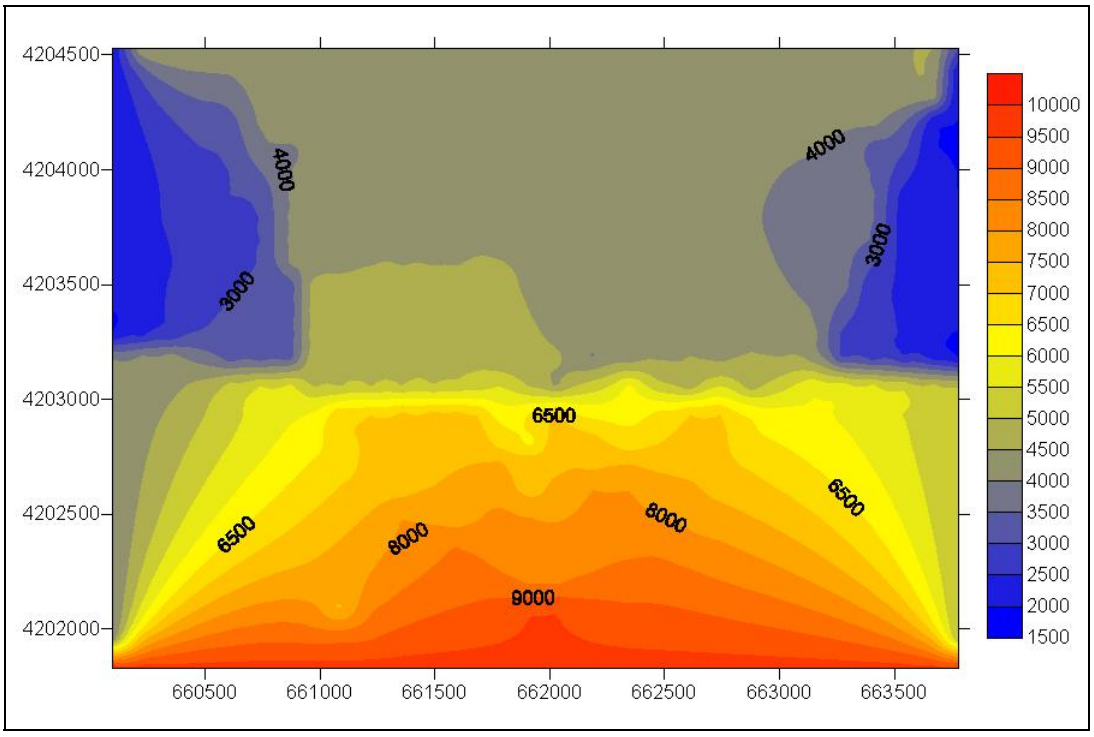

Figure 3.19 Pressures at the end of transient calibration

In temperature simulation, although a good match is satisfied in natural state modeling (Table 3.3), calibration couldn't be continued at the transient calibration part. That is basically because of the fact that, there aren't enough parameters in the simulation code giving the ability to change heat conduction parameters in the domain. That means, it is not possible to change parameters related with temperature one by one for each element but just for the whole elements. This property of model caused deficiently simulation of the field in terms of temperature variation in time.

Nevertheless, as much as the model allowed a calibration has been carried out in history matching period. Especially the results belonging to dates between years 2001-2005 are quite persuasive on the adequacy of the model for simulating the temperature decline in the well-bores.

In Figure 3.20, the temperature distribution in the modeling area before the deep wells R-1 and R-2 starts operation is illustrated. A regular distribution which resembles the contour map of steady state temperatures in Figure 3.9 is obtained at this period.

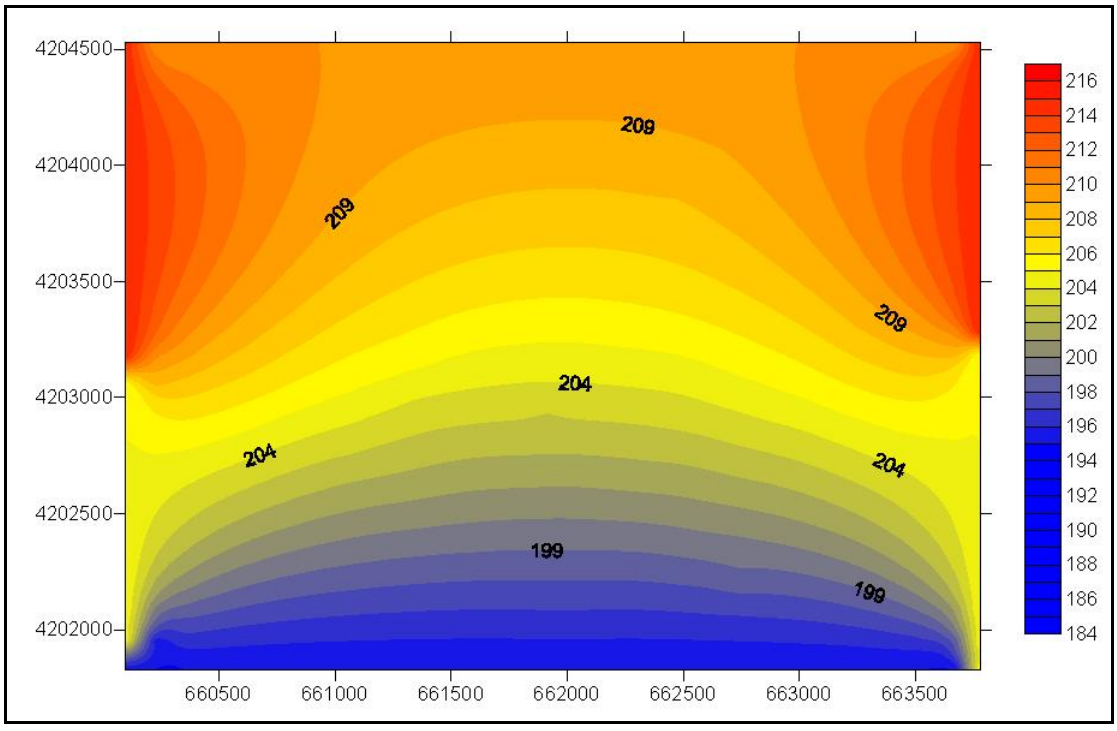

Figure 3.20 Temperatures distribution in the modeling area before R-1 and R-2 start operation

But, after beginning production from the well R-1 and reinjection from the well R-2 in the model, the shape of contour map is highly distorted (Figure 3.21). In this figure, a decrease in temperature right at the node where R-2 is found and in its vicinity could be recognized. This result is in agreement with the possible change at this zone occurs on account of the reinjection process.

Also the size of this change is satisfactory when compared with the data gained from literature (Figure 3.22). It is reported in (Yeltekin and Parlaktuna, 2006) that, although there was no significant change in the measured temperatures of KD-6 at 700 m during short term reinjection, full scale reinjection resulted with 3.4 °C decrease in temperature. This decrease is calculated as 2.03 °C at the end of transient calibration period which shows the end of year 2005.

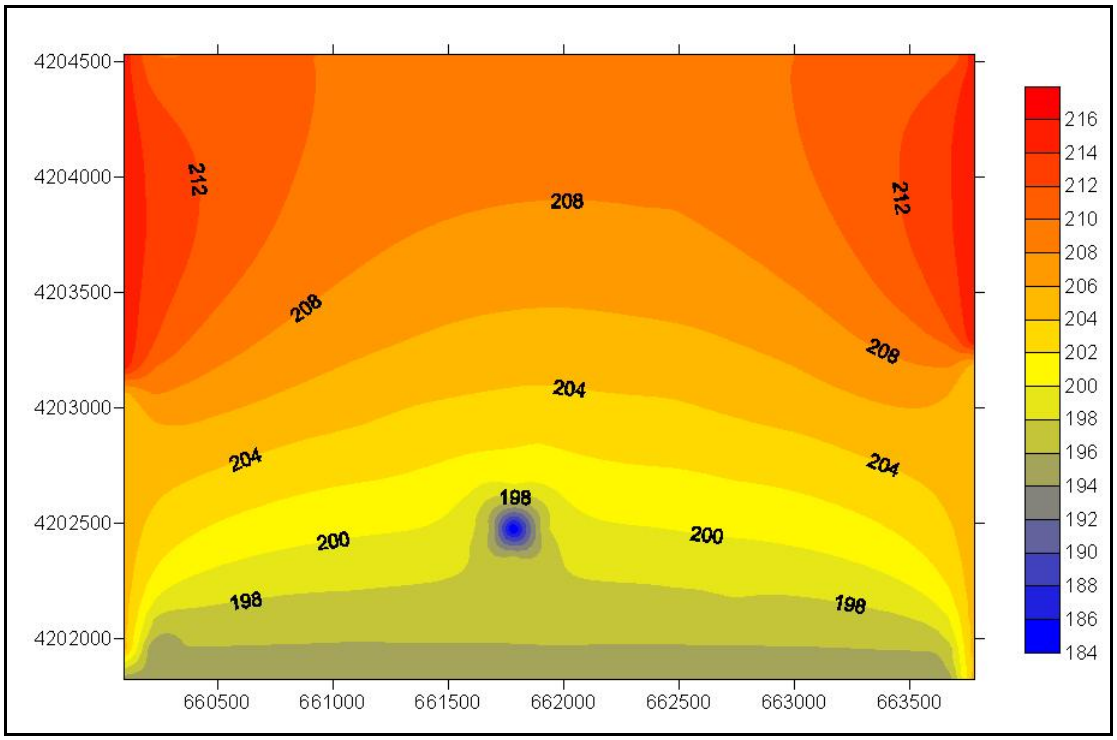

Figure 3.21 Temperatures distribution in the modeling area after R-1 and R-2 start operation

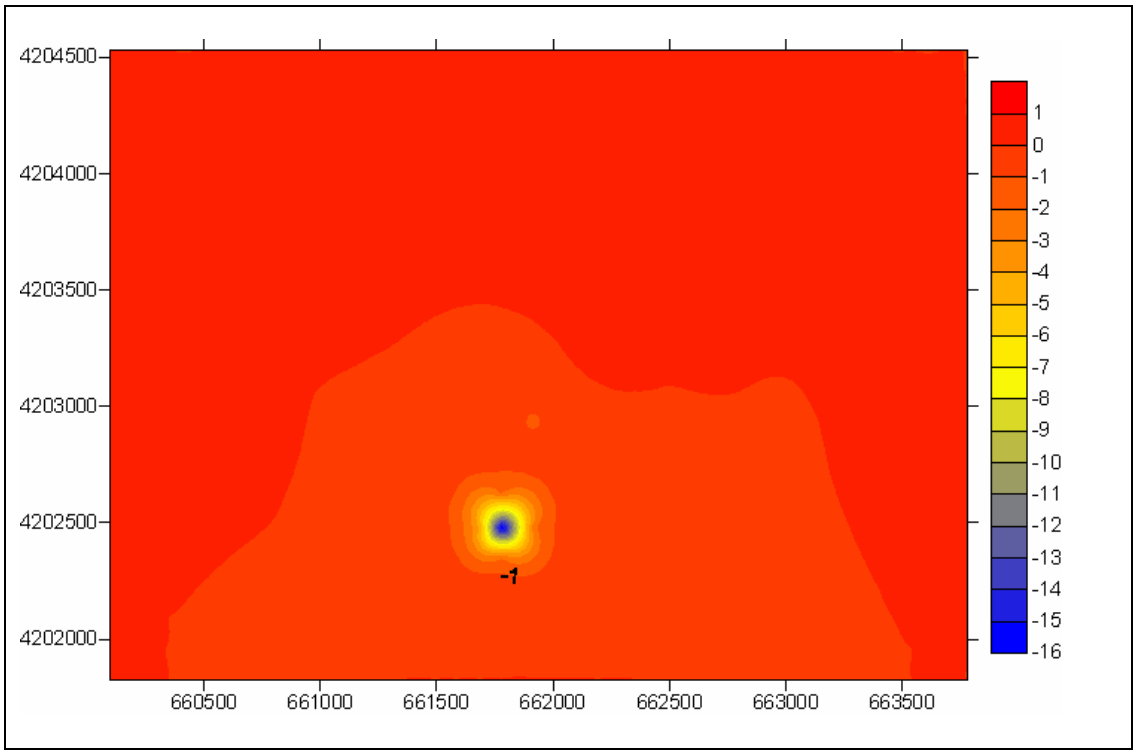

Figure 3.22 Temperature variation of the modeling area at the end of history matching period

3.5. The Effects of Wells R-1 and R-2 on Pressure Decline Profile of the System

At the charts above, decreasing trend in pressure stops approximately after 6000 days which shows the end of year 2000 and after this date, a steady or even increasing trend begins.

It has already been estimated that there is a decelerating behavior in the decrease of pressures at the KD wells after the end of 2000 (Yeltekin and Parlaktuna, 2006). This is mostly due to the effect of putting well R-1 into production and the well R-2 into full scale reinjection. These two effects seem to stop pressure decreases at the KD wells although the average fluid production rate from the field was increased at this period. It is estimated that the maximum production rate in the field can be as high as 1000 ton/h without experiencing any decline in water level of observation wells KD-1/A and KD-8 (Figure 3.23). This value was about 830 ton/h before full scale reinjection application (Yeltekin 2001).

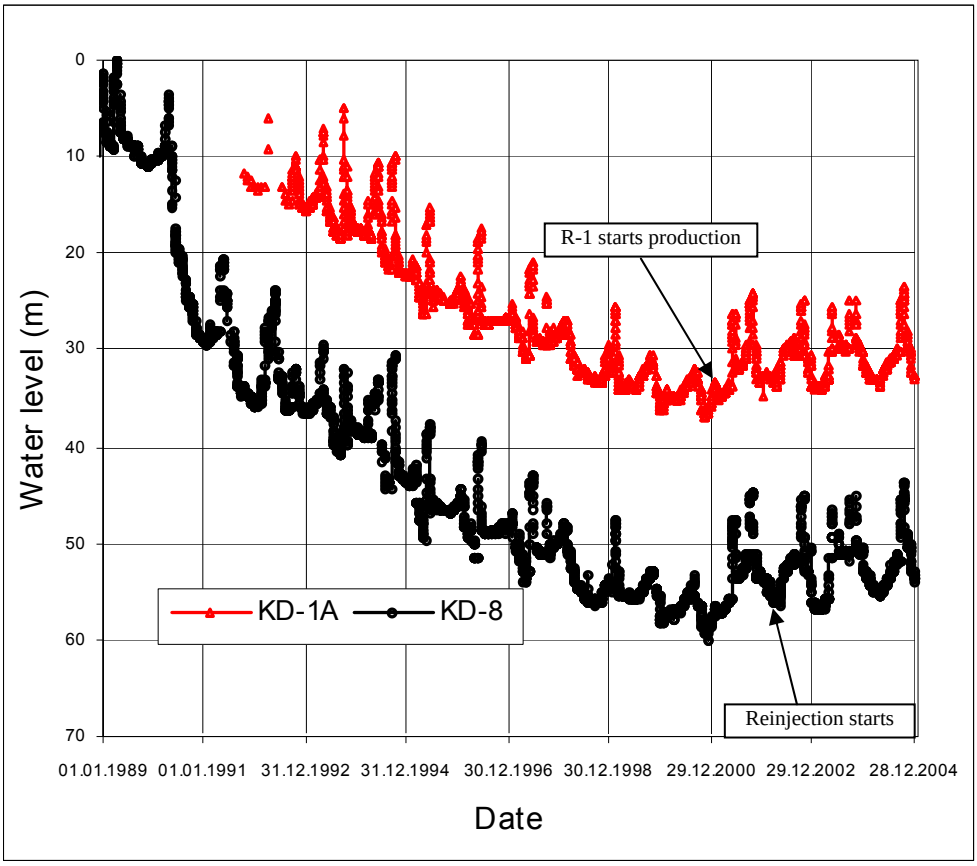

Figure 3.23 Water level measurements of KD-1/A and KD-8 between 01.01.1989-28.12.2004 (Taken from Yeltekin and Parlaktuna, 2006)

CHAPTER 4

PERFORMANCE PREDICTION OF THE STUDY AREA

In this chapter our aim is to forecast the performance of geothermal field under different production and reinjection scenarios.

A ten years period, from January 1, 2006 to December 31, 2015 was chosen for the performance prediction of Kızıldere Geothermal field. Reservoir properties given in Table 5.7 were used for performance prediction studies.

Production history of Kızıldere Geothermal Field from January 2001 to December 31, 2005 is used to provide the production data in place of already existing well-bores during performance prediction period.

Four different scenarios have been studied to observe the effects of adding new producers or injectors into the geothermal system. Table 4.1 lists the scenarios studied. Results of each prediction run are discussed separately in the following sections.

Table 4.1 Prediction Run list

Scenario	Details
1	No new production or reinjection well
2	Adding one producer well to the node 279 (R-3)
3	Adding one producer well to the node 156 (KD-2)
4	KD–15 is injector having the same injection rate with R-2

4.1. Regional Effects of Future Scenarios

4.1.1. Performance Prediction Run-1

In this prediction run, already existing production and reinjection wells (KD-6, KD-13, KD-14, KD-15, KD-16, KD-20, KD-21, KD-22, R-1 and R-2) produced 10 years more with their production history between January 2001 and December 2005. It is supposed that no additional re-injection or production operation will be done in this period.

Figure 4.1 shows the pressure contour map of the Kızıldere Geothermal field at the end of performance prediction period. It makes out that, the maximum decline in pressure would be observed at the southwest of the modelling area at the surrounding area of well R-1.

In Figure 4.2, change in the reservoir pressure at the end of ten years prediction period is demonstrated. In the contour map, blue color signifies greater decrease in pressure. So, the highest decrease is seen at R-1 region.

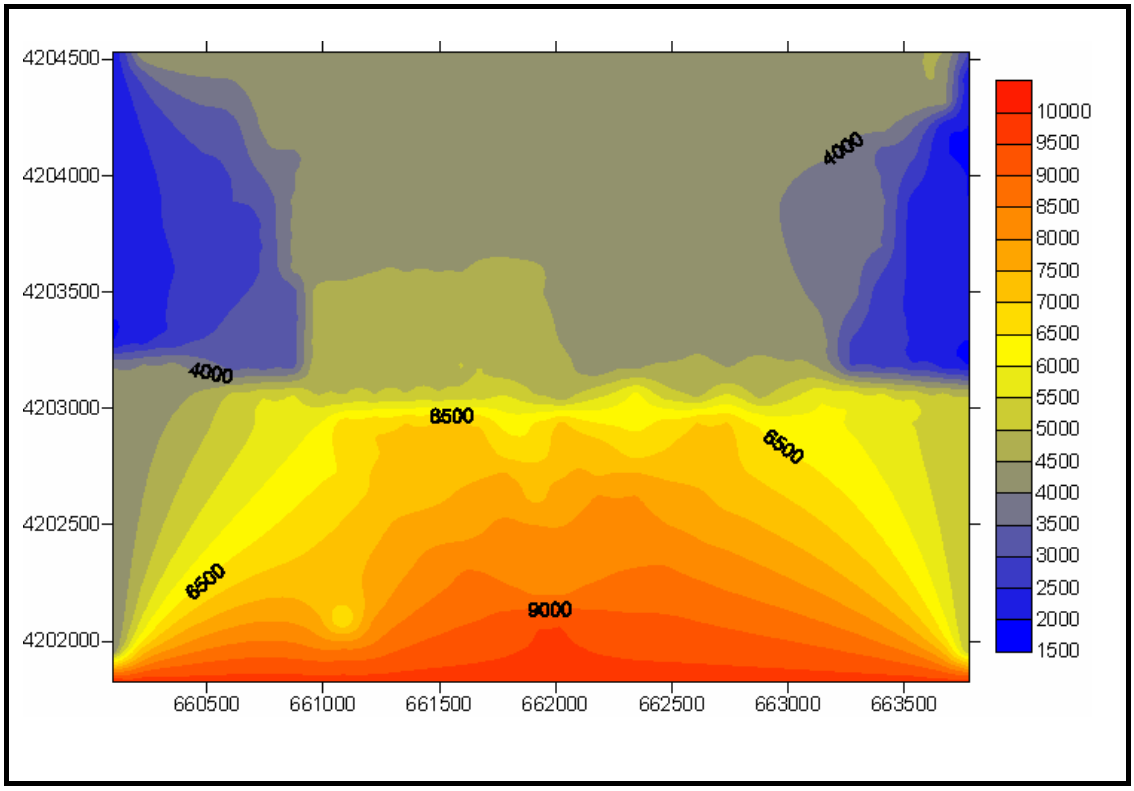

Figure 4.1 Pressure distribution of the modeling area in Prediction Run-1

Temperature distribution and change in temperature values are seen in Figure 4.3 and Figure 4.4 respectively. The decrease in reservoir temperature deepens at the end of prediction period. It reaches to 32°C at the R-2 location related with the reinjection and the effected zone gets larger compared to the end of transient calibration period Figure 3.21.

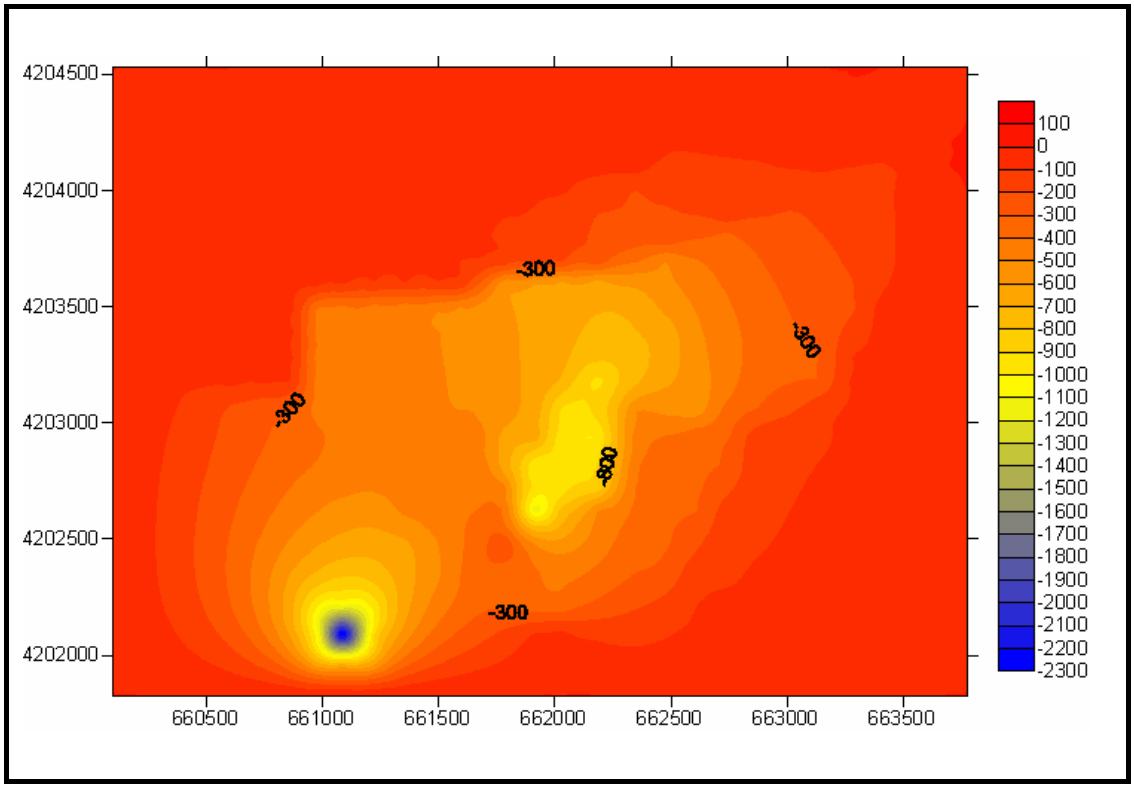

Figure 4.2 Pressure variation of the modeling area in Prediction Run-1

The changes in well-bore temperatures during the prediction period (between January 01, 2006 and December 31, 2015) are illustrated in Figure 4.5. It can be inferred from the graph that, the highest temperature decrease occurs in KD-6 with approximately 7 °C which is situated closer to the well R-2 than the other KD wells. Totally, 91.527.913 m^3 fluid is produced and 21.900.000 m^3 fluid is reinjected into the reservoir in this prediction trial.

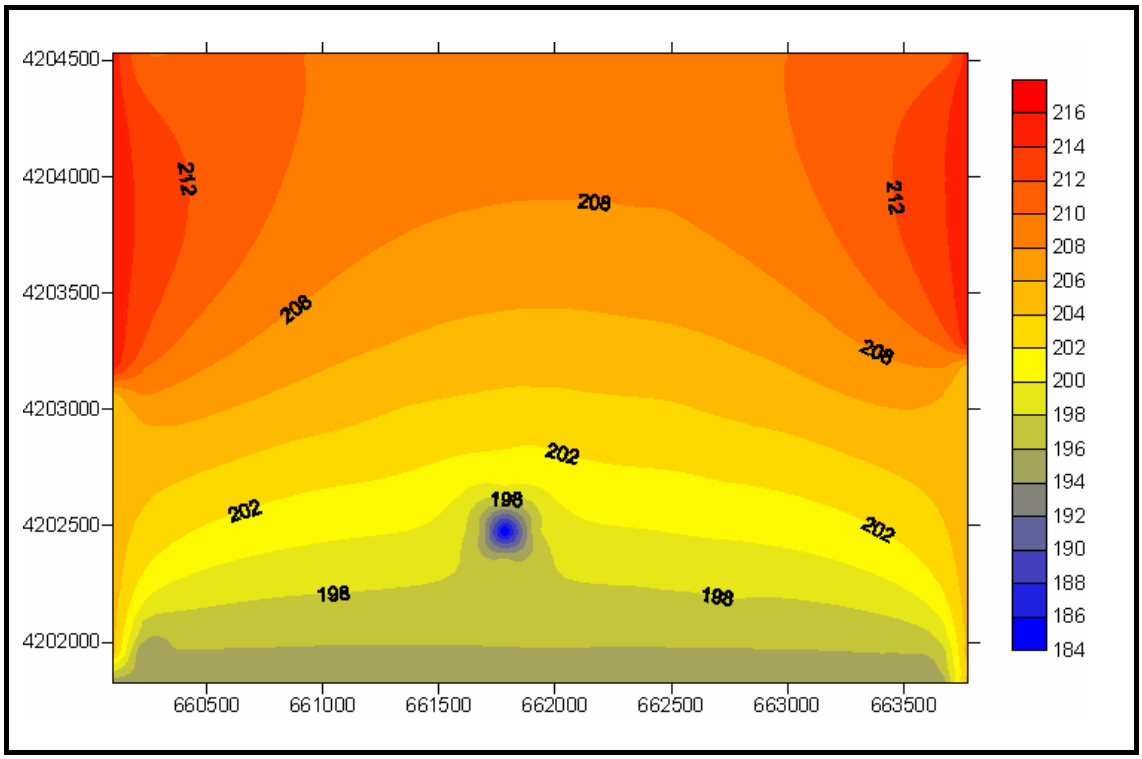

Figure 4.3 Temperature distribution of the modeling area in Prediction Run-1

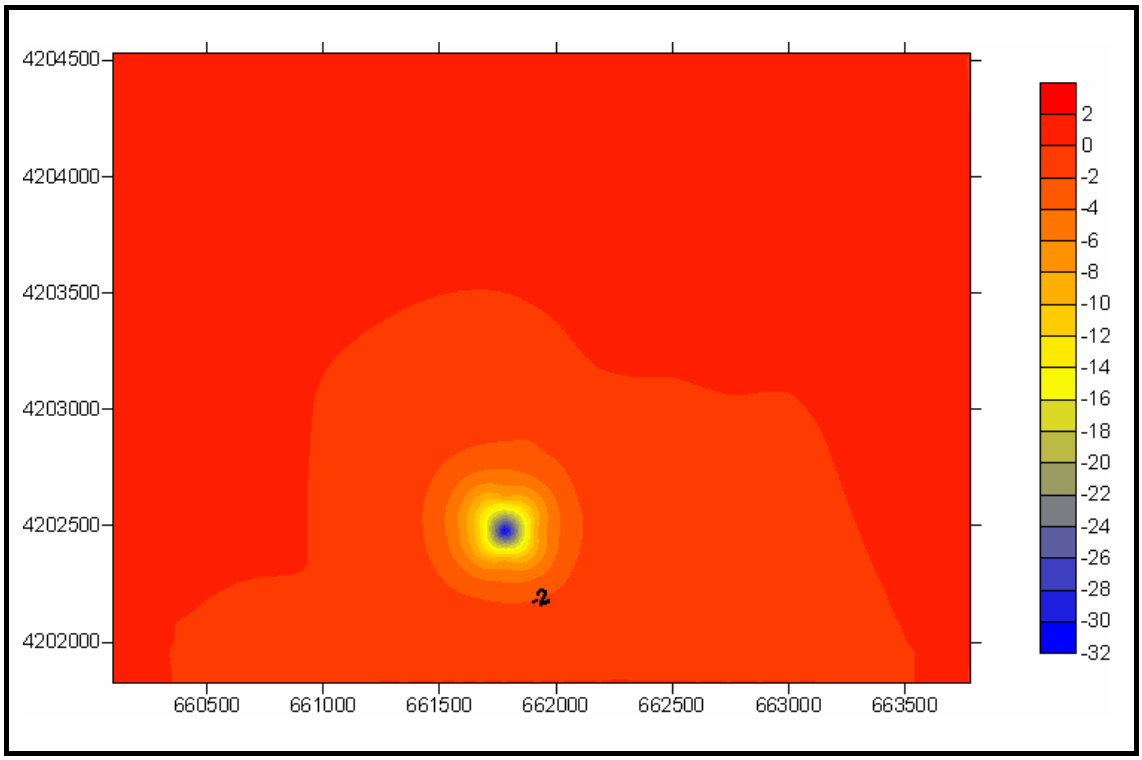

Figure 4.4 Temperature variation of the modeling area in Prediction Run-1

4.1.2. Performance Prediction Run-2

At this scenario a production well (R-3) is added to the operation regime of the area. Well R-3 was drilled in 2006 between wells R-1 and R-2 aiming to work as a reinjection well but up to the end of this study, it hasn't met the expectations both for production and reinjection. This could be due to the fact that, the geothermal reservoir does not have homogeneity in terms of fracture distribution resulting very different permeability values in small distances. If the insufficiency of this well could be handled it is supposed that it could be a production well.

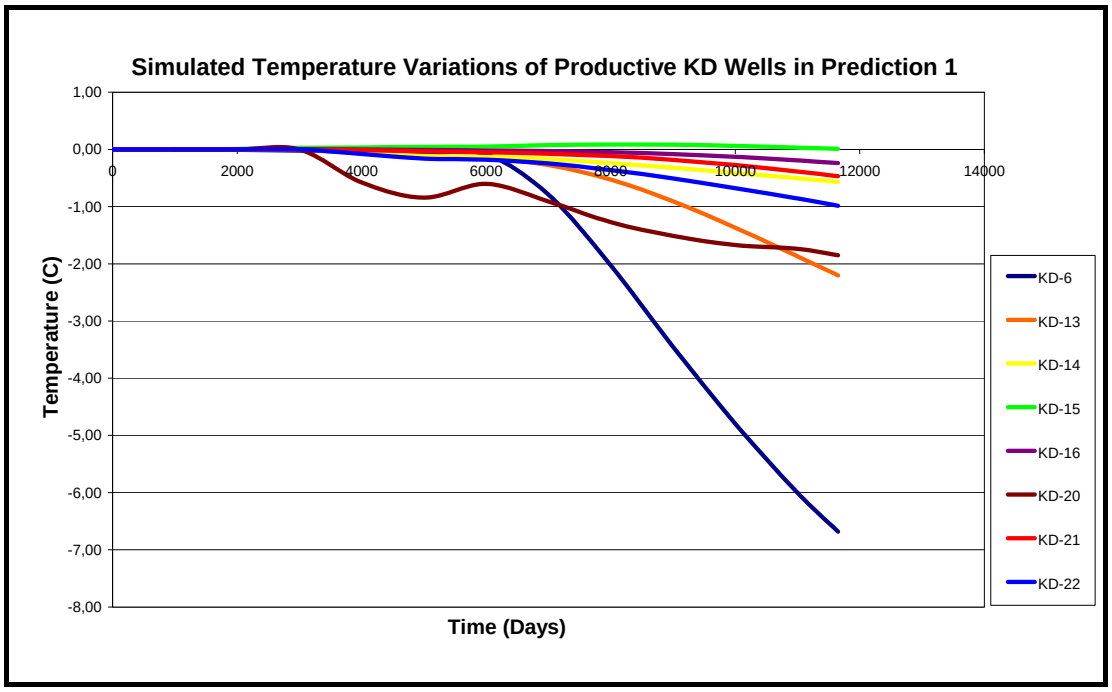

Figure 4.5 Overall demonstration of temperature drop in KD wells at the end of Prediction Run-1

So a new well has been created in the model located at the middle node between wells R-1 and R-2 and supposed that it has a production rate same as R-1. The reason of adding this well as a new production well is the common belief that the further expansion of the field should be toward the south and southwesterly region of the field. In the performance prediction period 1245 kPa decline in pressure at R-3 well was monitored.

The pressure declines at the bottom of the other production wells were more than performance Prediction Run-1 (without adding any producer and injector).

Pressure contour map of the Kızıldere Geothermal field for this run is given in Figure 4.7. As observed, addition of a new production well caused a higher-pressure decline in the field. The response of the other part of the field to the new production well is in the direction of increasing in pressure decline but not as much as in the SW corner.

In Figure 4.8 could be seen the temperature distribution of the modeling area after Prediction Run-2. Here, the results are quite similar with the results obtained from Prediction Run-1 meaning no big effect would be monitored by adding new wells to the field but reinjection wells.

Figure 4.9 shows the temperature decrease in the field. As similar to the Prediction Run-1, the decrease stays at 32 °C at R-2 location and lowers as growing distant from this well. The well KD-6 has experienced the highest temperature drop about 7°C being the nearest well to the reinjection well R-2 (Figure 4.10). In total, 103.466.336 m^3 fluid is produced and 21.900.000 m^3 fluid is reinjected into the reservoir in this prediction run period.

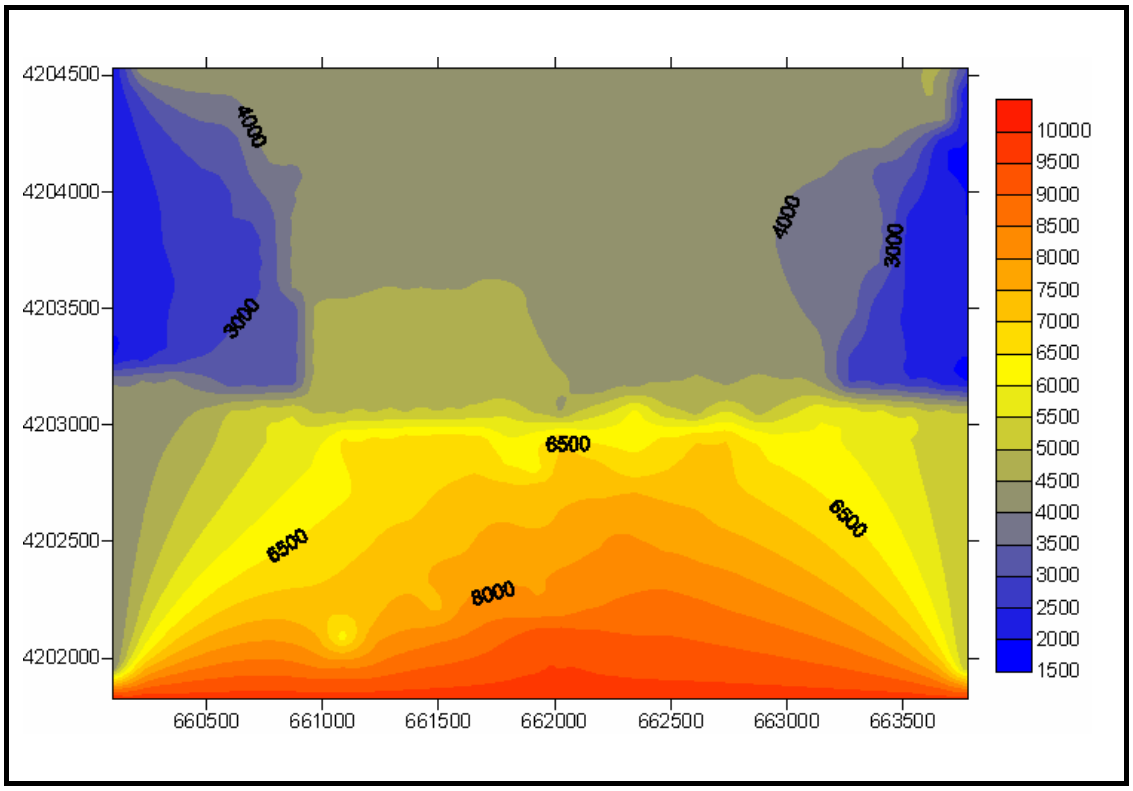

Figure 4.6 Pressure distribution of the modeling area in Prediction Run-2

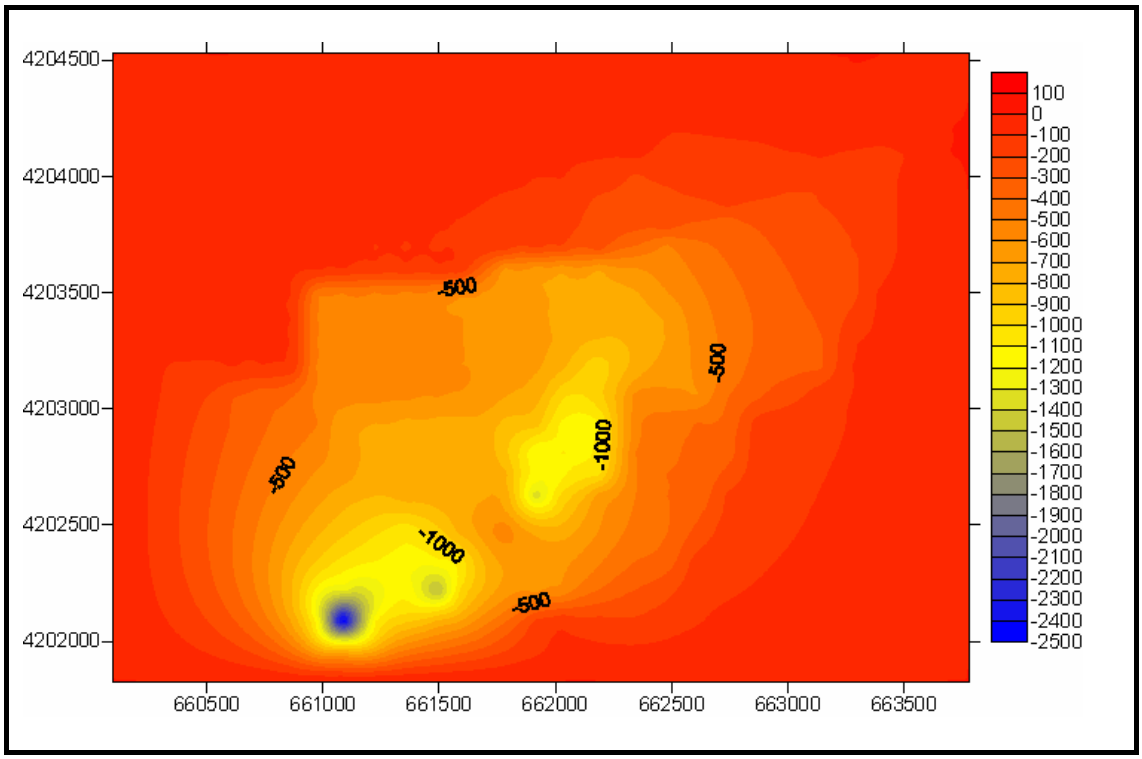

Figure 4.7 Pressure variation of the modeling area in Prediction Run-2

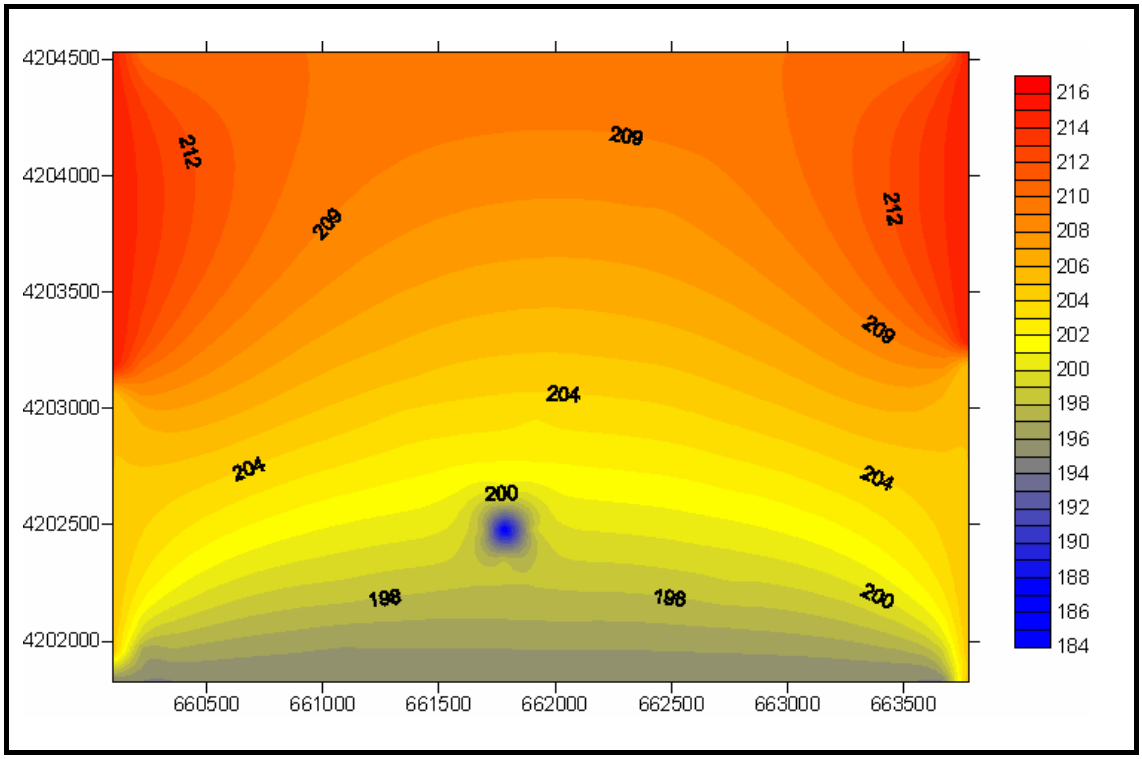

Figure 4.8 Temperature distribution of the modeling area in Prediction Run-2

4.1.3. Performance Prediction Run-3

At this scenario another production well (KD-2) at the SW corner of the field has been put into operation (Figure 3.4). It is aimed with this scenario to observe the possible effect of production from the southwestern parts of the field. Well KD-2 produced in the same production regime with R-1 in the prediction period and has experienced 1323 kPa decline in pressure. The pressure declines of the other production wells were more than Run-1 and also Run-2. SW corner of the field responded to well KD-2 with an increase in pressure decline compared to decline in Run-1 (Figure 4.11- Figure 4.12).

In Figure 4.13 and 4.14, contour maps of temperature distribution and temperature variation belonging to Prediction Run-3 are tabulated. These two maps are also very similar to their equivalents in Prediction Run-1 and Prediction Run-2. These results prove that production of the fluid from the field doesn't have important effect on the reservoir temperature.

The graph of temperature variation behavior of KD wells is seen in Figure 4.15. In this graph, the largest influenced well seems to be the well KD-6 which is the closest of all wells to the well R-2. In this prediction run, totally 103.466.336 m^3 fluid is produced and 21.900.000 m^3 fluid is reinjected into the reservoir.

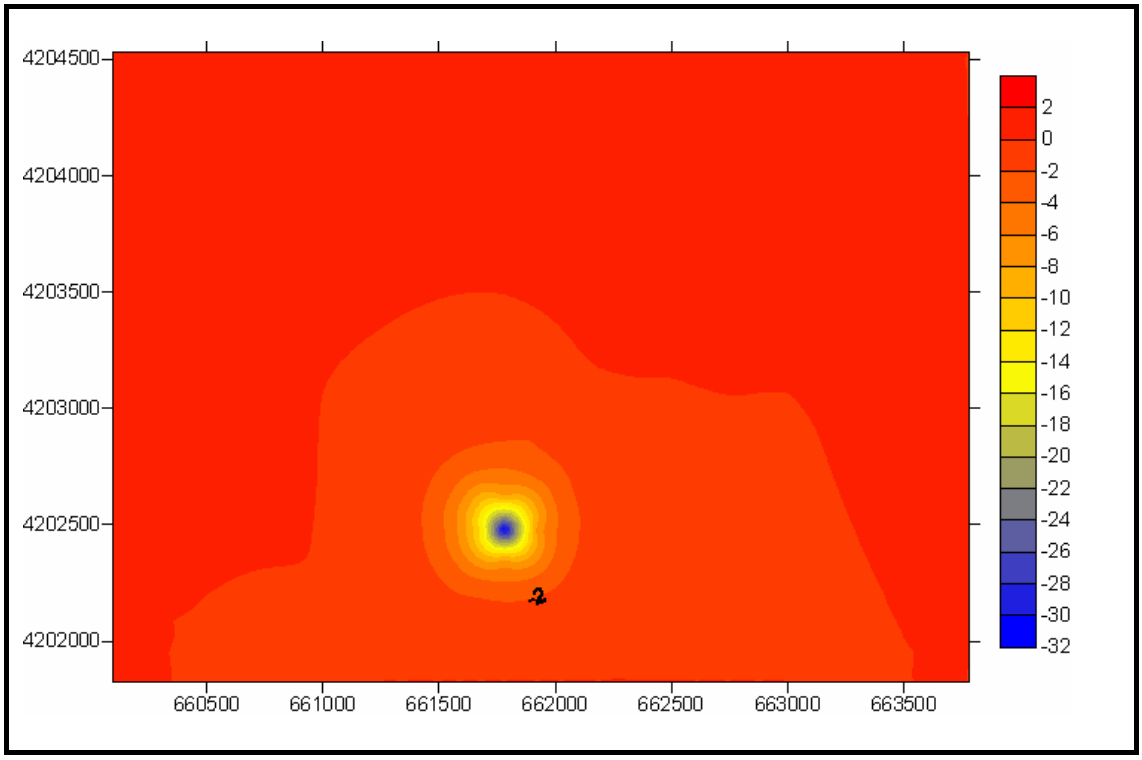

Figure 4.9 Temperature variation of the modeling area in Prediction Run-2

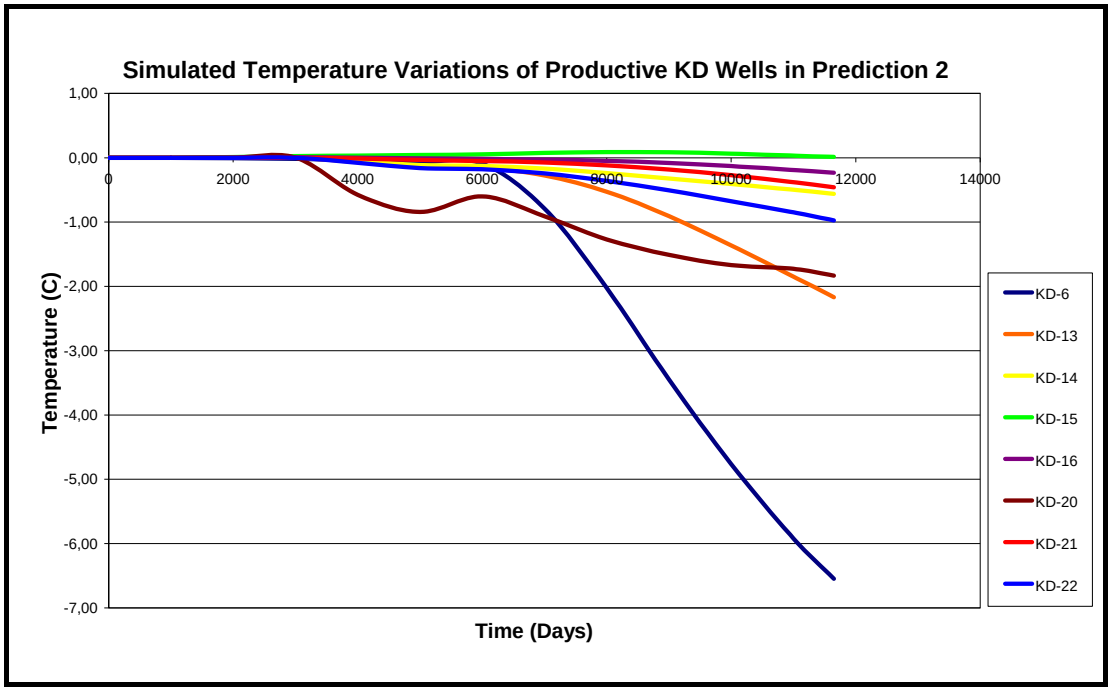

Figure 4.10 Overall demonstration of temperature drop in KD wells at the end of Prediction Run-2

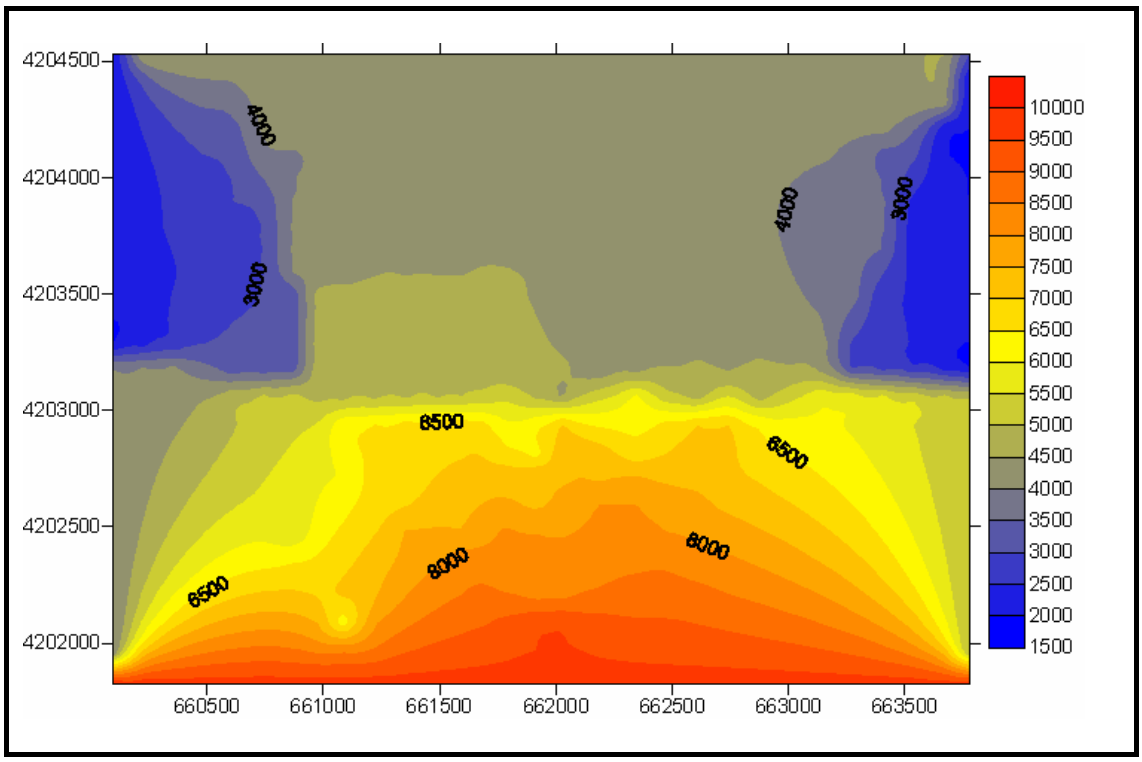

Figure 4.11 Pressure distribution of the modeling area in Prediction Run-3

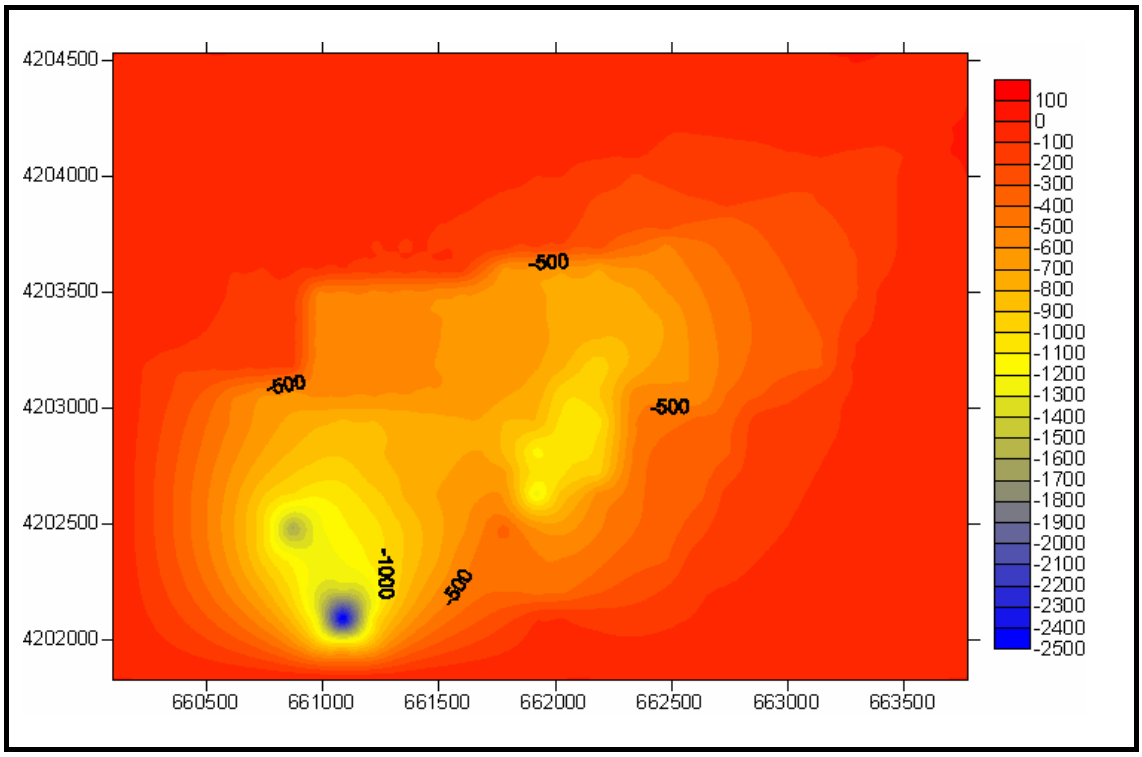

Figure 4.12 Pressure variation of the modeling area in Prediction Run-3

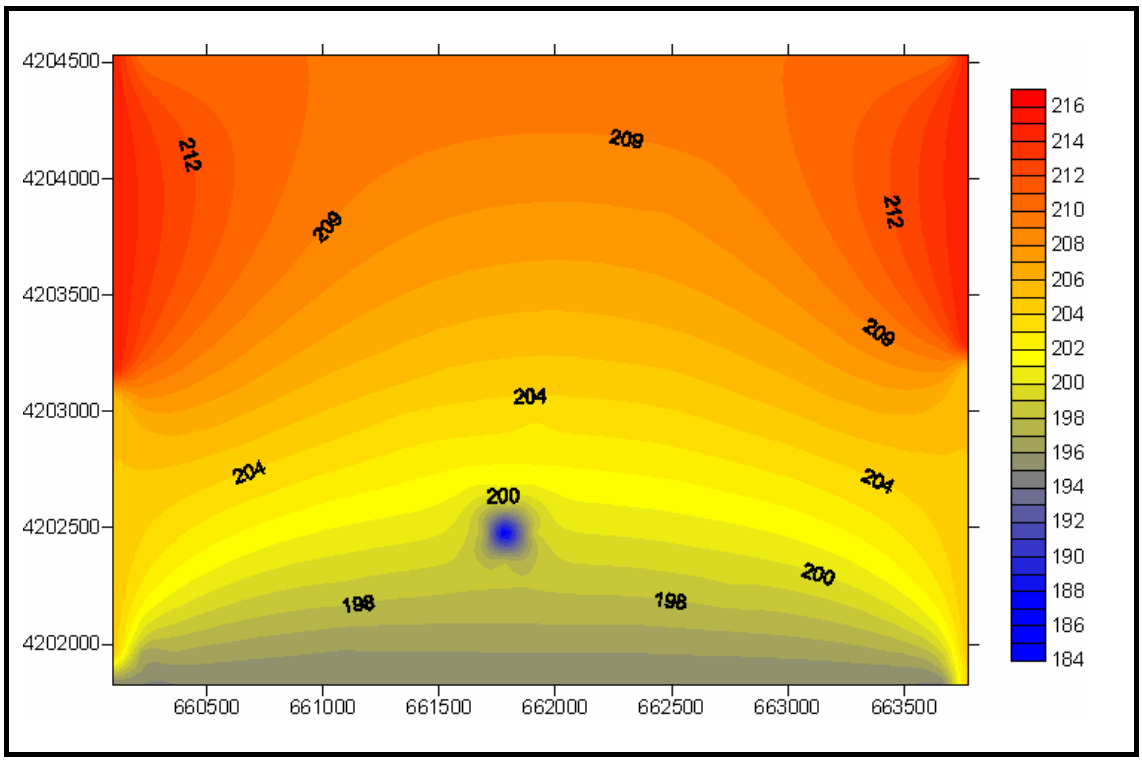

Figure 4.13 Temperature distribution of the modeling area in Prediction Run-3

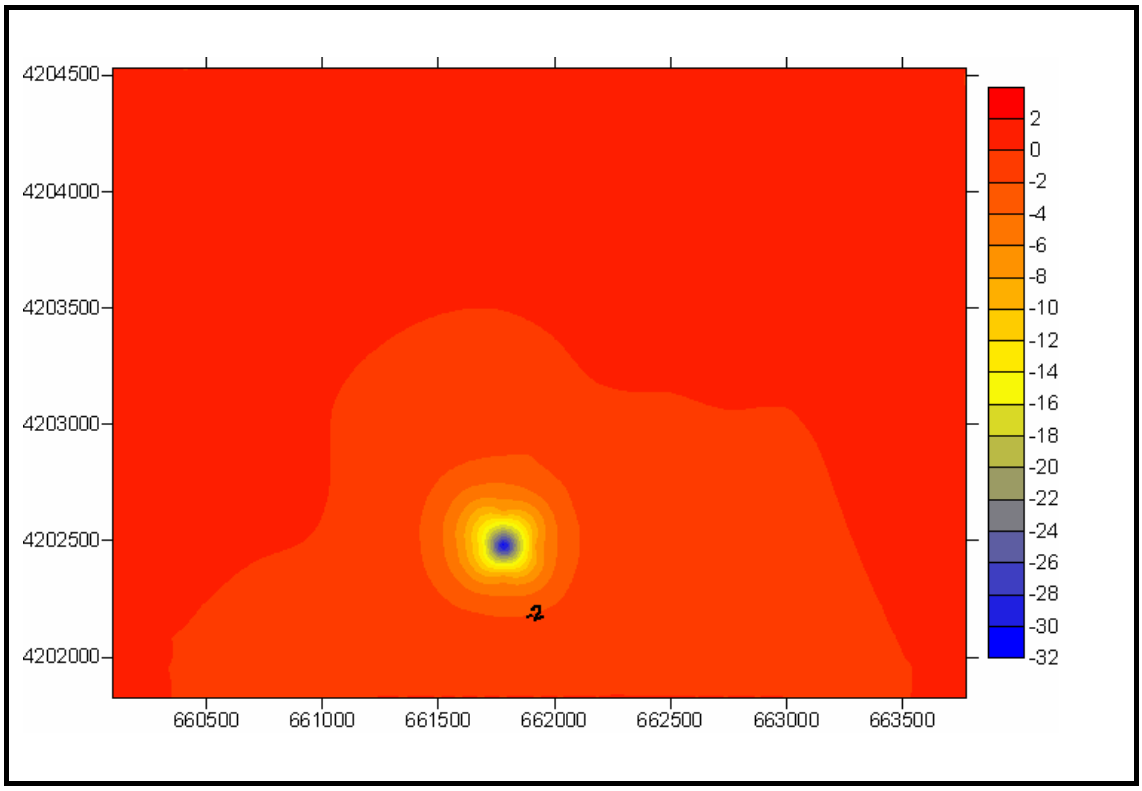

Figure 4.14 Temperature variation of the modeling area in Prediction Run-3

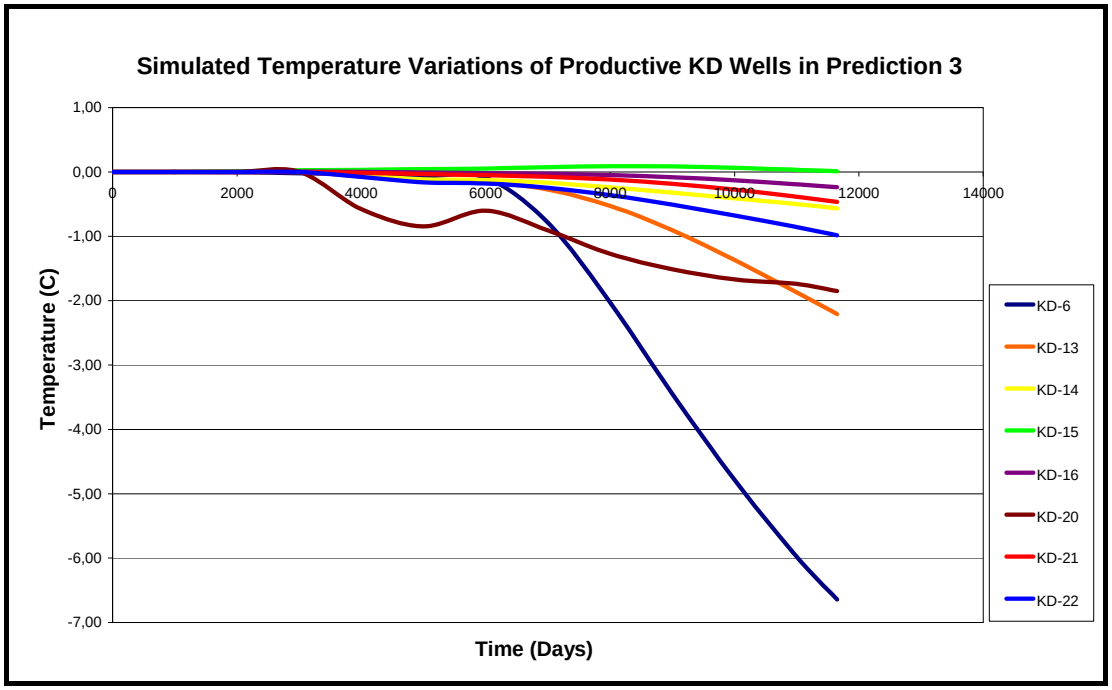

Figure 4.15 Overall demonstration of temperature drop in KD wells at the end of Prediction Run-3

4.1.4. Performance Prediction Run-4

In this run, the production well KD-15 was converted to a re-injection well. KD-15 is found at the northernmost of the production zone. After putting of deep wells R-1 and R-2 into service, its production is reduced since the needed amount is mostly met by R-1. Considering also that the KD wells are about to fill their economical life-span, its necessity has become questionable. So, in Prediction Run-4 the utilization of KD-15 as a reinjection well has been examined.

The re-injection rate of the fluid in this well is chosen to be the same with the rate of R-2, 250m^3/h and a continuous re-injection is done during the prediction period. The effect of the re-injection to the reservoir pressure was simulated. The amount of fluid re-injected corresponds to 20-25 % of the total produced fluid during performance prediction period.

Re-injection of fluid caused pressure increase in the field contrary to the other prediction runs (Figure 4.16 - Figure 4.17).

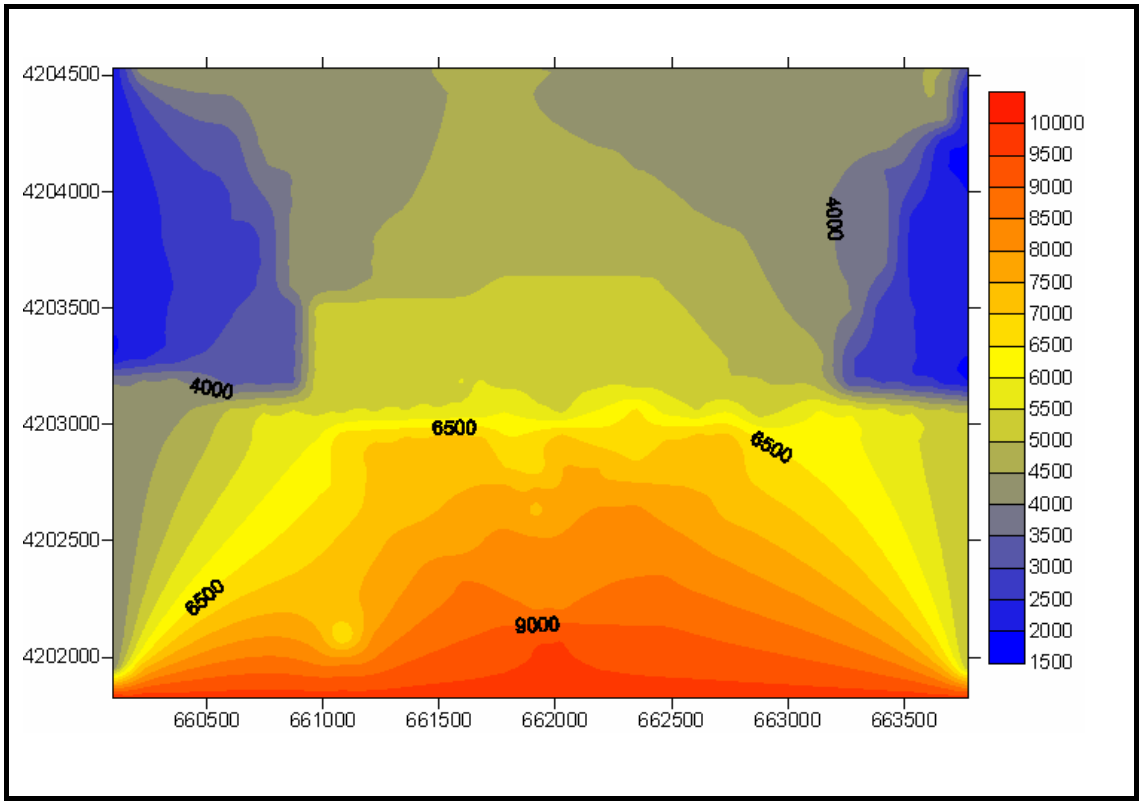

Figure 4.16 Pressure distribution of the modeling area in Prediction Run-4

In Figure 4.18 and Figure 4.19 are, respectively, the temperature distribution and temperature variation maps produced with the results obtained from Prediction Run-4. These two maps confirm that, reinjection had negative consequences on the temperature of the geothermal reservoir. In both maps, there appears another cooling point at the zone where reinjection has been applied. This cooling of reservoir temperature is about 32 °C at R-2 region and about 28 °C at KD-15 region.

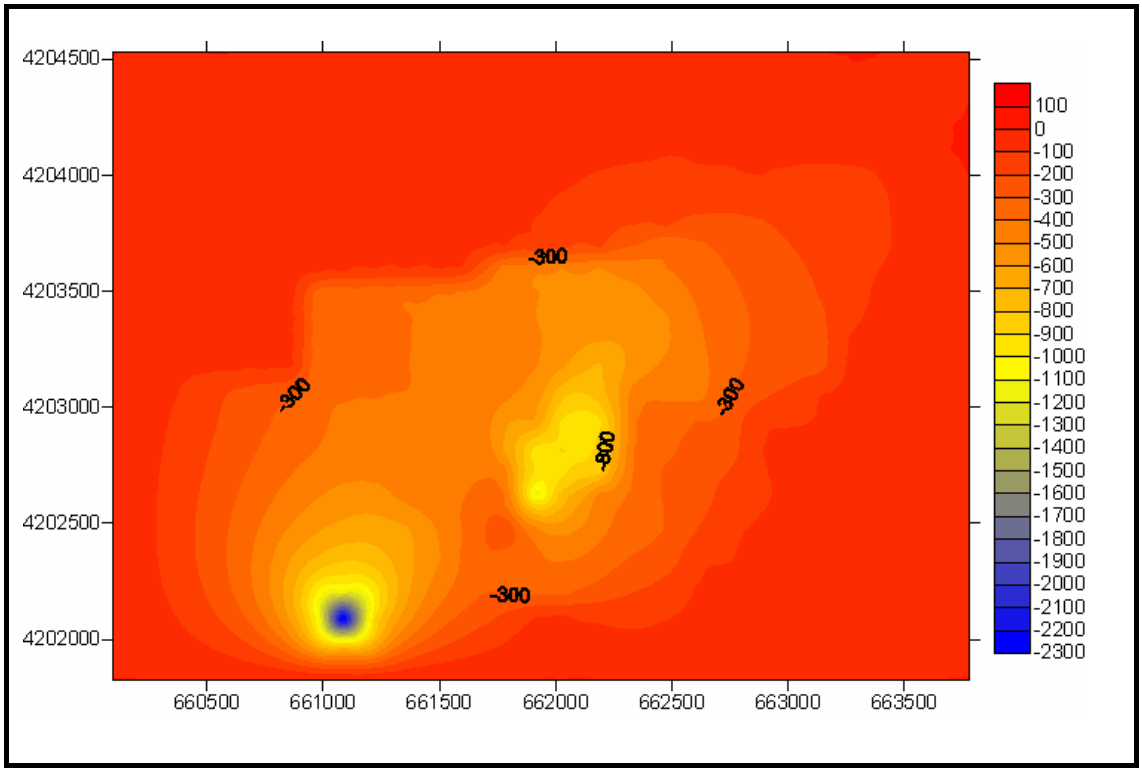

Figure 4.17 Pressure variation of the modeling area in Prediction Run-4

In Figure 4.20, a huge decrease in the temperature of the well KD-15 is remarkably manifested. This decrease is obviously related with the reinjection process applied from this well. But in this prediction run the negative effects of reinjection could be observed not only on the reinjection well but also on the other production wells nearby. 91.527.913 m^3 fluid is produced and 43.800.000 m^3 fluid is reinjected into the reservoir.

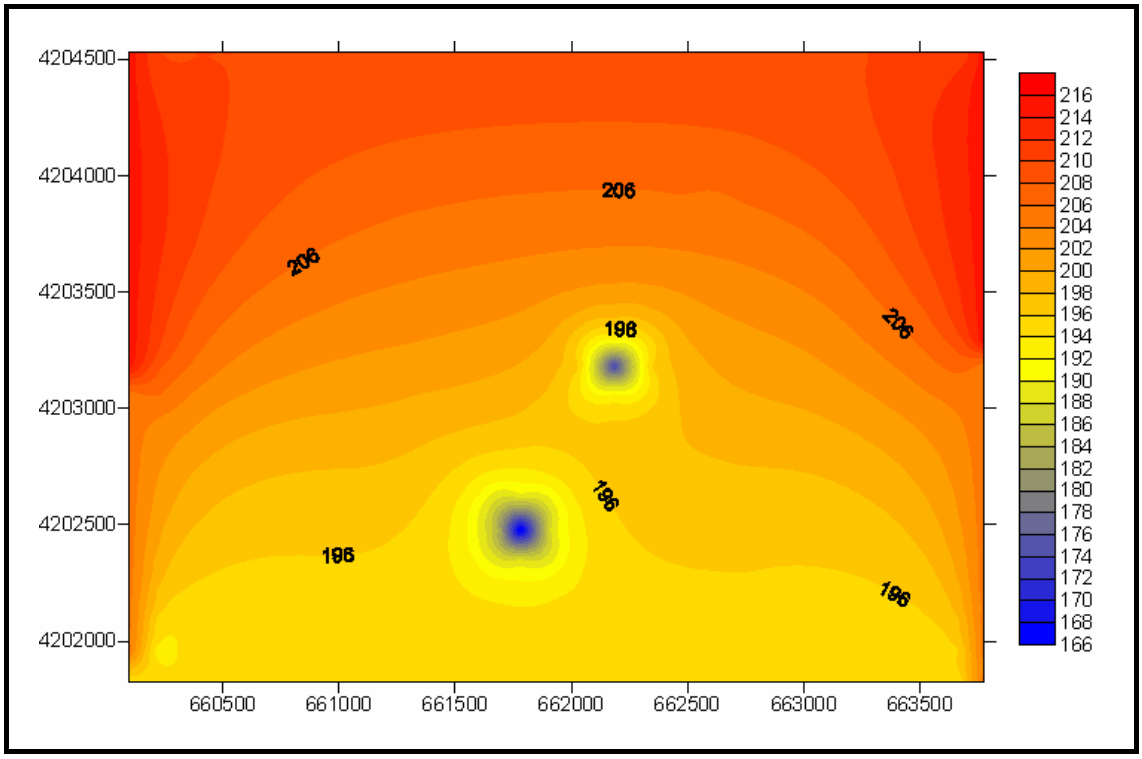

Figure 4.18 Temperature distribution of the modeling area in Prediction Run-4

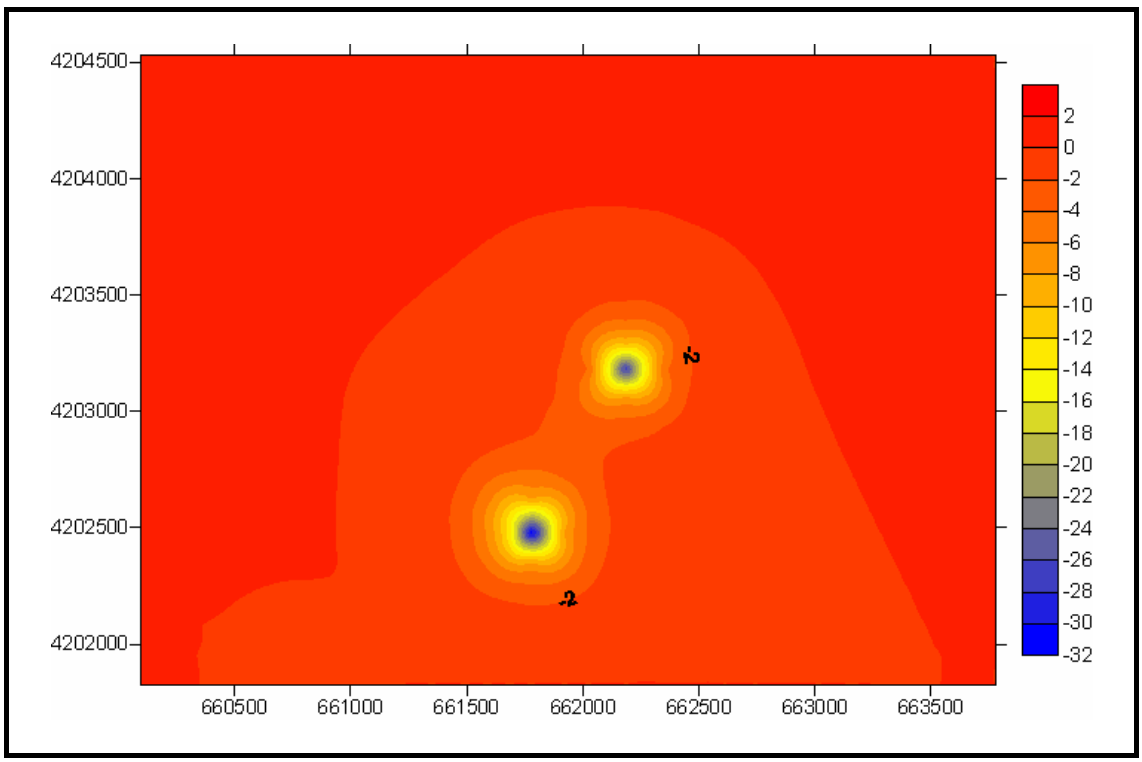

Figure 4.19 Temperature variation of the modeling area in Prediction Run-4

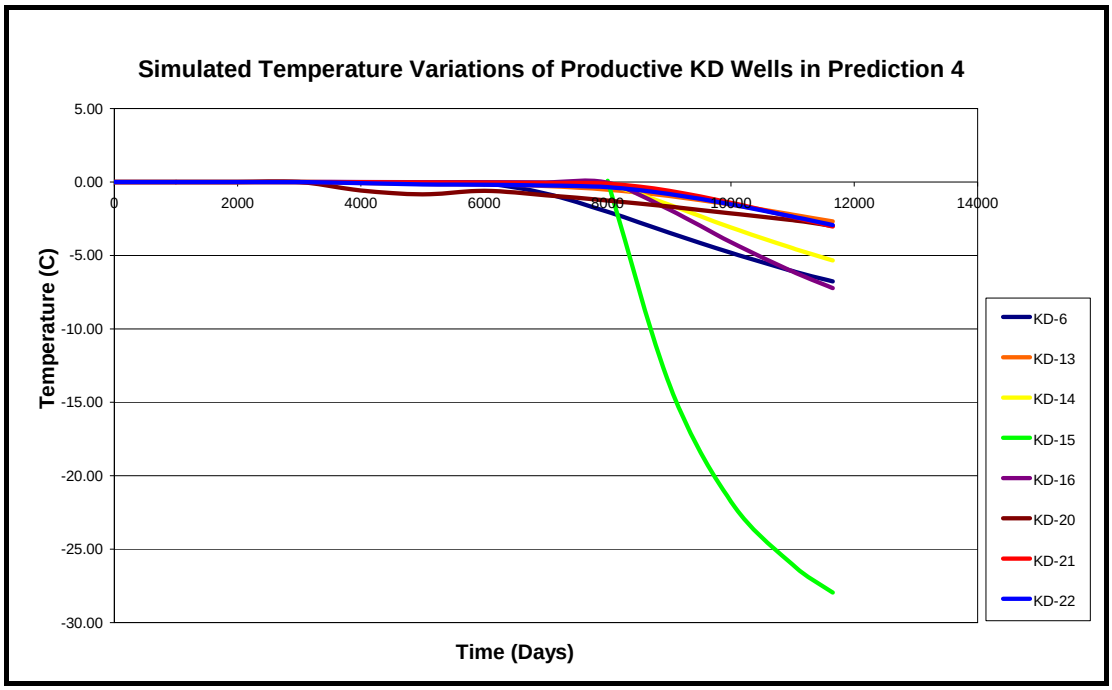

Figure 4.20 Overall demonstration of temperature drop in KD wells at the end of Prediction Run-4

4.2. Results of Scenarios at the Production and Reinjection Wells

In this section, effects of four different predictions to every single production and reinjection well are discussed separately. At this point, it is aimed to forecast the future behavior of operative wells under different operational regimes. So this could give an idea to the authorities that are responsible of Kızıldere Geothermal Field to decide about the manner how these wells should be utilized.

4.2.1. Performance Prediction of KD-6

At this well from the beginning of transient calibration to the end of year 2000 there appears a decline in bottom well-bore pressure but after this time an increasing trend in pressure starts (Figure 4.21). As explained before in Section 3.4, this behavioral change in pressure could be attributed to the addition of deep wells R-1 and R-2 to the already operating KD wells.

Similar to the other wells, in every prediction run, KD-6 exhibited a different response in terms of pressure. It could be seen in Figure 4.22 that, in Prediction Run-1, which assumes the conservation of present operational regime, KD-6 has a rise in pressure. In Prediction Run-2, this increasing halts because of the entrance of the well R-3 and in Prediction Run-3 because of the entrance of well KD-2 as new producers. When these two prediction runs are compared; second run has higher effect on the well KD-6 than third run, since the well R-3 is situated at a closer distance to KD-6 than the well KD-2. Prediction Run-4 has the highest positive effect on the well pressure with 170 kPa increase. This change is obviously due to the renovation of the well KD-15 as a reinjection well.

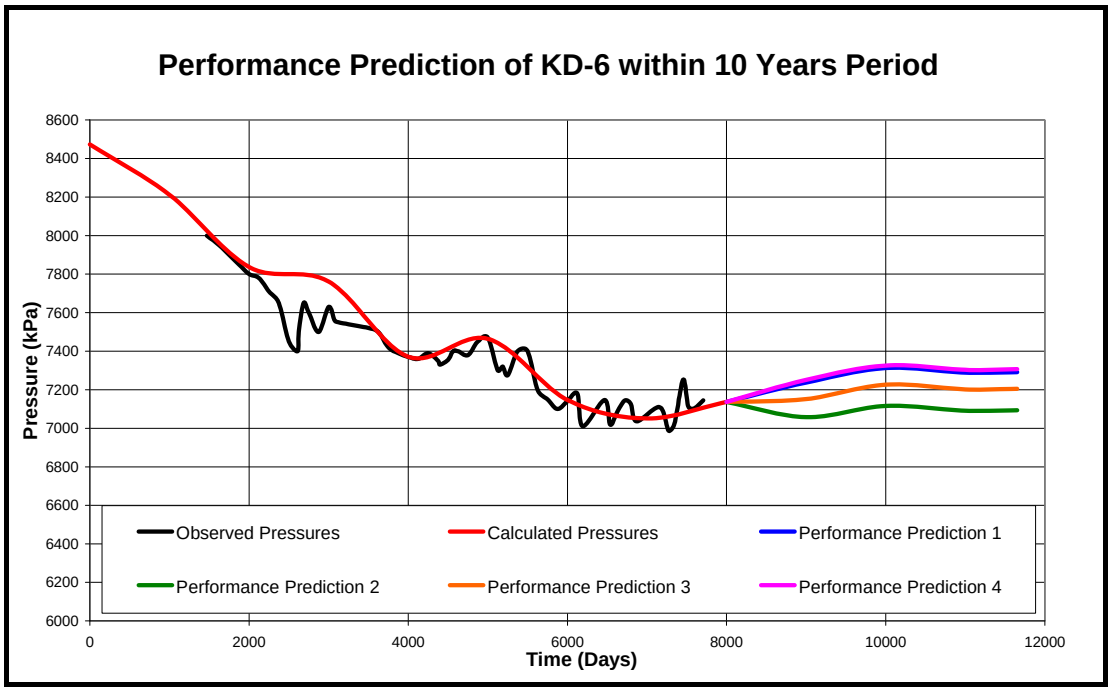

Figure 4.21 History matching and performance prediction run results of KD-6

In temperature aspects, KD-6 has not experienced different decrease profiles in different scenarios. It has about 7 °C decline in bottom hole temperature in all prediction runs. This result is quite concordant with the idea that, KD-6 is in the well R-2's influence zone (Yeltekin ad Parlaktuna, 2006).

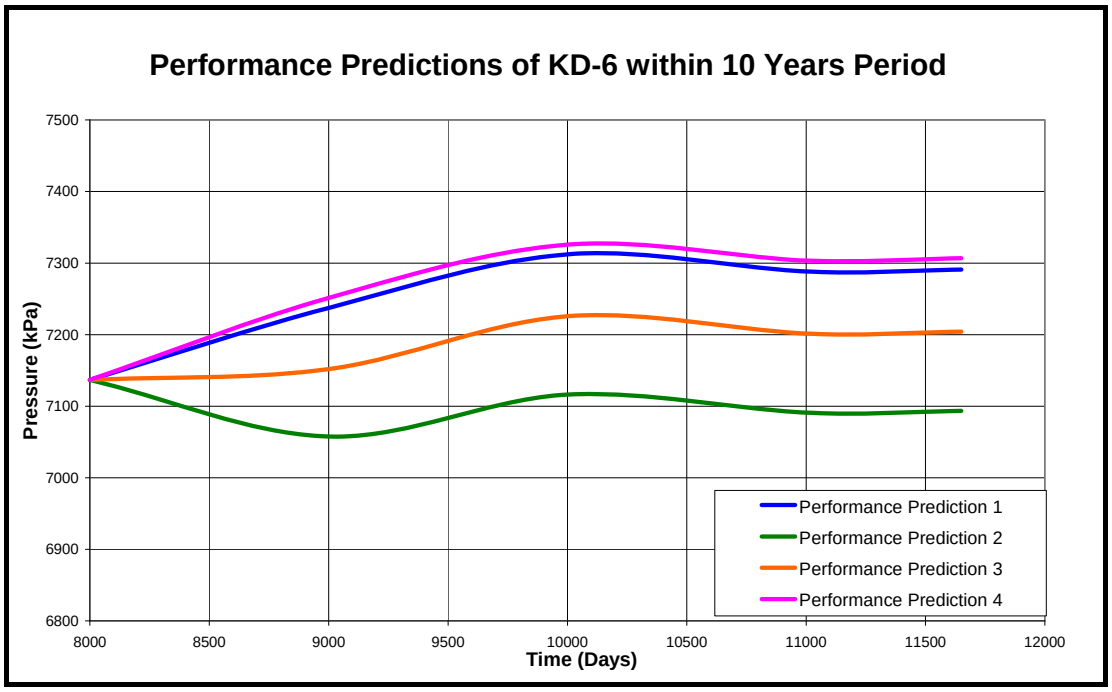

Figure 4.22 Performance prediction run curves of KD-6

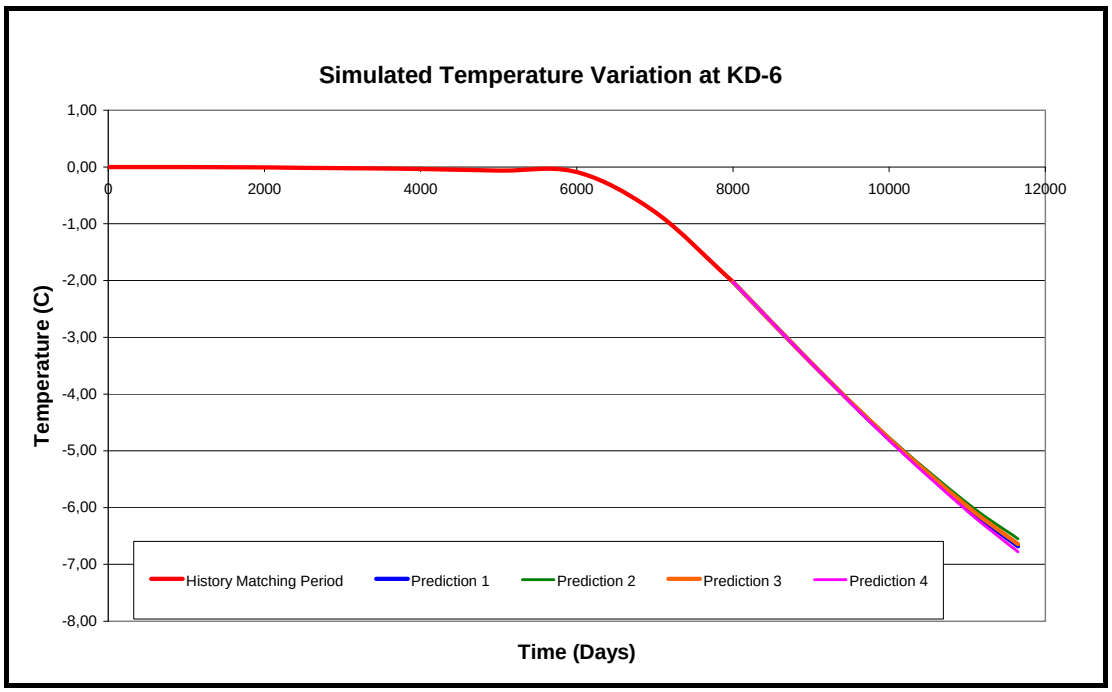

Figure 4.23 Temperature variation of well KD-6 in the modeling period

4.2.2. Performance Prediction of KD-13

Performance of the well KD-13 for different scenarios shows similarities to the performance of KD-6. Again there is an increase in Prediction Run-1 and Run-4 and stabilization in Run-2 and Run-3 (Figure 4.24).

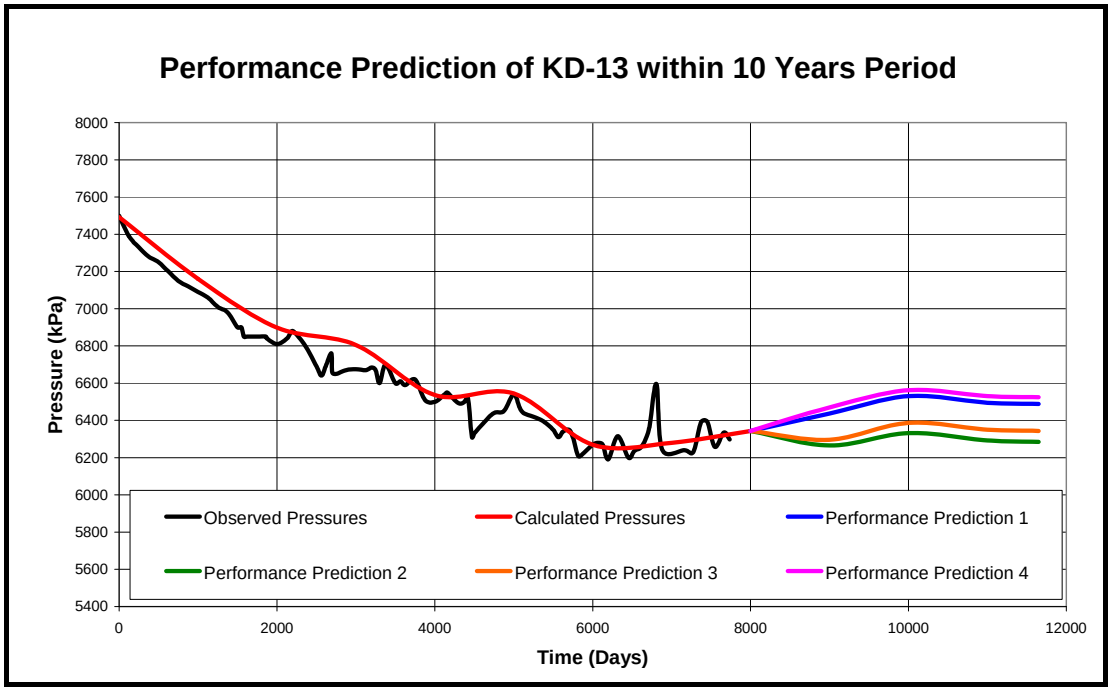

Figure 4.24 History matching and performance prediction run results of KD-13

In Figure 4.25, the change in bottom hole pressures of the well KD-13 could be identified precisely. Because of the situation of this well is nearer to the well KD-15 than KD-6 (Figure 3.4), its positive or negative effects are felt more intensively at this well. Thus, in Prediction Run-4, a higher increase is achieved in well pressure, namely 180 kPa, but a bigger decrease in temperature which is about 2.7 °C when compared with the well KD-6 (Figure 4.26).

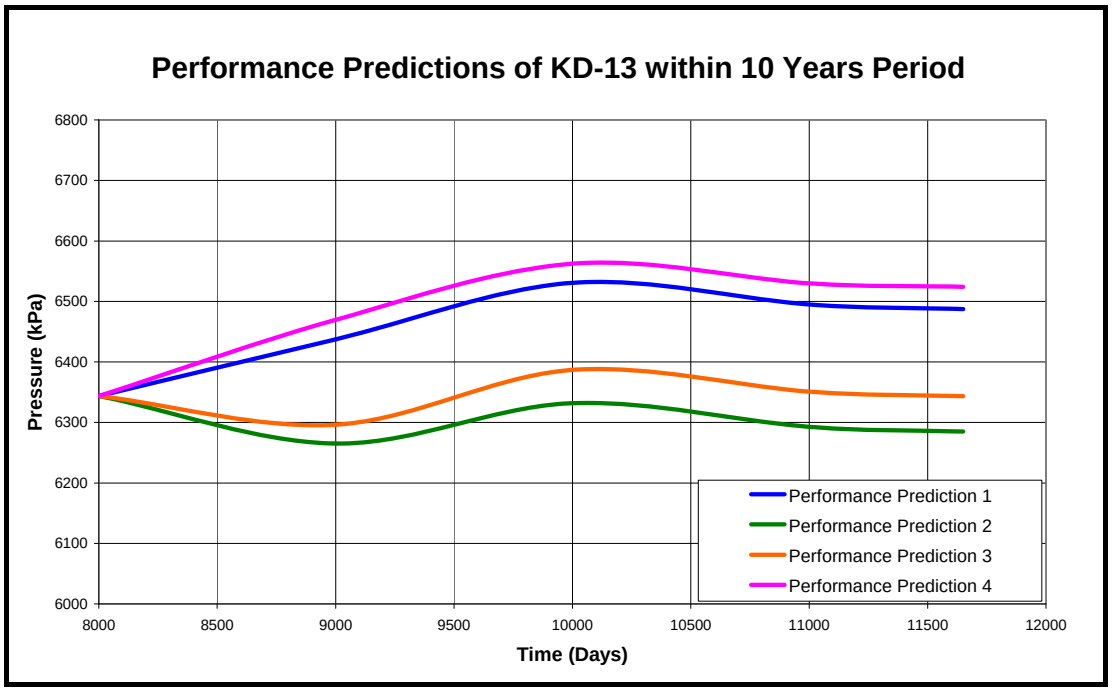

Figure 4.25 Performance prediction run curves of KD-13

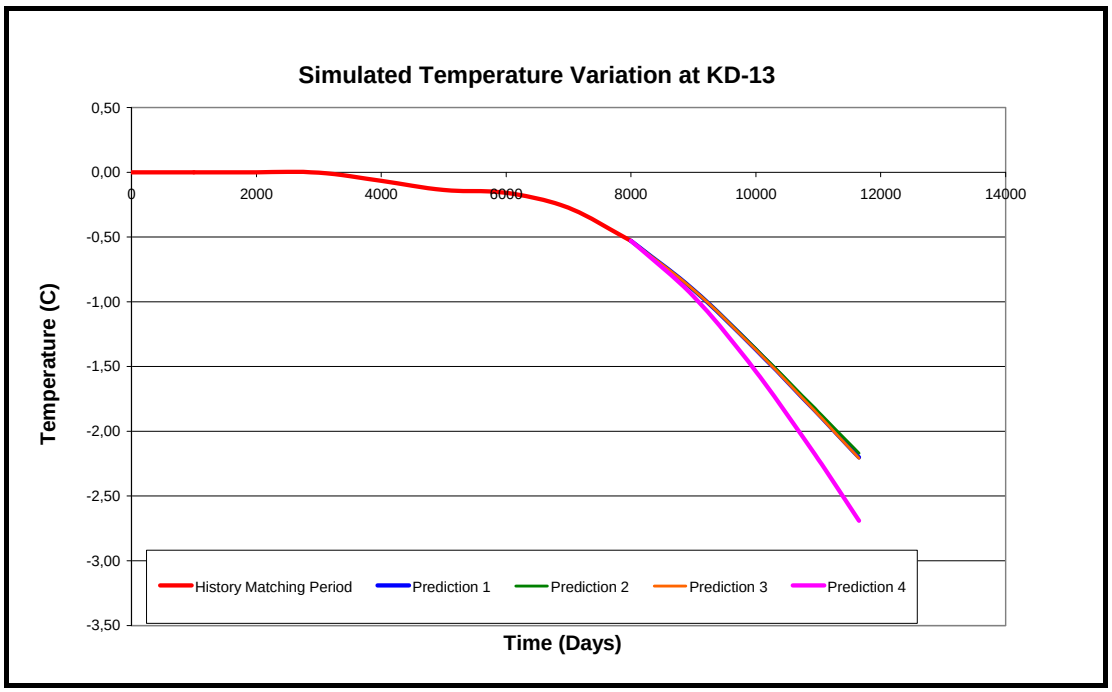

Figure 4.26 Temperature variation of well KD-13 in the modeling period

4.2.3. Performance Prediction of KD-14

At the well KD-14, as the calculated values from Prediction Run-1 Run-2 and Run-3 become similar, Run-4's effect gets evident. Settlement of the well is the sole reason for this divergence of the results (Figure 3.4).

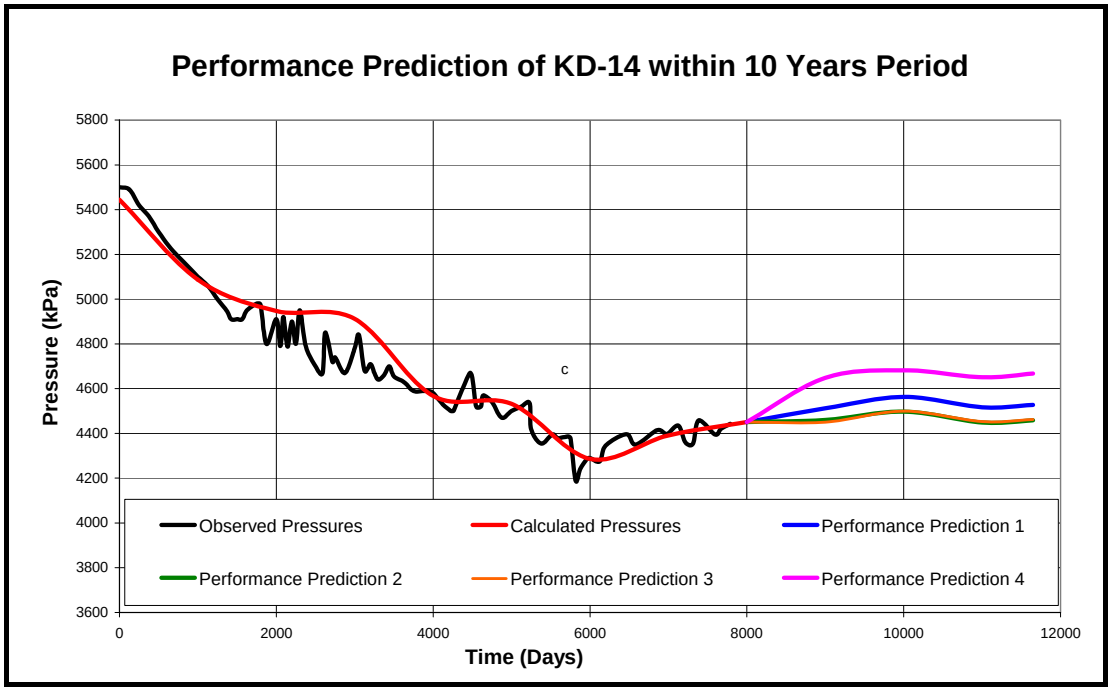

Figure 4.27 History matching and performance prediction run results of KD-14

As it could be understood from Figure 4.28, the Prediction Run-2 and Run-3 have approximately same outcomes on the well KD-14 and Prediction Run-1 has also given quite parallel results. But there is a high increase in bottom hole pressure of this well as a response to the Prediction Run-4. Likewise, well temperature fall in this prediction run is quite harsh, showing again the negative effect of reinjection on the production wells (Figure 4.29).

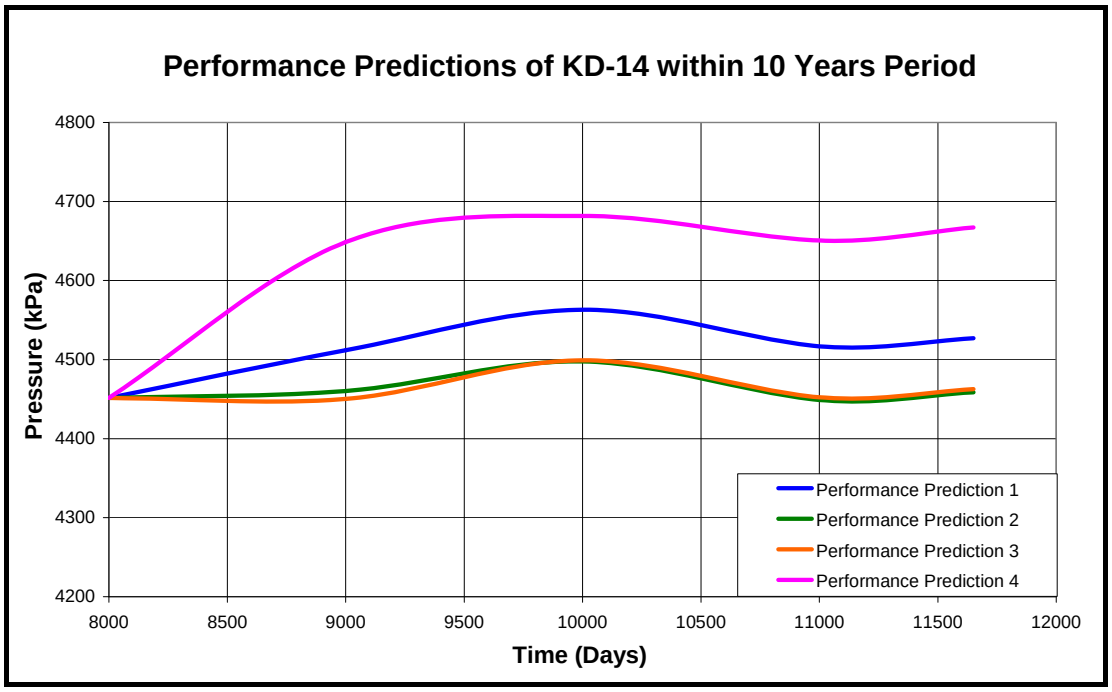

Figure 4.28 Performance prediction run curves of KD-14

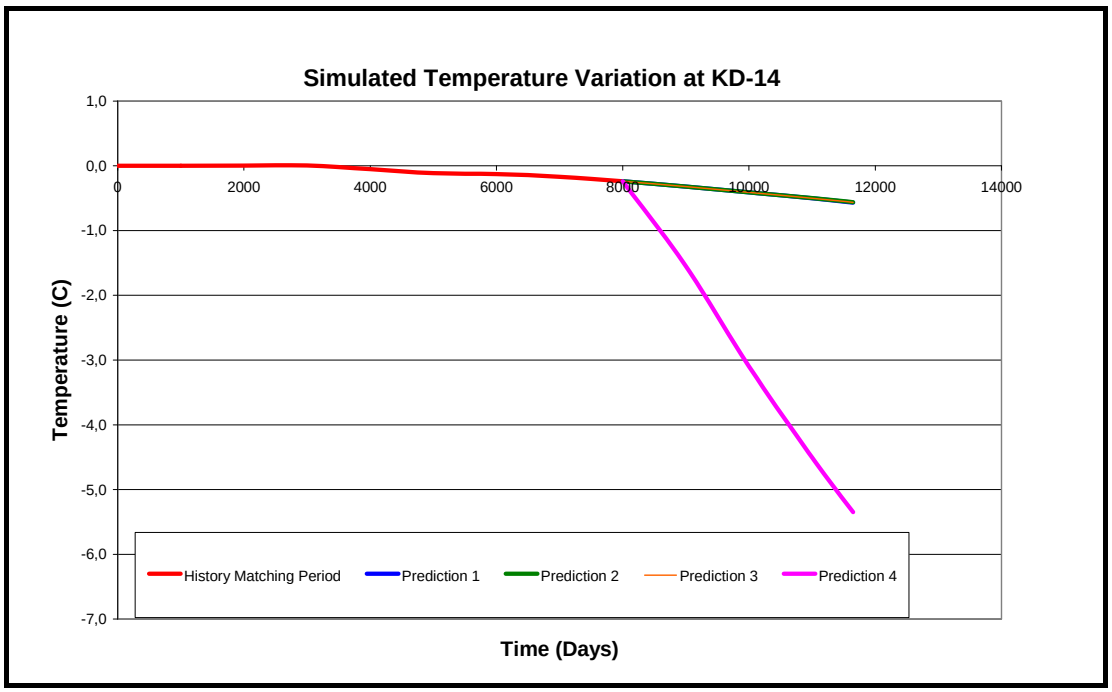

Figure 4.29 Temperature variation of well KD-14 in the modeling period

4.2.4. Performance Prediction of KD-15

Prediction runs created very low differences in well KD-15's pressure and temperature, except Prediction Run-4 (Figure 4.30). In the first three runs, general increasing trend in pressure continues. This shows that, KD-15 is quite preserved from the operational modifications at the other wells.

The largest difference is obtained in the forth prediction run. Being a reinjection well, KD-15 is supposed to have highest negative effects related with reinjection.

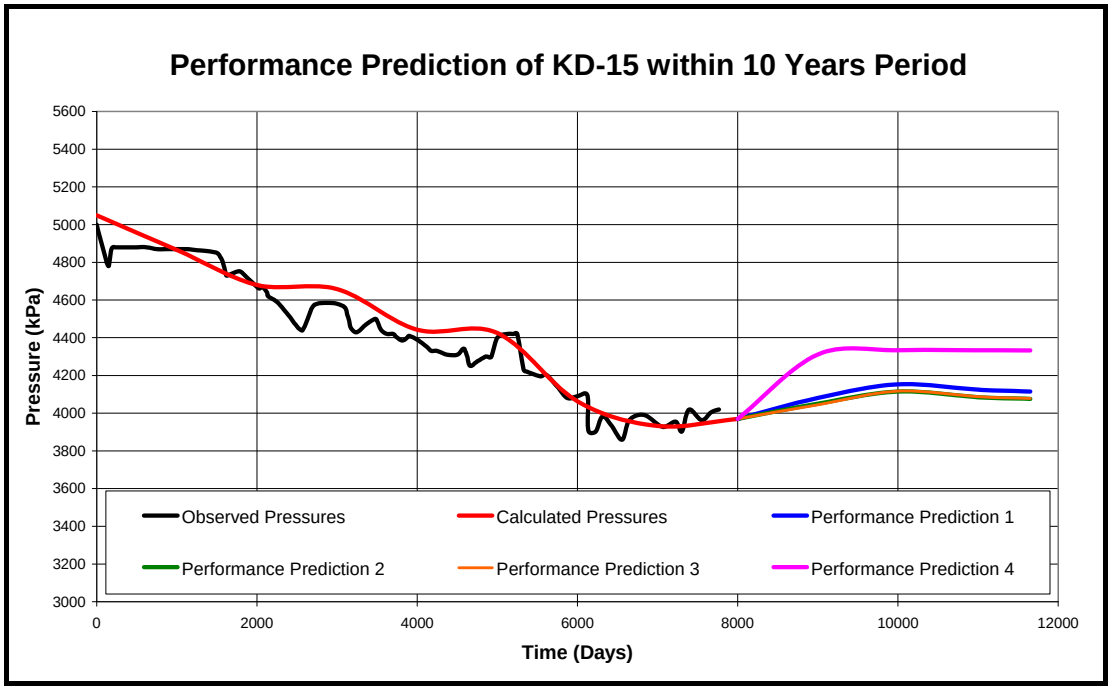

Figure 4.30 History matching and performance prediction run results of KD-15

Pressure increase in Prediction Run-1 is calculated to be 146 kPa, 107 kPa in Run-2 and 109 kPa in Run-3. In Prediction Run-4, a drastic raise which is 364 kPa is monitored (Figure 4.31).

Well-bore temperature is also highly affected in the Prediction Run-4. While experiencing roughly 0 °C decline in the other prediction runs, in Run-4, reservoir temperature looses about 28 °C at the well location (Figure 4.32).

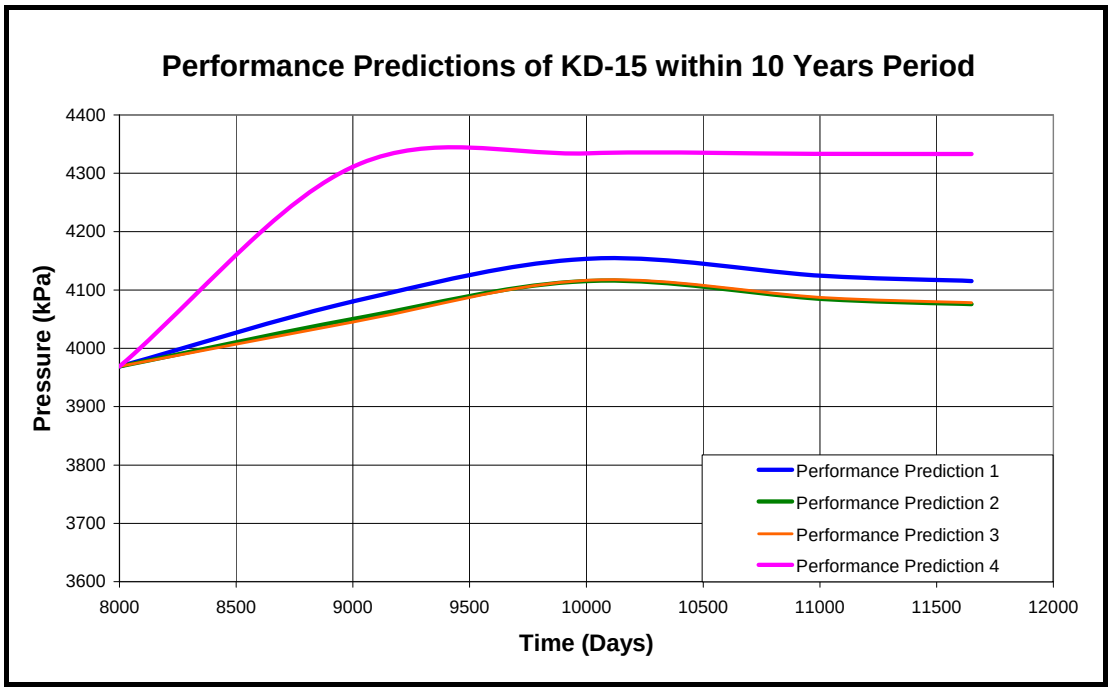

Figure 4.31 Performance prediction run curves of KD-15

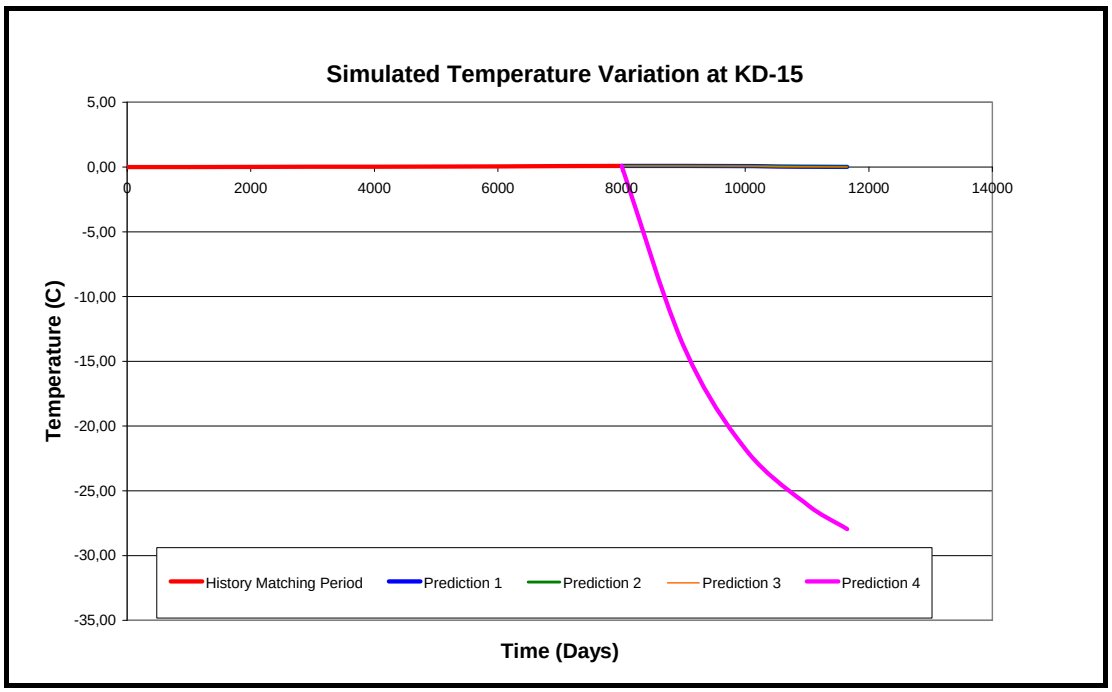

Figure 4.32 Temperature variation of well KD-15 in the modeling period

4.2.5. Performance Prediction of KD-16

Like the wells KD-14 and KD-15, an increasing trend is observed at the well KD-16, as a result of all performance predictions (Figure 4.33). The amount of this increase varies with the proximity of the producer or injector of that particular prediction run.

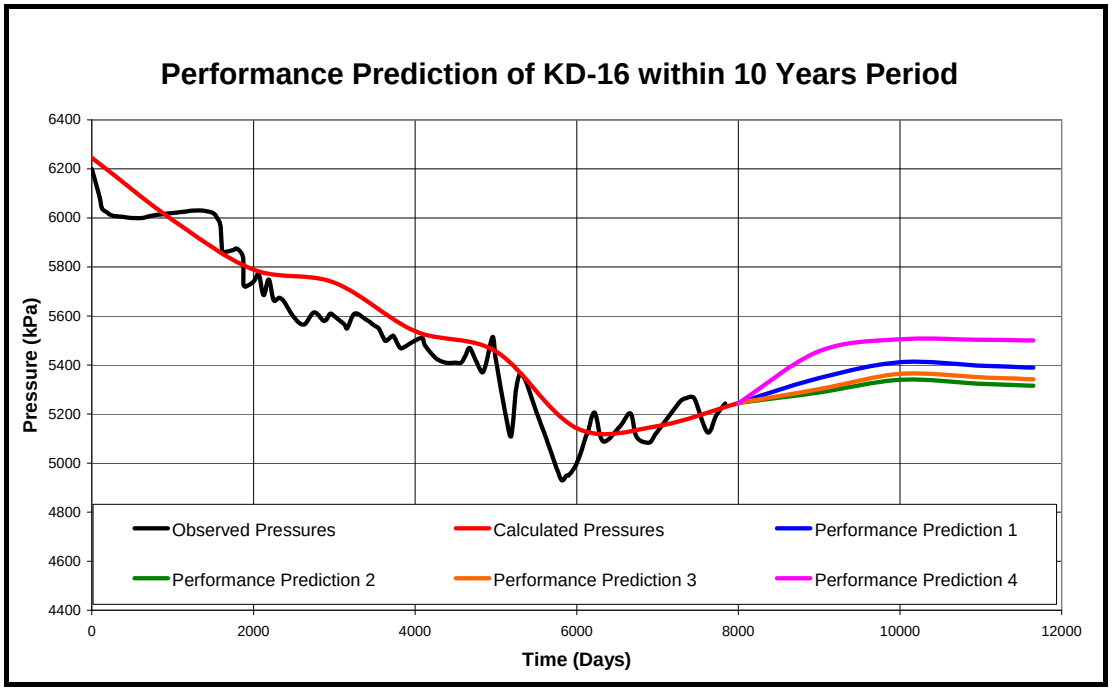

Figure 4.33 History matching and performance prediction run results of KD-16

While Prediction Run-1 results in 145 kPa increase, Run-2 adds 71 kPa and Run-3 adds 97 kPa to the well-bore pressure of the KD-16 well. Prediction Run-4 has higher influence, so that a 256 kPa is gained at the end of this prediction (Figure 4.34).

In temperature variations, prediction runs from 1 to 3 has given 0.25 °C decrease, on the other hand in Prediction Run-4, there is a drop at the range of 7.5 °C (Figure 4.35).

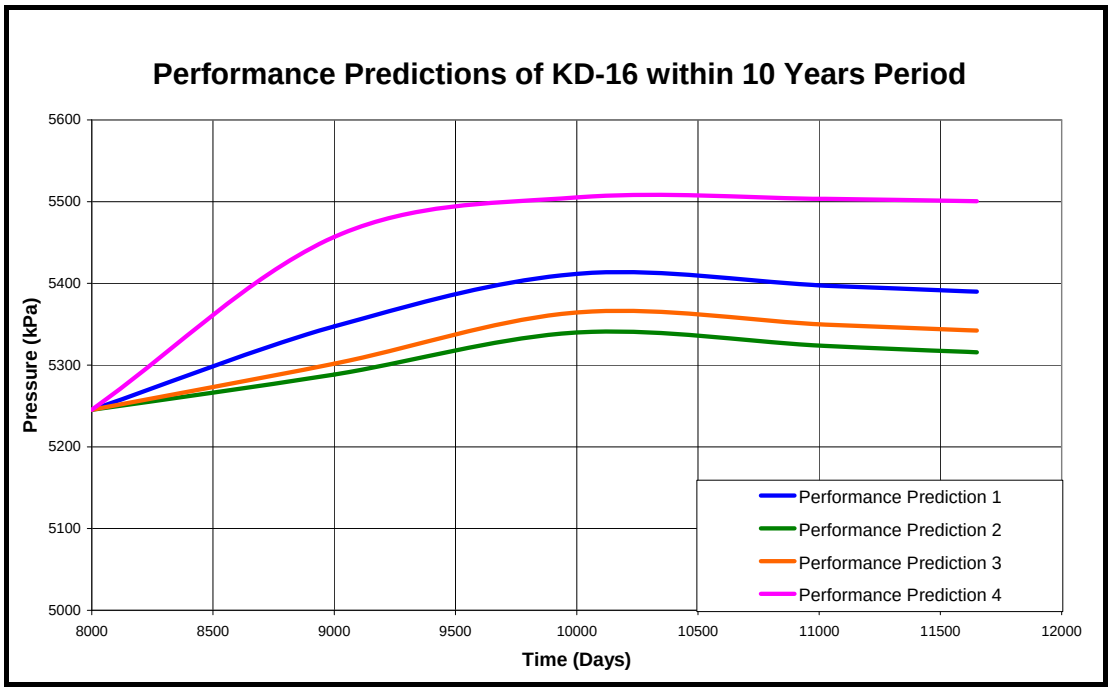

Figure 4.34 Performance prediction run curves of KD-16

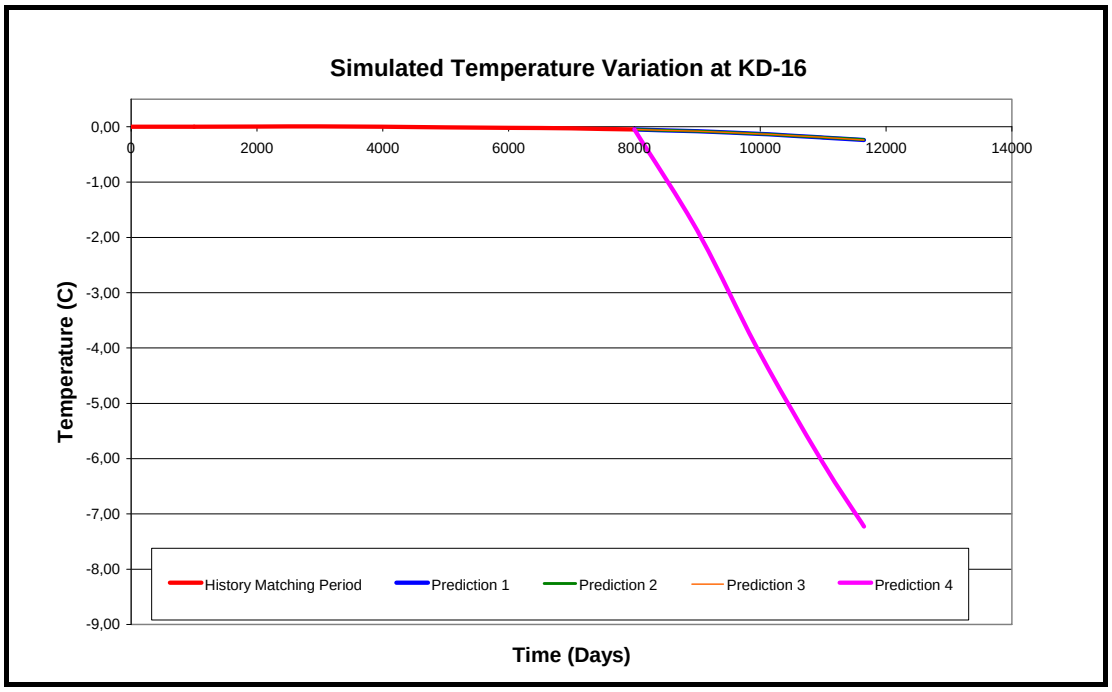

Figure 4.35 Temperature variation of well KD-16 in the modeling period

4.2.6. Performance Prediction of KD-20

At the well KD-20 there is an increasing trend at the end of history matching. This trend is continued in Prediction Run-4, while the other runs give declining pressure profiles (Figure 4.36).

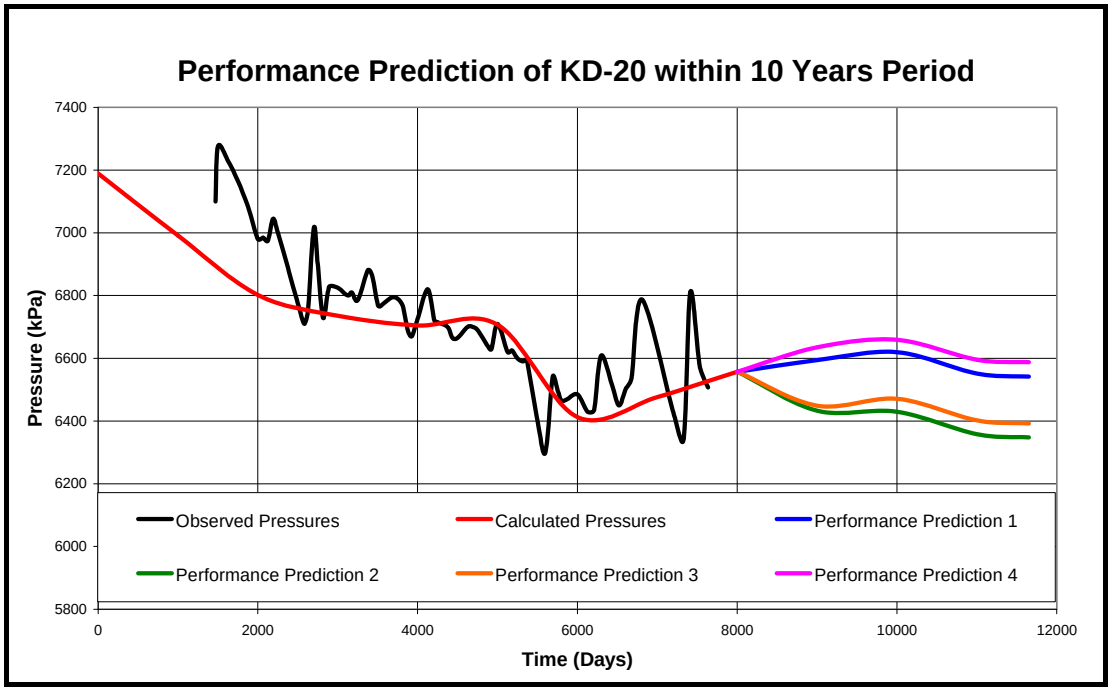

Figure 4.36 History matching and performance prediction run results of KD-20

In Prediction Run-1, decline could be considered negligible with 16 kPa (Figure 4.37). So, the bottom-hole pressure of KD-20 could be regarded as constant in this run.

In Prediction Runs 2 and 3, there is an apparent pressure decrease caused by the production wells added to the system. This is 209 kPa in Prediction Run-2 and 165 kPa in Prediction Run-3. In Prediction Run-4 an increase is calculated as 30 kPa.

Temperature variation of the well is quite large in also history matching period. The decreasing trend continues in the prediction periods up to 3 °C in Prediction Run-4 and up to approximately 2 °C in the other prediction runs (Figure 4.38).

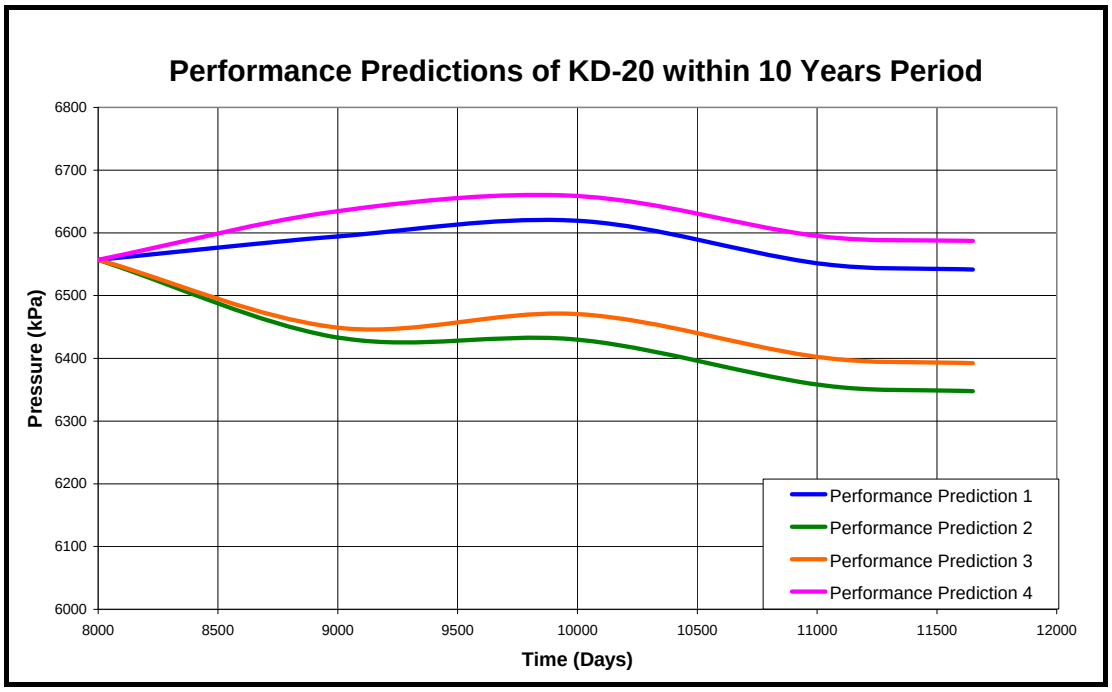

Figure 4.37 Performance prediction run curves of KD-20

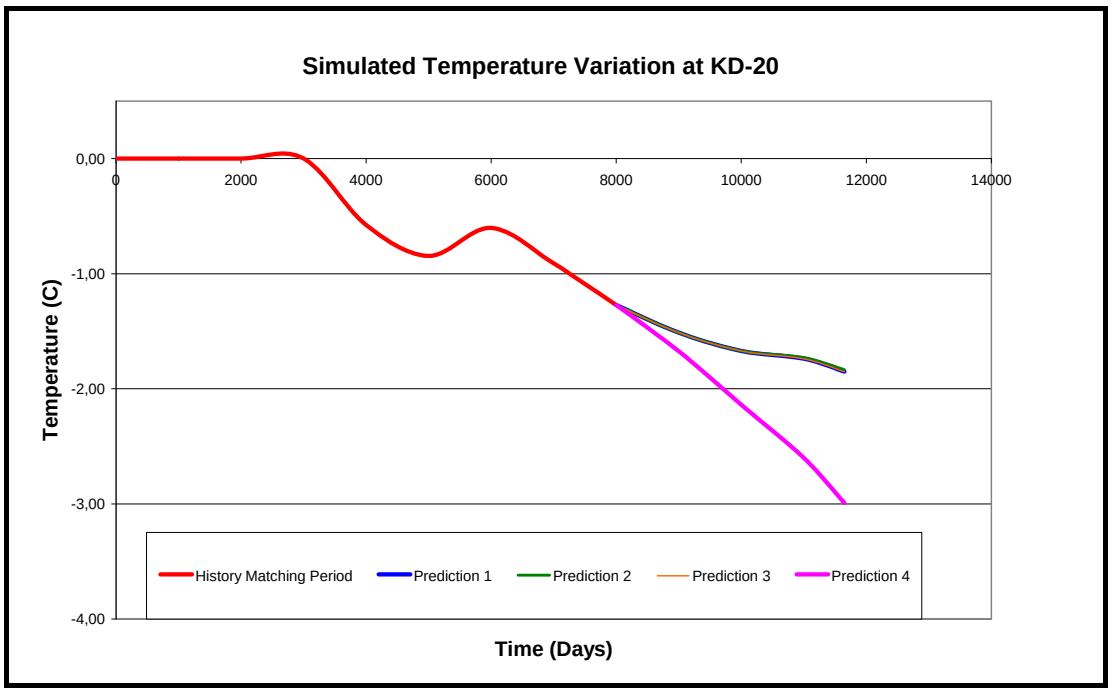

Figure 4.38 Temperature variation of well KD-20 in the modeling period

4.2.7. Performance Prediction of KD-21

In all of the prediction runs of KD-21, there appear increases in the bottom-hole pressures. Because that the situation of the well in the geothermal field is sufficiently far away from the newly added wells of the prediction runs (Figure 3.4), all the predictions have affected more or less in the same way and this resulted in a regularly spaced geometry in the prediction curves (Figure 4.39).

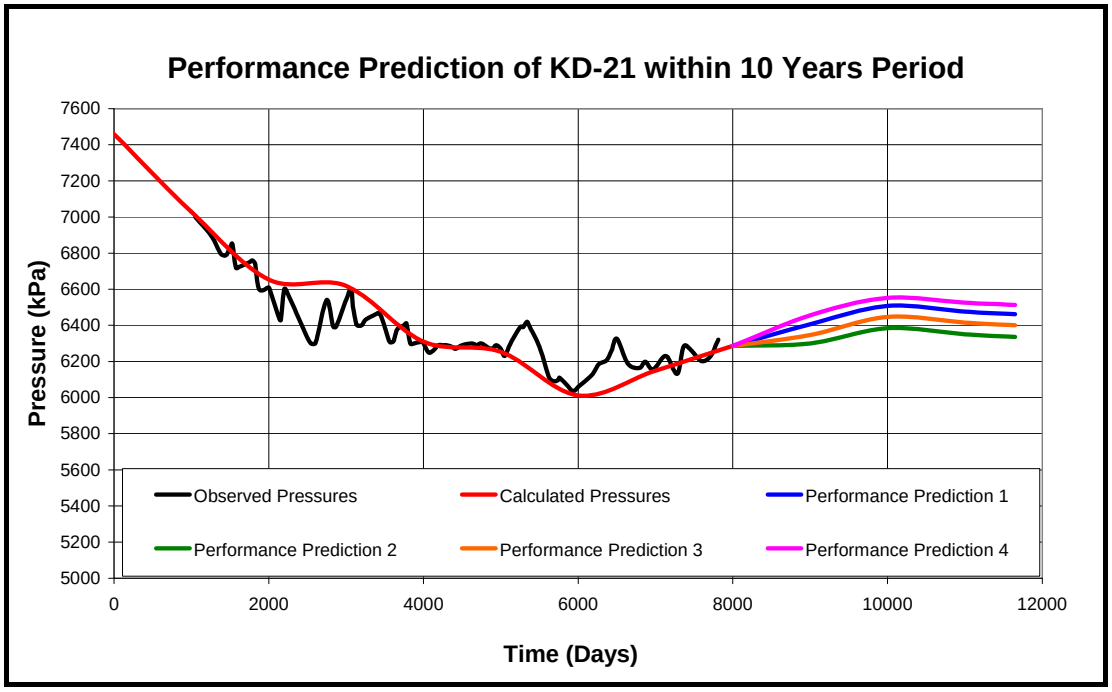

Figure 4.39 History matching and performance prediction run results of KD-21

In Prediction Run-1 increase in well pressure is found to be 176 kPa, in Prediction Run-2 this increase stays at 50 kPa, in Prediction Run-3 again ascends to 114 kPa and in Prediction Run-4 reaches to 228 kPa (Figure 4.40).

Temperature decline profile of this well is quite similar to the profiles of the wells KD-14 and KD-16. The drop is at 0.5 °C in the Prediction Runs 1, 2 and 3, and at 3 °C in the Prediction Run-4 (Figure 4.41).

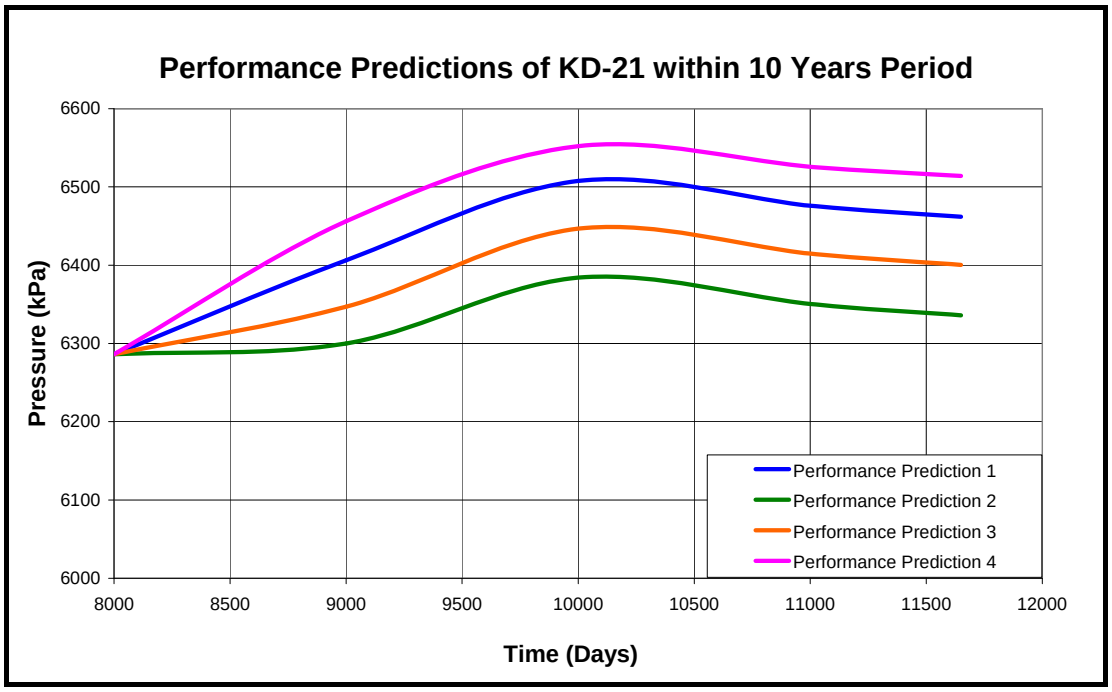

Figure 4.40 Performance prediction run curves of KD-21

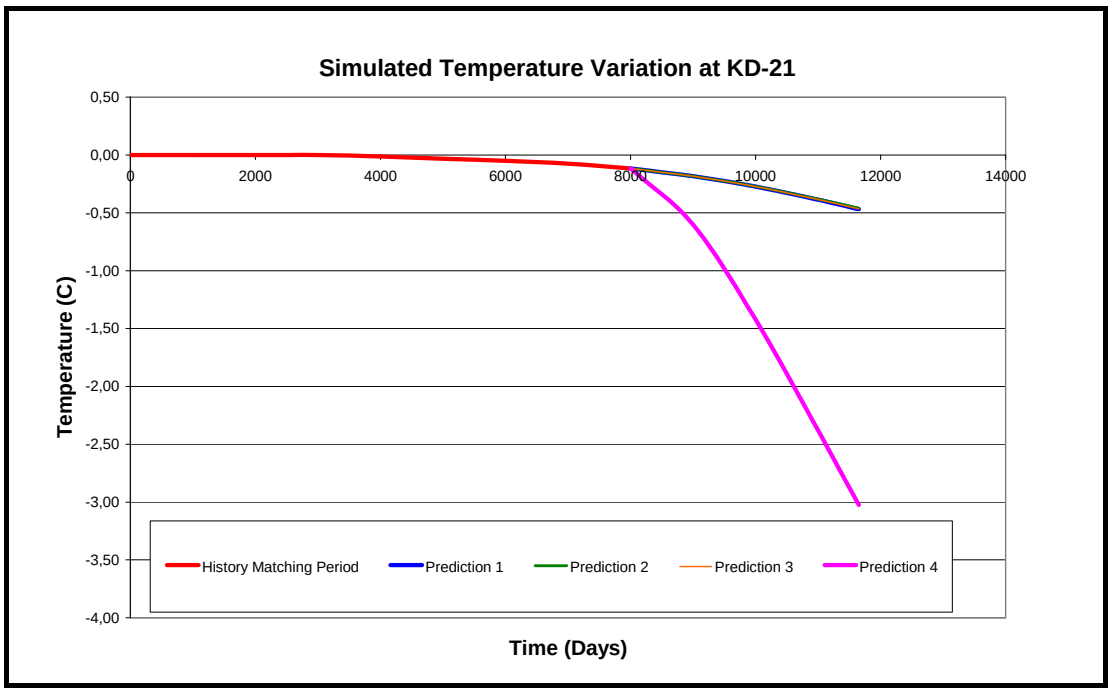

Figure 4.41 Temperature variation of well KD-21 in the modeling period

4.2.8. Performance Prediction of KD-22

In the Performance Prediction Runs 1 and 4, bottom-hole pressure of the well KD-22 has increased. In Prediction Runs 2 and 3 this pressure has dropped.
But the general trend in pressure response seems stabilized (Figure 4.42).

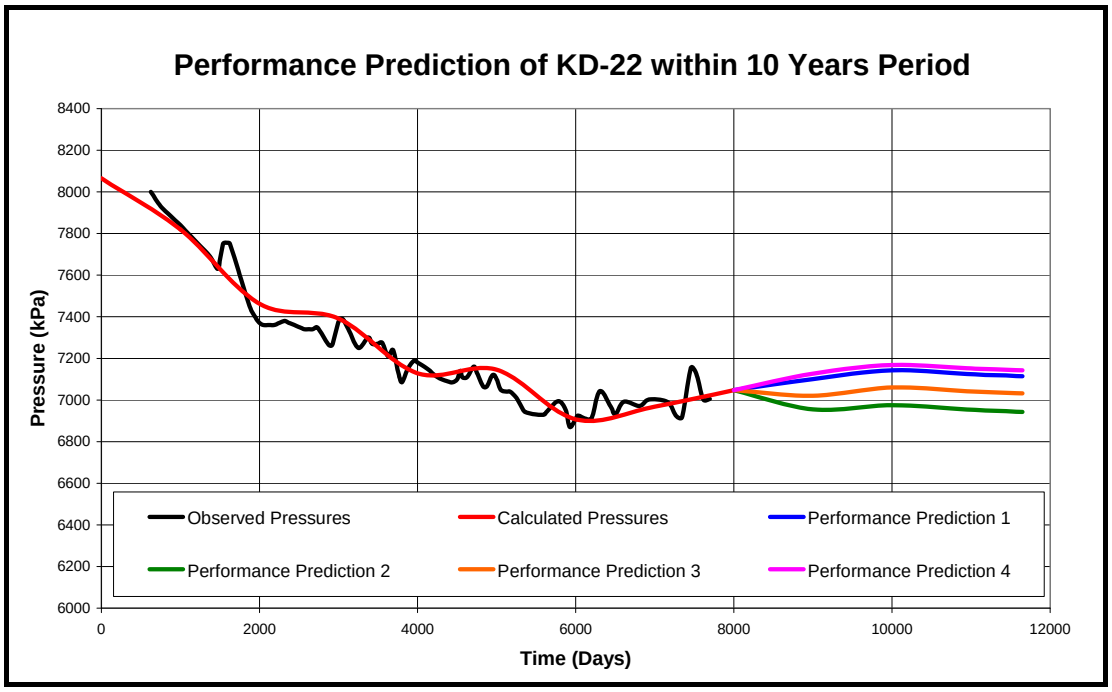

Figure 4.42 History matching and performance prediction run results of KD-22

In the first prediction run, the well pressure has experienced a 67 kPa increase (Figure 4.43). Second run resulted with 104 kPa decrease. In the third run a small decrease as 16 kPa and Prediction Run-4 an increase as 96 kPa has been observed.
In terms of temperature, there is a decrease about 3°C in the Prediction Run-4 and about 1°C decrease in the other prediction runs (Figure 4.44).

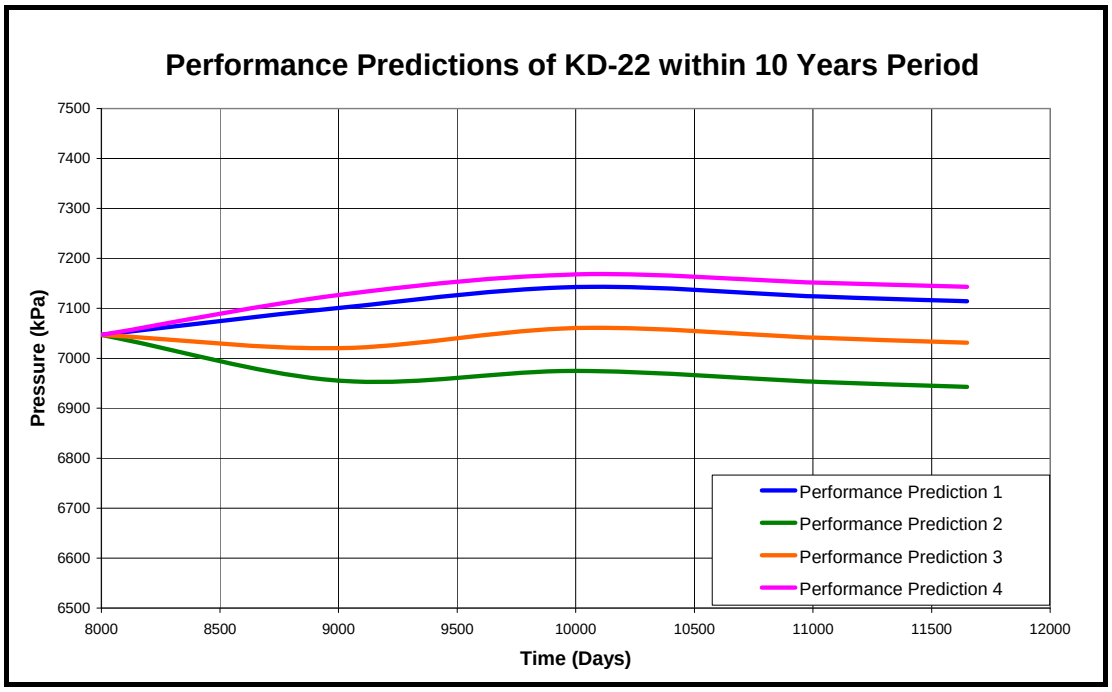

Figure 4.43 Performance prediction run curves of KD-22

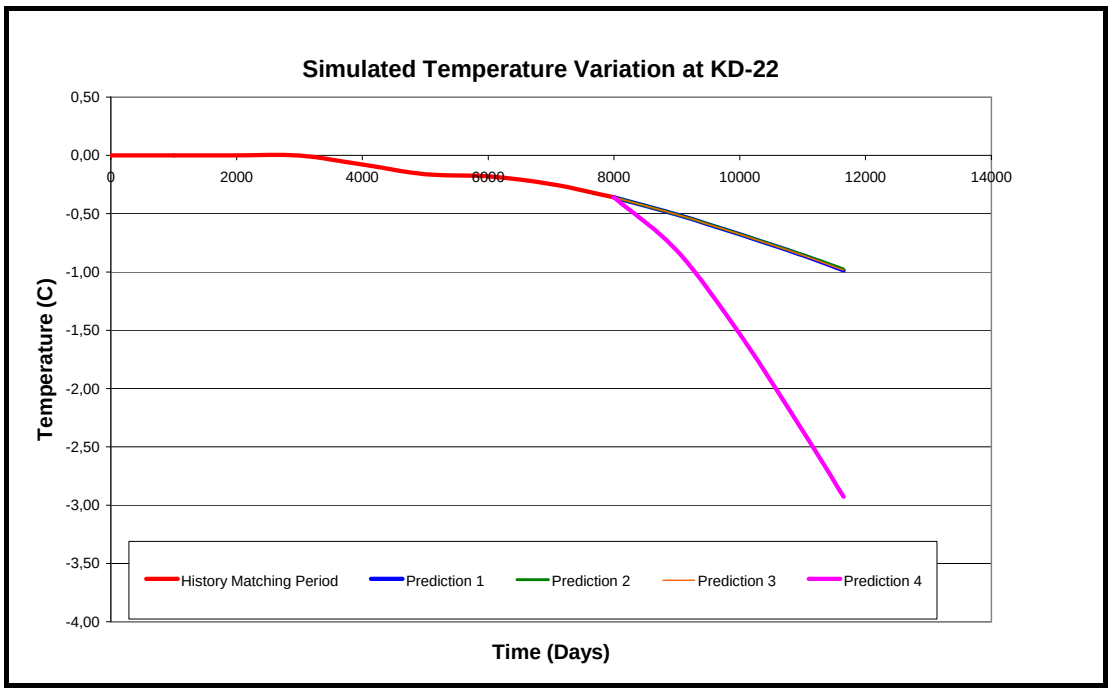

Figure 4.44 Temperature variation of well KD-22 in the modeling period

4.2.9. Performance Prediction of R-1

At the well R-1 a drastic decrease in pressure has been observed after it has been put into operation after 6000 days period. This decrease continues also in the prediction periods but lowering after a while (Figure 4.45). At the end of prediction runs, the decline profile gets almost flat. The decrease gets bigger with the addition of new production wells in prediction Runs 2 and 3.

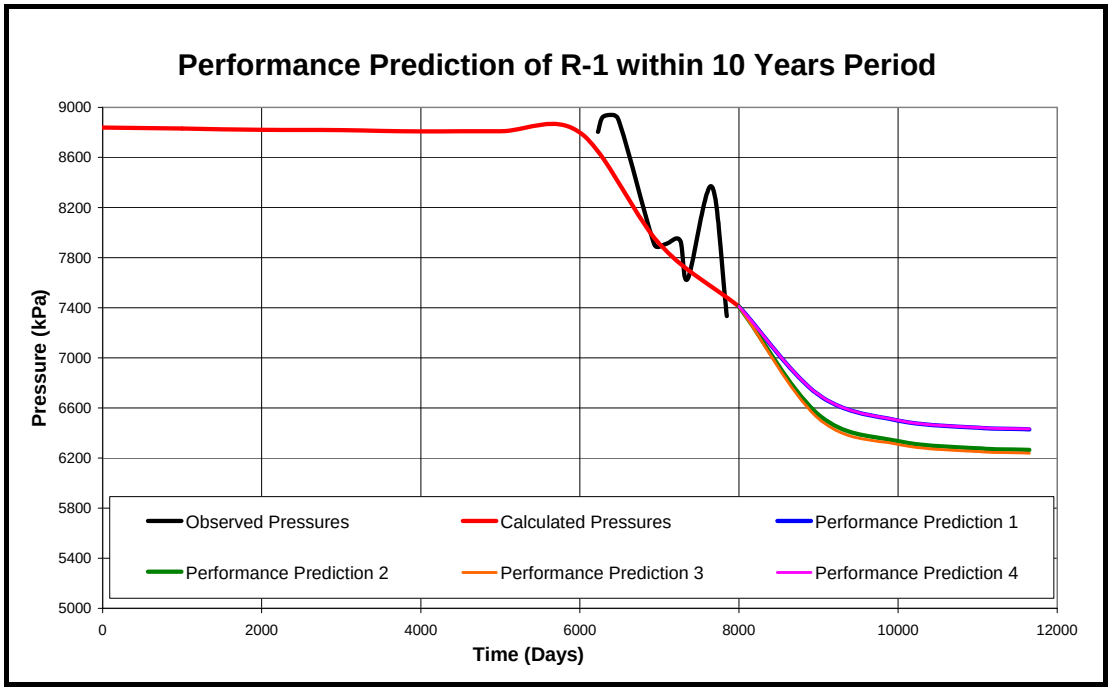

Figure 4.45 History matching and performance prediction run results of R-1

In Performance Prediction Run-1, 880 kPa drop is calculated. In Prediction Run-2, this value is 1145 kPa and in Prediction Run-3 it is 1170 kPa. In the forth prediction, the decline is found to be 978 kPa (Figure 4.46).

The bottom-hole temperature of the well R-1 hasn't been affected by the addition of any other production or reinjection well. This could be explained with the quite independent location of this well which is far away from the other production wells but closer to the constant temperature boundaries. The highest decline in temperature for this well is calculated as 0.13 °C in Prediction Run-3 (Figure 4.47).

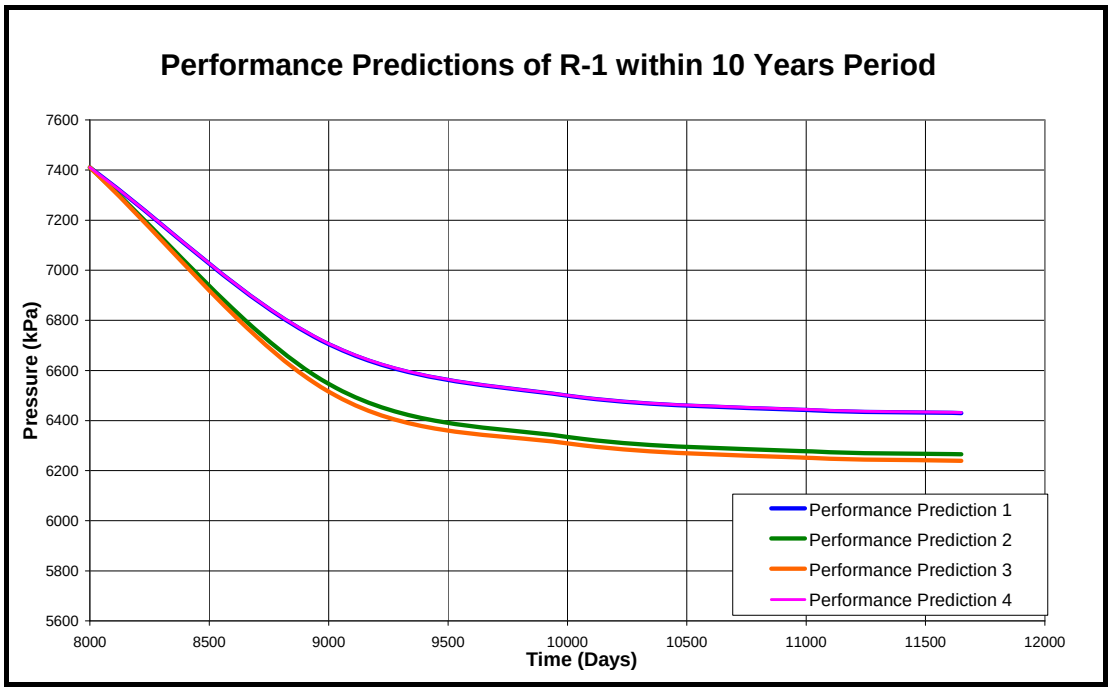

Figure 4.46 Performance prediction run curves of R-1

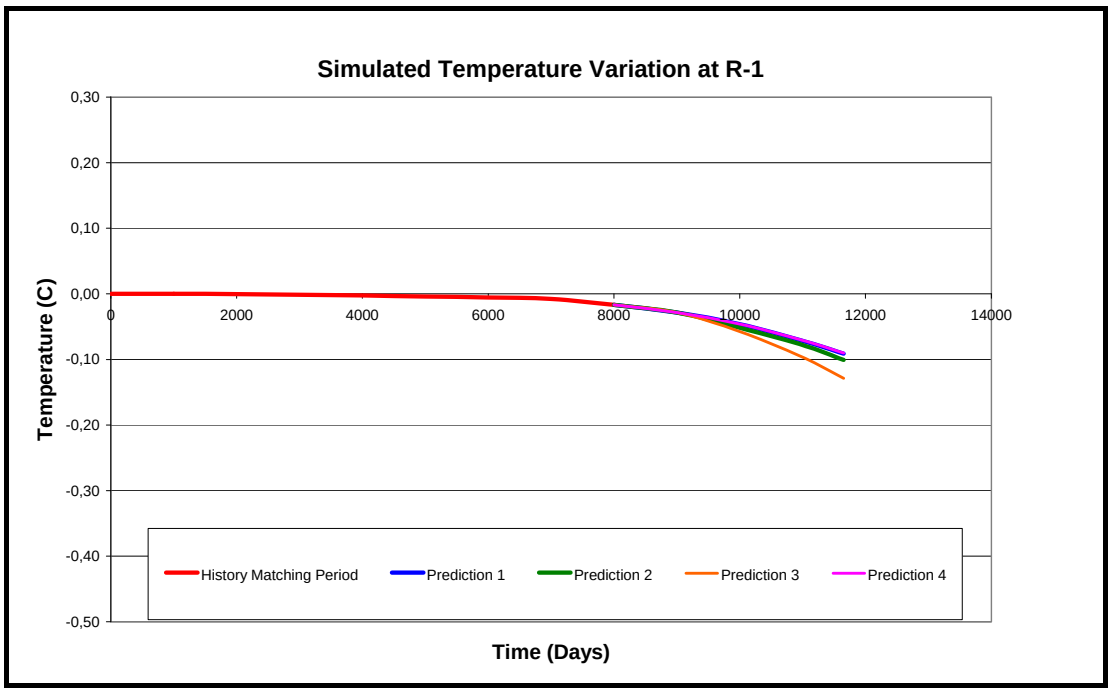

Figure 4.47 Temperature variation of well R-1 in the modeling period

4.2.10. Performance Prediction of R-2

The well R-2 has also started operating as a reinjection well after 6000 days period which shows the end of the year 2000. After this time, the increasing of well pressure starts. This trend also continues in the Performance Prediction Runs 1 and 4. But in Prediction Runs 2 and 3, the well shows high decline profiles with the effects of production from the wells R-3 and KD-2 (Figure 4.48).

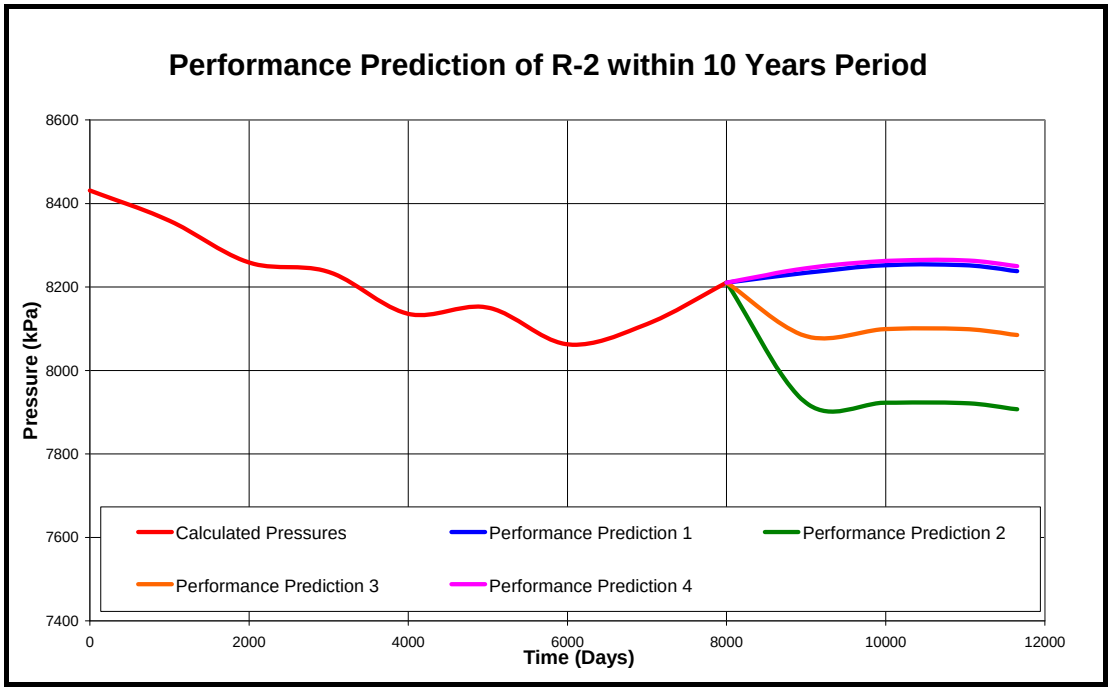

Figure 4.48 History matching and performance prediction run results of R-2

In Prediction Run-1, there is a small increase as 28 kPa in the well pressure of R-2. In the second prediction a decrease as 303 kPa is calculated. In Prediction Run-3 again a decrease as 125 kPa is found. Prediction Run-4 gives an increase as 40 kPa to the bottom-hole pressure of this well (Figure 4.49).

From the Figure 4.50, it can be inferred that, there is no effect of the prediction runs to the temperature change in the well R-2. It is understood from the graph that, the only effect in the temperature behavior of R-2 is the reinjection process from itself. Here the cooling of the well reaches to 32 °C at the end of all prediction periods (Figure 4.50).

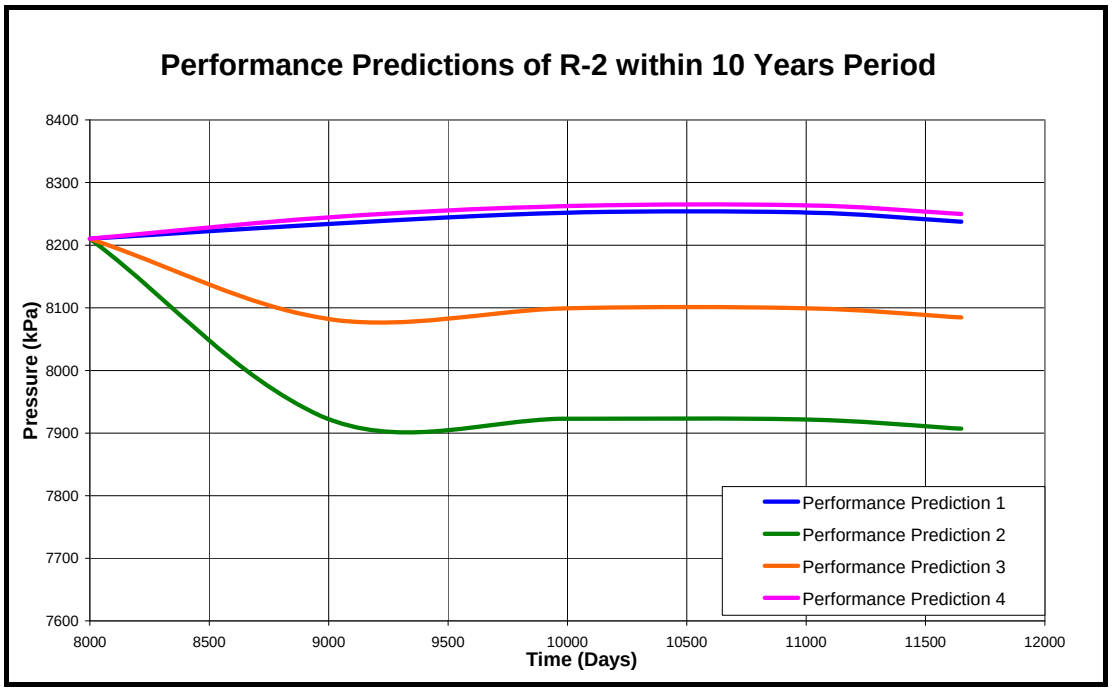

Figure 4.49 Performance prediction run curves of R-2

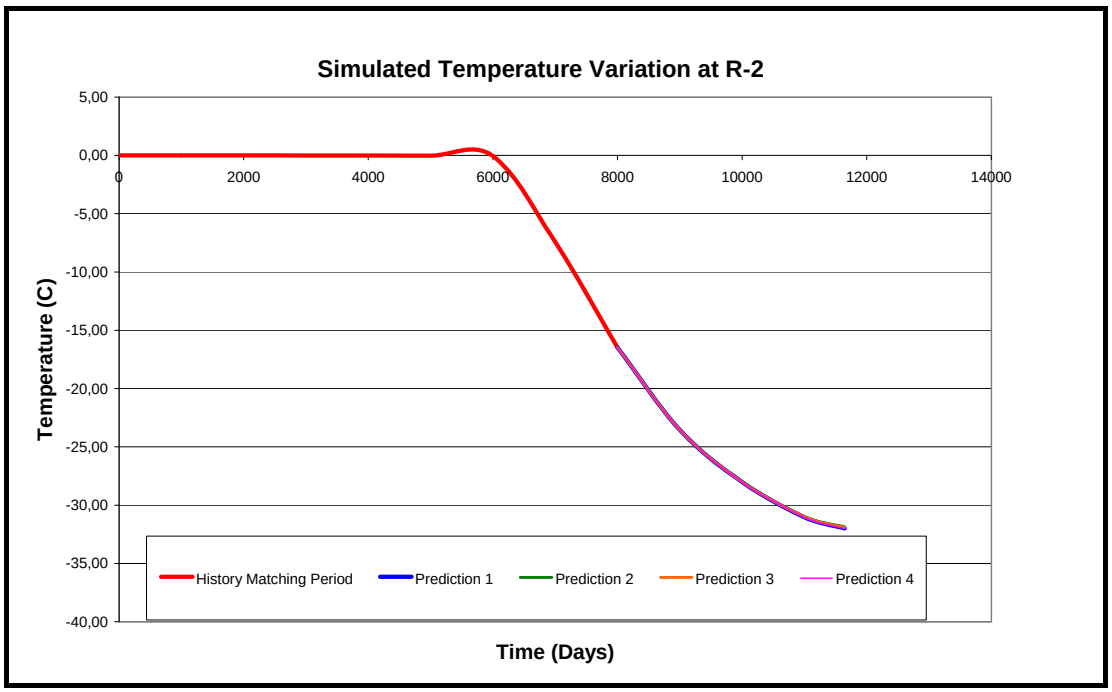

Figure 4.50 Temperature variation of well R-2 in the modeling period

CHAPTER 5

DISCUSSION AND CONCLUSIONS

Being one of the highest potential and the energy producing geothermal fields in Turkey, Kızıldere Geothermal Field gets always immense attention of research. Moreover, there are still problems that have to be solved in this field related with the production. This study is dedicated to make a foreseeing of the future state of geothermal field and to suggest acceptable solutions to the current problems of the field with minimizing the adverse effects. For this purpose, a numerical model of Kızıldere Geothermal Field is created and questions in mind are implemented to the model as performance prediction runs. The numerical model of the field is generated by employing a two dimensional simulation code, SUTRA-VERSION 1284-2D of U.S. Geological Survey.

While developing the conceptual model;

1. Only saturated flow and steady-state transport are assumed to be effective within the domain.
2. The thickness of producing zone is fixed to a level at the vertical extent of reservoir which is equal to the depth of İğdecik Formation.
3. As two deep wells R-1 and R-2 have very high pressure values, their pressures are normalized by subtracting the hydrostatic pressures below the depth of İğdecik Formation. Thus, they have considered as shallow wells with high production capacities.
4. The fault zones found in the region are assumed to possess lower permeabilities compared to the rest of the area.

Two of the basic operational problems in Kızıldere Geothermal Field have been the decrease in reservoir pressure of the field due to the production from KD wells and disposal of the waste water after energy production.

For solving these problems, a re-injection project has been put into practice and two deep wells R-1 (producer) and R-2 (injector) started operation after year 2000. Since the debut of these wells, there appear steady and even increasing trends in pressures of KD wells (Yeltekin and Parlaktuna, 2006).

Effects of these wells to the system are considered and tried to be simulated in the model. It could be suggested that an appropriate profile is achieved at the end of history matching.

After the calibration processes give satisfactory results, the performance of geothermal field is predicted under different production and reinjection scenarios. Four different conditions are studied (Table 4.1) and the following conclusions are drawn from the analysis of the results of these prediction runs:

1. In the first performance prediction trial of the field with existing wells resulted in an increasing trend in the pressures of most of the wells, other than R-1. In temperatures, a drop about 7°C in KD-6 and about 2°C in KD-13 and KD-20 is calculated. Totally, 91.527.913 m^3 fluid is produced and 21.900.000 m^3 fluid is reinjected into the reservoir in this prediction trial (Table 5.1).

2. Among the second performance prediction run, a newly drilled deep well, R-3 is recommended to be a producer having a production rate same with R-1. At the end of this trial, the bottom-hole pressure of the wells close to the well R-3 like KD-6, KD-13, KD-20, KD-22, R-1 and R-2 have experienced a drop, while the others haven't been affected or had small increases. Temperature decrease in this prediction run is quite similar to the results of Prediction Run-1. Again, the drops in well temperatures about 7°C in KD-6 and about 2°C in KD-13 and KD-20 are replicated. In total, 103.466.336 m^3 fluid is produced and 21.900.000 m^3 fluid is reinjected into the reservoir in this prediction run period (Table 5.1).

3. The third prediction run assumes the observation well KD-2 is converted to a production well having again a production rate same with R-1. Probably, the settlement of KD-2 is quite far away from the production well, no big pressure decrease has occurred in this prediction trial. Only in KD-20, R-1 and R-2 bottom-hole pressures have reduced in small amounts. Also in temperature, no big decline in well temperatures has been monitored. Resembling results to the other two runs are computed showing that the production from the well KD-2 has negligible effects on the reservoir temperature. In this prediction run, totally 103.466.336 m^3 fluid is produced and 21.900.000 m^3 fluid is reinjected into the reservoir (Table 5.1).

4. In the forth prediction, the production well KD-15 is converted to a reinjection well with a re-injection rate same with R-2 which is 250 m^3/h and a continuous re-injection is done during the prediction period. This operation has raised the bottom-hole pressures of most of the well, with the exception of the well R-1. On the other hand, there have been great decreases in the well temperatures of KD-15 and the production wells close to it. In KD-15 28 °C, in KD-16 7 °C, in KD-14 5.5 °C, and in KD-20 KD-21 and KD-22 3 °C of temperature drop has occurred at the end of the

prediction period. 91.527.913 m^3 fluid is produced and 43.800.000 m^3 fluid is reinjected into the reservoir (Table 5.1).

Table 5.1 Production and reinjection amounts used in prediction runs

Prediction Run No.	Total Production (m^3)	Total Reinjection (m^3)	Percentage of Reinjection in Production (%)
1	91.527.913	21.900.000	23,9
2	103.466.336	21.900.000	21,2
3	103.466.336	21.900.000	21,2
4	91.527.913	43.800.000	47,9

With considering the limitations of the tools in hand in evaluating the results gained from this model, quite meaningful outcome are obtained from this study.

- The first important question has been related with the effect of production from the first deep well R-1. In the model, the effected zone is estimated as in Figure 4.2. This zone doesn't cover the production region. Also at R-1 the decline in pressure is predicted to be in the range 980-1145 kPa which is acceptable when the actual pressures in the well R-1 which are much higher in reality are regarded.
- The second actual question of the field is the full-scale reinjection from the well R-2 and related cooling at the production wells. The basic aim of reinjection is increasing of reservoir pressure and giving the production wells pressure support. This purpose is achieved with putting R-2 into operation. But a temperature fall in the well KD-6 has been reported in literature and the extent of this decrease is still questionable.

  The model has given a decline profile at KD-6 reaching about 7 °C in ten years period. Reinjection from R-2 doesn't have a strong influence on the other production wells.

- Another important issue is the utilization of R-3 as a production well. This well was drilled as a reinjection well between R-1 and R-2 wells. It was supposed to have similar properties with R-1 or R-2 but it hasn't met the expectations up to the end of this study. In this study, a prediction run is planned to test the effect of this well if it had a production rate same with R-1. In this run, even though a decrease is seen in the neighborhood of R-3, no important effect is monitored in the bottom-hole pressures of the production wells (Figure 4.7). In the performance prediction period 1245 kPa decline in pressure at R-3 well has been calculated.
- The other aspect under consideration is the shifting of the production zone to the southwest sector of the field. This proposal is practiced by converting the well KD-2 which is found at the southwest of the area to a production well having the same production rate with R-1. KD-2 has experienced 1323 kPa decrease in bottom-hole pressure in the prediction period. This essay has given better results than the prediction run which is related with the production from R-3 in terms of pressure decrease in the other production wells. These results show that production from both R-3 and KD-2 are acceptable applications in the future operations of Kızıldere Geothermal Field.
- Finally, the condition of converting the KD wells to reinjection wells has been envisaged. After putting deep wells R-1 and R-2 into service, productions of KD wells are reduced since the needed amount is mostly met by R-1. Considering also that the KD wells are about to fill their economical life-span, the utilization of KD-15 as a reinjection well has been examined in the last prediction run. A continuous re-injection is done from the well during the prediction period having the same rate with R-2. The effect of the re-injection to the reservoir pressure has been simulated. The amount of fluid re-injected corresponds to 20-25 % of the total produced fluid during performance prediction period. Re-injection of the fluid from KD-15 has given the highest-pressure support of all the prediction runs, but the amount of fluid to be re-injected for this purpose is too high to be injected from this well. A huge decrease in the temperature of the well KD-15 is remarkably manifested in Figure 4.20. But in this prediction run the negative effects of reinjection could be observed not only on the reinjection well but also on the other production wells nearby. So this result supports the idea that application should be outside the production well region since the adverse affects of reinjection (early breakthrough, cooling) were experienced in short period of time (Yeltekin and Parlaktuna, 2006).

REFERENCES

Antics, M.A., 1998. Computer modeling of an over-pressured medium enthalpy geothermal reservoir located in deep sedimentary basin. Proceedings of the 23rd Workshop on Geothermal Reservoir Engineering, Stanford University, Stanford, California, 26–28 January 1998, pp. 362–367.

Aunzo, Z., Steingrimsson, B., Bodvarsson, G.S., Escobar, C., Quintanilla, A., 1989. Modeling studies of the Ahuachapa´n geothermal field, El Salvador. Proceedings of the 14th Workshop on Geothermal Reservoir Engineering Report, Stanford University, Stanford, California, 24–26 January 1989, pp. 287– 295.

Battistelli, A., Chersica, A., Ferragina, C., Matarrese, G., Pieroni, M., 1998. Simulation of the transport of aromatic amines in unsaturated zone for the evaluation of an environmental remediation project. Proceedings of the TOUGH Workshop ‘98, Berkeley, California, 4–6 May 1998, pp. 136–141.

Battistelli, A., Calore, C., Pruess, K., 1997. The simulator TOUGH2/EWASG for modeling geothermal reservoirs with brines and non-condensible gas. Geothermics 26 (4), 437–464.

Bertani, R., Cappetti, G., 1995. Numerical simulation of the Monteverdi zone (western border of the Larderello geothermal field). Proceedings World Geothermal Congress ‘95, Florence, 18–31 May 1995, pp. 1735–1740.

Bodvarsson, G.S., Gislason, G., Gunnlaugsson, E., Sigurdsson, O., Stefansson, V., Steingrimsson, B., 1993. Accuracy of reservoir predictions for the Nesjavellir geothermal field, Iceland. Proceedings of the 18th Workshop on Geothermal Reservoir Engineering, Stanford University, Stanford, California, 26– 28 January 1993, pp. 273–278.

Bodvarsson, G.S., Bjornsson, S., Gunnarsson, A., Gunnlaugsson, E., Sigurdsson, O., Stefansson, V., Steingrimsson, B., 1991. The Nesjavellir geothermal field, Iceland: 2. Evaluation of the generating capacity of the system. Journal of Geothermal Science and Technology 2 (4), 229–261.

Bodvarsson, G.S., Bjornsson, S., Gunnarsson, A., Gunnlaugsson, E., Sigurdsson, O., Stefansson, V., Steingrimsson, B., 1988. A summary of modeling studies of the Nesjavellir geothermal field, Iceland. Proceedings of the 13th Workshop on Geothermal Reservoir Engineering, Stanford University, Stanford, California, 19–21 January 1988, pp. 83–91.

Bodvarsson, G.S., 1988. Model predictions of the Svartsengi reservoir, Iceland. Water Resources Research 24 (10), 1740–1746.

Bodvarsson, G.S., Pruess, K., Lippmann, M.J., 1986. Modeling of geothermal systems. Journal of Petroleum Technology (September), 1007–1021.

Bozkurt, E., 2001, Neotectonics of Turkey – a synthesis, Geodinamica Acta, Vol. 14, pp. 3-30.

Bullivant, D.P., O'Sullivan, M.J., Blakeley, M.R., 1995. A graphical interface for a geothermal reservoir simulator. Proceedings World Geothermal Congress '95, Florence, 18–31 May 1995, pp. 2971–2976.

Burnell, J.G., 1992. Modeling mass, energy and chloride flows in the Rotorua geothermal system. Geothermics 21 (1/2), 261–280.

Butler, S.J., Sanyal, S.K., Henneberger, R.C., Klein, C.W., Gutierrez P., H., de Leon V., J.S., 2000. Numerical modeling of the Cerro Prieto geothermal field, Mexico. Proceedings World Geothermal Congress, Kyushu-Tohuku, Japan, May 28–June 10, 2000, pp. 2545–2550.

Cheng, H.P., Yeh, G.T., 1998. Development and demonstrative application of a 3-D numerical model of subsurface flow, heat transfer, and reactive chemical transport: 3DHYDROGEOCHEM. Journal of Contaminant Hydrology 34, 47–83.

Cheng, P., Lau, K.H., 1973. Numerical modeling of Hawaiian geothermal resources. Geothermics 2, 90–93.

Cohen, H.A., Dart, C.J., Akyüz, H.S., Barka, A., 1995. Syn-rift sedimentation and structural development of the Gediz and Büyük Menderes graben, western Turkey. Journal of Geological Society, London 152, 629–638.

Dagan, G., Neuman, S.P. (Eds.), 1997. Subsurface Flow and Transport: A Stochastic Approach. Cambridge University Press, New York.

Dominco, E. (1974). Geothermal Energy Survey of Western Anatolia, Project Findings and Recommendations, Report to United Nations Development Program. New York, USA.

Dora O., Candan, O., Dürr, S., Oberhanslı, R., 1997, New evidence on the geotectonic evolution of the Menderes Massif. In: Pişkin O, Ergün M, Savaşcın Y., Tarcan, G., (eds) Proc International Earth Sciences Colloquium on the Aegean Region, İzmir-Güllük, Turkey, pp 53–72.

Dumont, J.F., Uysal, Ş., Şimşek, Ş., 1979, Karamanderesi, I.H., Letouzcy, F., Güneybatı Anadolu'daki grabenlerin oluşumu, Min. Res. Expl. Inst. Turkey Bull., Vol. 92, pp. 7–17.

Duvarcı, E., 2001, Geolectric structure of inland area of the Gökova rift, southwest Anatolia and its tectonic implications, J. Geodyn., Vol. 31, pp. 33–48.

Ediger, V.¸ Ş., and E. Kentel. 1999. Renewable energy potential as an alternative to fossil fuels in Turkey. Energy Convers. Mgmt. 40:743–755.

Eltez, M. 1997. Geothermal Energy Report, Prepared for the Scientific and Technical Research Council of Turkey, TUBITAK (in Turkish).

Erdoğan, B., Güngör, T., 1992, Menderes Masifinin Kuzey Kanadının Stratigrafisi ve Tektonik Evrimi, Turk. Assoc. Petrol. Geol. Bull., Vol. 4, pp. 9 – 34.

Erişen, B., Akkuş, İ., Uygur, N., Koçak, A., (Eds.), 1996. Türkiye Jeotermal Envanteri, MTA, Ankara, 480 sayfa.

Eyidoğan H., 1988, Rates of crustal deformation in western Turkey as deduced from major earthquakes, Tectonophysics, Vol. 148, pp. 83–92.

Finsterle, S., Pruess, K., 1999. Automatic calibration of geothermal reservoir models through parallel computing on a workstation cluster. Proceedings of the 24th Workshop on Geothermal Reservoir Engineering, Stanford University, Stanford, California, 25–27 January 1999, pp. 123–130.

Finsterle, S., Pruess, K., 1995. Solving the estimation-identification problem in two-phase flow modeling. Water Resources Research 31(4), 913–924.

Gelhar, L.W., 1993. Stochastic Subsurface Hydrology. Prentice-Hall, Englewood Cliffs, NJ.

Gemici, Ü., Tarcan, G., 2002, Hydrogeochemistry of the Simav geothermal field, western Anatolia, Turkey, Journal of volcanology and geothermal research, Vol. 116, pp. 215-233.

Glover, P.W.J., Matsuki, K., Hikima, R., Hayashi, K., 1998. Fluid flow in synthetic rough fractures and application to the Hachimantai geothermal Hot Dry Rock test site. Journal of Geophysical Research 103 (B5), 9621–9635.

Grant, M.A., Donaldson, I.G., Bixley, P.F., 1982. Geothermal Reservoir Engineering. Academic Press, New York.

Günerhan, G. G., Koçar, G., and Hepbaşlı, A., 2001. Geothermal energy utilization in Turkey. Int. J. Energy Res. 25:769–784.

Hadgu, T., Zimmerman, R.W., Bodvarsson, G.S., 1995. Coupled reservoir-wellbore simulation of geothermal reservoir behavior. Geothermics 24 (2), 145–166.

Halfman, S.E., Lippmann, M.J., Bodvarsson, G.S., 1986. Quantitative model of the Cerro Prieto geothermal field. Proceedings of the 11th Workshop on Geothermal Reservoir Engineering, Stanford University, Stanford, California, 21–23 January 1986, pp. 127–134.

Hanano, M., Seth, M.S., 1995. Numerical modeling of hydrothermal convection systems including super-critical fluid. Proceedings World Geothermal Congress ‘95, Florence, 18–31 May 1995, pp. 1681– 1686.

Hepbaşlı , A., A. Özdamar, and N. Özalp. 2001. Present status and potential of renewable energy sources in Turkey. Energy Sources 23:631–648.

Hodges, R.A., Falta, R.W., Finsterle, S., 1998. Three-dimensional simulation of DNAPL transport at the Savannah River site. Proceedings of the TOUGH Workshop ‘98, Berkeley, California, 4–6 May 1998, pp. 136–141.

Hu, B., 1995. Reservoir simulation of the Yangbajian geothermal field in Tibet, China. Proceedings World Geothermal Congress ‘95, Florence, 18–31 May 1995, pp. 1691–1695.

Ingebritsen, S.E., Sorey, M.L., 1985. Quantitative analysis of the Lassen hydrothermal system, northcentral California. Water Resources Research 21(6), 853–868.

Ishido, T., Tosha, T., 1998. Feasibility study of reservoir monitoring using repeat self-potential measurements. Transactions Geothermal Resources Council 22, 171–177.

Ishido, T., Sugihara, M., Pritchett, J.W., Ariki, K., 1995. Feasibility study of reservoir monitoring using repeat gravity measurements at the Sumikawa geothermal field. Proceedings World Geothermal Congress ‘95, Florence, 18–31 May 1995, pp. 853–859.

Kaya, O., 1982. Tersiyer sırt yitmesi: Doğu Ege bölgelerinin yapısı ve mağmatikliği için olasılı bir mekanizma, Türkiye Jeoloji Kurumu, Batı Anadolu’nun genç¸ tektoniği ve volkanizması paneli, 39–58 (in Turkish).

Kaygusuz, K. 1996. Rural energy resources: Applications and consumption in Turkey. Energy Sources 19:549–557.

Ketin, I., 1983. Türkiye Jeolojisine Giriş, Istanbul Teknik Üniversitesi Yayını, No. 32.

Kissling, W.M., Brown, K.L., O’Sullivan, M.J., White, S.P., Bullivant, D.P., 1996. Modeling chloride and CO_2 chemistry in the Wairakei geothermal reservoir. Geothermics 25, 285–305.

Lefebvre, R., Smolensky, J., Hockley, D., 1998. Modeling of acid mine drainage physical processes in the Nordhalde of the Ronnenburg mining district of Germany. Proceedings of the TOUGH Workshop ‘98, Berkeley, California, 4–6 May 1998, pp. 228–233.

McClusky, S., Balassanian, S., Barka, A., Demir, C., Ergintav, S., Georgiev, I., Gurkan, O., Hamburger, M., Hurst, K., Kahle, H., Kastens, K., Kekelidze, G., King, R., Kotzev, V., Lenk, O., Mahmoud, S., Mishin, A., Nadariya, M., Ouzounis, A., Paradissis, D., Peter, Y., Prilepin, P., Reilinger, P., Sanli, I., Seeger, H., Tealeb, A., Toksöz, M.N., Veis, G., 2000. Global Positioning System constraints on plate kinematics and dynamics in the Eastern Mediterranean and Caucasus. Journal of Geophysical Research 105 (B3), 5695–5719.

McGuinness, M.J., White, S.P., Young, R.M., Ishizaki, H., Ikeuchi, K., Yoshida, Y., 1995. A model of the Kakkonda geothermal reservoir. Geothermics 24, 1–48.

McGuinness, M.J., Blakeley, M., Pruess, K., O'Sullivan, M.J., 1993. Geothermal heat pipe stability: solution selection by upstreaming and boundary conditions. Transport in Porous Media 11, 71–100.

Menzies, A.J., Forth, J.L., 1995. Modeling the response of the geothermal system at Lihir Island, Papua New Guinea, to mine dewatering. Proceedings of the TOUGH Workshop '95, Berkeley, California, 20– 22 Mar. 1995, pp. 245–251.

Menzies, A.J., Pham, M., 1995. A field-wide numerical simulation model of The Geysers geothermal field, California, USA. Proceedings World Geothermal Congress '95, Florence, 18–31 May 1995, pp.1697– 1702.

Mercer Jr., J.W., Pinder, G.F., 1973. Galerkin finite-element simulation of a geothermal reservoir. Geothermics 2, 81–89.

Mertoğlu, O., and N. Başarır. 1995. Geothermal Utilization and Applications in Turkey. In Proceedings of the World Geothermal Congress, Florence, Italy, 1:345–349.

Mertoğlu, O., F. M. Mertoğlu, and N. Başarır. 1993. Direct use of heating applications in Turkey. Annual meeting, California. Geothermal Resources Council Transactions 17:19–22.

Moller, N., Greenberg, J.P., Weare, J.H., 1998. Computer modeling for geothermal systems: predicting carbonate and silica scale formation, CO_2 breakout and H_2S exchange. Transport in Porous Media 33, 173–204.

Moridis, G., Pruess, K., 1998. T2SOLV: An enhanced package of solvers for the TOUGH2 family of reservoir simulation codes. Geothermics 27 (4), 415–444.

MTA. 1993. General Directorate of Mineral Research and Exploration Institute of Turkey (MTA in Turkish initials), Geothermal Energy, Department of Raw Material Exploration of MTA, Ankara, pp. 1–16.

Murathan, A., Alıcılar, A., and Ar, I., 1999. An optimization example for electricity production from geothermal sources by using double stage systems. Energy Edu. Sci. Techno. 3:42–47.

Murray, L., Gunn, C., 1993. Toward integrating geothermal reservoir and wellbore simulation: TETRAD and WELLSIM. Proceedings of the 15th New Zealand Geothermal Workshop, Auckland, New Zealand, 10–12 November 1993, pp. 279–284.

Nakanishi, S., Iwai, N., 2000. Reservoir simulation study of the Onikobe geothermal field, Japan. Proceedings World Geothermal Congress, Kyushu-Tohuku, Japan, May 28–June 10, 2000, pp. 2159– 2164.

Oral, M.B., 1994. Global Positioning System (GPS) measurements in Turkey (1988–1992): Kinematics of the Africa–Eurasia plate collision zone. PhD Thesis, MIT.

Osato, K., Sato, T., White, S.P., Burnell, J., Yokomoto, S., 1998. Development of an integrated geothermal reservoir modeling system (database & mapping system for reservoir modeling/simulation/ management, pre-processor and post-processor system. Proceedings of the 23rd Workshop on Geothermal Reservoir Engineering, Stanford University, Stanford, California, 26–28 January 1998, pp. 152–160.

O'Sullivan M. J., Pruess K., Marcelo, J. L., 2001. State of the art of geothermal reservoir simulation, Geothermics 30 (2001) 395–429

O'Sullivan, M.J., Bullivant, D.P., Follows, S.E., Mannington, W.I., 1998. Modeling of the Wairakei -Tauhara geothermal system. Proceedings of the TOUGH Workshop '98, Berkeley, California, 4–6 May 1998, pp. 1–6.

O'Sullivan, M.J., Barnett, B.G., Razali, M.Y., 1990. Numerical simulation of the Kamojang geothermal field, Indonesia. Transactions Geothermal Resources Council 14, 1317–1324.

O'Sullivan, M.J., 1985. Geothermal reservoir simulation. Energy Research 9, 313–332.

O'Sullivan, M.J., Bodvarsson, G.S., Pruess, K., Blakeley, M.R., 1985. Fluid and heat flow in gas-rich geothermal reservoirs. Society of Petroleum Engineers Journal 25 (2), 215–226.

Ölçenoğlu, K., 1986. Scaling in the reservoir in Kızıldere geothermal field, Turkey. Geothermics 15, 731–734.

Parini, M., Acuna, J.A., Laudiano, M., 1996. Reinjected water return at Miravalles geothermal reservoir, Costa Rica: numerical modeling and observations. Proceedings of the 21st Workshop on Geothermal Reservoir Engineering, Stanford University, Stanford, California, 22–24 January 1996, pp. 127–134.

Parini, M., Cappetti, G., Laudiano, M., Bertani, R., Monterrosa, M., 1995. Reservoir modeling study of the Ahuachapan geothermal field (El Salvador) in the frame of a generation stabilization project. Proceedings World Geothermal Congress '95, Florence, 18–31 May 1995, pp. 1543–1548.

Paton, S., 1992. Active normal faulting, drainage patterns and sedimentation in southwestern Turkey. Journal of Geological Society, London 149, 1031–1044.

Pritchett, J.W., 1995. STAR: A geothermal reservoir simulation system. Proceedings World Geothermal Congress '95, Florence, 18–31 May 1995, pp. 2959–2963.

Pruess, K., Oldenburg, C., Moridis, G., 1998. An overview of TOUGH2, Version 2.0. Proceedings of the TOUGH Workshop '98, Berkeley, California, 4–6 May 1998, pp. 307–314.

Pruess, K., 1997. On vaporizing water flow in hot sub-vertical rock fractures. Transport in Porous Media 28, 335–372.

Pruess, K., Narasimhan, T.N., 1985. A practical method for modeling fluid and heat flow in fractured porous media. Society of Petroleum Engineers Journal 25 (1), 14–26.

Pruess, K., Weres, O., Schroeder, R., 1983. Distributed parameter modeling of a producing vapor-dominated geothermal reservoir: Serrazzano, Italy. Water Resources Research 19 (5), 1219–1230.

Roberts, S.C., 1988. Active Normal Faulting in Central Greece and western Turkey. PhD Thesis, University of Cambridge, England.

Rose, P.E., Goranson, C., Salls, D., Kilbourn, P., 1999. Tracer testing at Steamboat Hills, Nevada, using fluorescein and 1,5-naphthalene disulfonate. Proceedings of the 24th Workshop on Geothermal Reservoir Engineering, Stanford University, Stanford, California, 25–27 January 1999, pp. 17–23.

Rose, P.E., Apperson, K.D., Johnson, S.D., Adams, M.C., 1997. Numerical simulation of a tracer test at Dixie Valley, Nevada. Proceedings of the 22nd Workshop on Geothermal Reservoir Engineering, Stanford University, Stanford, California, 27–29 January 1997, pp. 169–176.

Sakagawa, Y., Aoyama, K., Ikeuchi, K., Takahashi, M., Kato, O., Doi, N., Tosha, T., Ominato, T., 426 M.J. O'Sullivan et al. / Geothermics 30 (2001) 395–429

Sanyal, S.K., 2000. Forty years of production history at The Geysers geothermal field, California- the lessons learned. Proc. World Geothermal Congress, Kyushu-Tohoku, Japan, 28 May–10 Jun. 2000.

Sanyal, S.K., Pham, M., Iwata, S., Suzuki, M., Inoue, T., Yamada, K., Futagoishi, M., 2000b. Numerical simulation of the Wasabizawa geothermal field, Akita Prefecture, Japan. Proceedings World Geothermal Congress, Kyushu-Tohuku, Japan, May 28–June 10, 2000, pp. 2189–2194.

Serpen, U., Satman, A., 2000. Reassessment of the Kızıldere Geothermal Reservoir, World Geothermal Congress, Kyushu-Tohoku, Japan, 28 May-10 June 2000.

Simiyu, S.M., 1999. Seismic application to geothermal evaluation and exploitation- Southern Lake Naivasha area, Kenya Rift. Proceedings of the 24th Workshop on Geothermal Reservoir Engineering, Stanford University, Stanford, California, 25–27 January 1999, pp. 305–311.

Stevens, J.L., Garg, S.K., Luu, L., Barker, T.G., Pritchett, J.W., Truesdell, A.H., 1995. GEOSYS: An X/ MOTIF-based system for analysis and management of geothermal data. Proceedings World Geothermal Congress '95, Florence, 18–31 May, 1995, pp. 2951–2953.

Suarez Arriaga, M.C., Samaniego V., F., Rodriguez, F., 1996. Some mismatches occurred when simulating fractured reservoirs as homogeneous porous media. Proceedings of the 21st Workshop on Geothermal Reservoir Engineering, Stanford University, Stanford, California, 22–24 January 1996, pp. 179–186.

Şalk, M., Altıner, Y., Ergün, M., 1999. Geodynamics of Western Turkey. Proceedings of the International Conference on Earthquake Hazard and Risk in the Mediterranean Region. V.II, 179–188, 18–22 October 1999, Turkish Republic of Northern Cyprus.

Şengör, A.M.C., Görür, N., Şaroğlu, F., 1985, Strike-slip faulting and related basin formation in zones of tectonic escape: Turkey as a case study, in: Biddle K.T., Christie-Blick N. (Eds.), Strike-slip Faulting and Basin Formation, Soc. Econ. Paleontol. Mineral. Sp. Pub., Vol. 37, pp. 227–264.

Şimşek, Ş., Doğdu, M.S., Akan, B., Yıldırım, N., 2000. Chemical and isotopic survey of geothermal reservoirs in Western Anatolia, Turkey. In: Proceedings of the World Geothermal Congress 2000, pp. 1765–1770.

Şimsek, S. 1997. Geothermal education studies in Turkey. Turkish Geothermal Association Bulletin 1:19–20 (in Turkish).

Şimşek, Ş., Yıldırım, N., Gülgör, A., 2005. Developmental and environmental effects of the Kızıldere geothermal power project, Turkey. Geothermics 34 (2005) 239–256.

Şimşek, Ş., 1985. Geothermal model of Denizli, Sarayköy–Buldan area. Geothermics 14, 393–417.

Tarcan, G., Gemici, Ü., Aksoy, N., 2005, Hydrogeological and geochemical assessments of the Gediz Graben geothermal areas, western Anatolia, Turkey, Environmental Geology, Vol. 47, pp. 523-534.

Tokita, H., Yahara, T., Kitakoga, I., 1995. Cooling effect and fluid behavior due to reinjected hot water in the Hatchobaru geothermal field, Japan. Proceedings World Geothermal Congress '95, Florence, 18–31 May 1995, pp. 1869–1874.

Tsang, Y.W., Birkholzer, J.T., 1999. Predictions and observations of the thermal-hydrological conditions in the single heater test. Journal of Contaminant Hydrology 38(1–3), 385–425.

Tulinius, H., Sigurdsson, O., 1989. Two-dimensional simulation of the Krafla-Hvitholar geothermal field, Iceland. Proceedings of the 14th Workshop on Geothermal Reservoir Engineering, Stanford University, Stanford, California, 24–26 January 1989, pp. 87–93.

Tulinius, H., Spencer, A.L., Bodvarsson, G.S., Kristmannsdottir, H., Thorsteinsson, T., Sveinbjornsdottir, A.E., 1987. Reservoir studies of the Seltjarnarnes geothermal field, Iceland. Proceedings of the 12th Workshop on Geothermal Reservoir Engineering, Stanford University, Stanford, California, 20–22 January 1987, pp. 67–75.

Vinsome, P.K.W., Shook, G.M., 1993. Multi-purpose simulation. 1991. Journal of Petroleum Science and Engineering 9 (1), 29–38.

Voss, C. I., 1984. SUTRA: A Finite-Element Simulation Model for Saturated-Unsaturated Fluid-Density-Dependent Ground-Water Flow with Energy Transport or Chemically-Reactive Single-Species Solute Transport, U.S. Geological Survey Water-Resources Investigations Report 84-4369

WECTNC. 1994. Sixth Energy Congress of Turkey, World Energy Council-Turkish National Committee, Izmir, Energy Statistics. Izmir, Turkey.

Weir, G.J., White, S.P., 1996. Surface deposition from fluid flow in a porous medium. Transport in Porous Media 25, 79–96.

Westaway, R., 1993. Neogene evolution of the Denizli region of western Turkey. Journal of Structural Geology 15, 37–53.

White, S.P., Young, R.M., Kissling, W.M., 1998. Using ITOUGH2 to improve geothermal reservoir models. Proceedings of the TOUGH Workshop '98, Berkeley, California, 4–6 May 1998, pp. 25–29.

White, S.P., Mroczek, E.K., 1998. Permeability changes during the evolution of a geothermal field due to dissolution and precipitation of quartz. Transport in Porous Media 33, 81–101.

Wu, Y.S., Haukwa, C., Bodvarsson, G.S., 1999. A site-scale model for fluid and heat flow in the unsaturated zone of Yucca Mountain, Nevada. Journal of Contaminant Hydrology 38 (1–3), 185–215.

Xu, T., Pruess, K., 2000. Hydrothermal fluid flow and mineral alteration in a fractured rock under multiphase H_2O-CO_2 mixture conditions. Proceedings of the World Geothermal Congress, Kyushu- Tohuku, Japan, 28 May–10 June 2000, pp. 2983–2988.

Xu, T., Pruess, K., 1998. Coupled Modeling of Non-Isothermal Multiphase Flow, Solute Transport and Reactive Chemistry in Porous and Fractured Media: 1. Model Development and Validation. Report: LBNL-42050, Lawrence Berkeley National Laboratory, Berkeley, California.

Yamaguchi, S., Akibayashi, S., Rokugawa, S., Fujinaga, Y., Tenma, N., Sato, Y., 2000. The numerical modeling study of the Hijiori HDR test site. Proceedings World Geothermal Congress, Kyushu- Tohuku, Japan, May 28–June 10, 2000, pp. 3975–3980.

Yeltekin, K., 2001. Characterization and modeling of Kızıldere geothermal field, Thesis for the degree of Master of Science in the Department of Petroleum and Natural Gas Engineering, Middle East Technical Univercity, Turkey.

Yeltekin, K., Parlaktuna, M., Akın, S. (2002), "Modeling of Kızıldere Geothermal Reservoir, Turkey", 27th Workshop on Geothermal Reservoir Engineering, Stanford University, Stanford, California, January, 27-30, 2002

Yeltekin, K., Erkan, B. (2002a), "Denizli Kızıldere Jeotermal Enerji Sahası 1996-2001 Yılları Çalışma Raporu", MTA Report (in Turkish).

Yeltekin, K., Parlaktuna, M., (2006), "Interpretation of reinjection tests in Kızıldere Geothermal Field, Turkey" Proceedings, 31st Workshop on Geothermal Reservoir Engineering, Stanford University, Stanford, California, January 30-February 1, 2006

Yıldırım, N., Ölmez, E., 1999. Kızıldere (Denizli–Sarayköy) sahasında açılan yeni kuyular ile üretim kuyuları arasındaki hidrokimyasal ilişki. Batı Anadolu Hammadde Kaynakları Sempozyumu Baksem 99, Izmir, Turkey.